2005-09-21

Compliant ortho-planar spring behavior under complex loads

Nathan Oliver Rasmussen
Brigham Young University - Provo

BEHAVIOR OF COMPLIANT ORTHO-PLANAR SPRINGS UNDER COMPLEX LOADS

by

Nathan O. Rasmussen

A thesis submitted to the faculty of

Brigham Young University

in partial fulfillment of the requirements for the degree of

Master of Science

Department of Mechanical Engineering

Brigham Young University

December 2005

BRIGHAM YOUNG UNIVERSITY

GRADUATE COMMITTEE APPROVAL

of a thesis submitted by

Nathan O. Rasmussen

This thesis has been read by each member of the following graduate committee and by majority vote has been found to be satisfactory.

Date	Robert H. Todd, Chair
Date	Larry L. Howell
Date	Spencer P. Magleby

BRIGHAM YOUNG UNIVERSITY

As chair of the candidate's graduate committee, I have read the thesis of Nathan O. Rasmussen in its final form and have found that (1) its format, citations, and bibliographical style are consistent and acceptable and fulfill university and department style requirements; (2) its illustrative materials including figures, tables, and charts are in place; and (3) the final manuscript is satisfactory to the graduate committee and is ready for submission to the university library.

Date

Robert H. Todd
Chair, Graduate Committee

Accepted for the Department

Matthew R. Jones
Graduate Coordinator

Accepted for the College

Alan R. Parkinson
Dean, Ira A. Fulton College of Engineering and Technology

ABSTRACT

BEHAVIOR OF COMPLIANT ORTHO-PLANAR SPRINGS

UNDER COMPLEX LOADS

Nathan O. Rasmussen

Mechanical Engineering

Master of Science

This thesis presents research on the feasibility of applying compliant-ortho-planar springs (COPS) to rotational applications. The primary motivation of this research is the application of COPS to a continuously variable transmission (CVT). The design space limitations, loading conditions, stresses, stress concentrations, and limitations of current design tools, such as pseudo-rigid-body models (PRBM) for COPS, are discussed. A new 3D PRBM is presented along with a discussion on the possible applications of such to a rotating COPS. Stress stiffening and lateral stability are two major phenomena occurring in a rotating COPS. Both phenomena are a direct result of the inertial loads a COPS would be subjected to in a rotational environment. The results show how stress stiffening and lateral buckling in the legs are influenced by design parameters. Conclusions and recommendations for further research are recommended.

ACKNOWLEDGMENTS

I would like to thank many for their patience, kindness, and support of my education. I am grateful to my Father in Heaven for placing such people in my path and for the opportunities he has given me to study at this great university. I know that only with his help it was possible to get an education here.

I am grateful to my loving wife, Courtney, who has encouraged and supported me through these many long years in school. I owe a great deal of thanks to her for her patience. I appreciate her taking care of the homefront which includes our three little ones - Porter, Haley, and Elijah. I would like to thank them as they have also been patient in my absence from time to time. I am indebted to my parents for teaching me principles of integrity and hard work. They have been a great support and influence in my life and I appreciate their encouraging me to get an education.

I am grateful for my thesis advisor, Robert H. Todd, who has had an enormous influence on me personally as well as my research. I cannot thank him enough for the many, many hours he has spent in my behalf offering advice, support, and encouragement. He has been an excellent mentor and teacher and has certainly made a difference in my life and education.

I would also like to thank Spencer Magleby and Larry Howell, for their guidance, encouragement and support. They have been great to work with.

A special thanks to many colleges and friends in the lab for their ears and minds especially Jon Wittwer for his many hours of instruction and help in setting up some of the software programs for my research. I would not have been able to accomplish nearly as much as I did without his willingness to share his expertise.

I would also like to thank the Center of Excellence for their contribution in funding my research.

Contents

List of Tables

List of Figures

Chapter 1

Introduction

1.1 Thesis Motivation

Research in the area of compliant mechanisms has experienced tremendous growth in recent years. This growth has been fueled by simplified methods of modeling large nonlinear deflections of compliant links using rigid body mechanics. This simplified model has aided compliant mechanism designers in analysis and synthesis and has accelerated the derivation of many different classes or types of compliant mechanisms [1].

Ortho-planar mechanisms are comprised of both compliant and rigid-body mechanisms. Ortho-planar mechanisms are defined as mechanisms in which all the links can be located simultaneously in a single plane. In some cases compliant ortho-planar mechanisms exhibit a force-deflection relationship much like a spring and have been classified as ortho-planar springs. Traditional ortho-planar springs, such as spider, disc, and volute springs, have been used to provide force-displacement behavior in compact spaces, but there are inherent disadvantages in these types of springs. Compliant ortho-planar springs (COPS) can potentially eliminate many of the problems associated with traditional ortho-planar springs. Some of these advantages include less rotation of the platform, no required clearance, increased displacement, and improved fatigue life [2, 3]. An example of a COPS can be seen in Figure 1.1.

COPS designs may be appropriate for a number of potential applications. They have successfully been implemented in the control of industrial valves [3]. Other

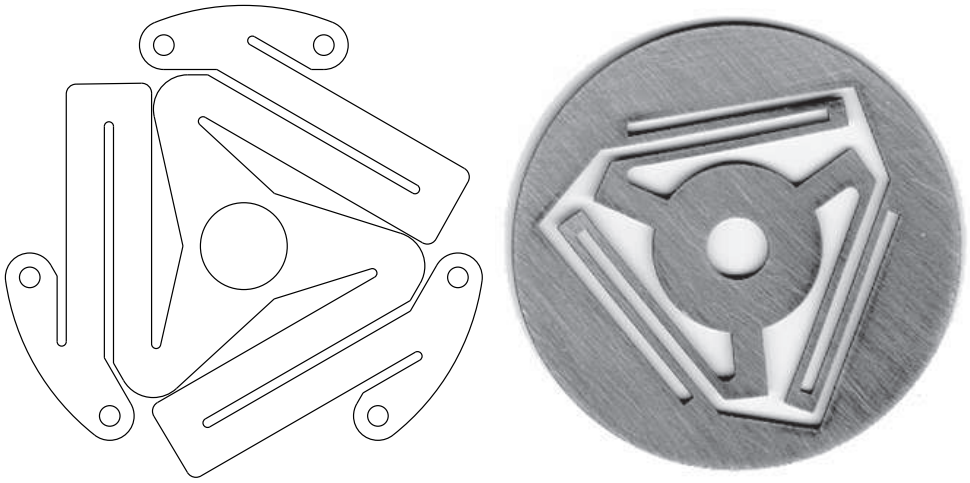

Figure 1.1: Typical compliant ortho-planar springs (COPS).

suggested applications include electrical contacts, keyboards, compact space applications, positioning and centering, compact camping gear, speakers, circuit boards, damping devices, precision antennae, and touch probes. COPS may possibly replace most any type of spring. It is important to note however that the many applications for COPS, both realized and suggested, function under loads which are static or quasi-static in nature.

Although there is adequate knowledge for analyzing spring designs utilized in quasi-static applications, there is still much to be learned from applying COPS to rotational applications. Some new challenges result which were not present in static applications. Some of these challenges are the increase in complexity and number of additional design parameters, the ability to understand the implications of a choice in design parameters, the need for new simple analysis tools, and a clear method for understanding how to approach problems given these new load conditions.

The primary motivation for this research is the application of COPS to composite v-belt continuously variable transmissions (CVT). A thorough review of CVT's can be found in Appendix A. Figure 1.2 (a) shows a CAD model of a CVT drive clutch with a coil spring and one with a COPS (b). In a CVT a COPS may be subject to

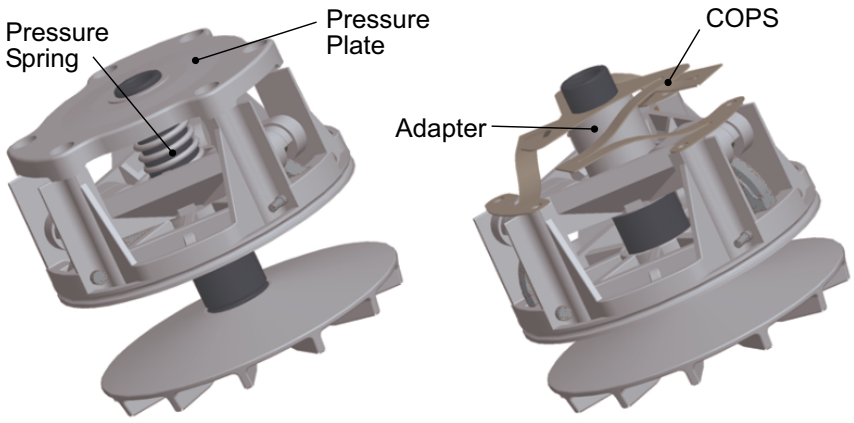

Figure 1.2: A rendition of the P-90 Polaris drive clutch (a) and a COPS adapted to fit within the existing design.

three or four types of loads: large orthogonal deflections, fluctuating inertial loads, and possibly imbalance or a moment applied to the axis of rotation.

A composite v-belt CVT performance is dependent on three elements: the spring constant, cam profile, and weights. In order to change the spring constant a new coil spring must be purchased and replaced. In order to fine tune the CVT a number of different coil springs may be purchased before the correct one is found. The tunability of a CVT would be greatly enhanced by replacing a box of coil springs with a stack of COPS as shown in Figure 1.3. There may also be some weight and space advantages with the redesign of a CVT specifically to accommodate COPS. There is, however, a lack of knowledge about how COPS behave while subjected to inertial loads. Two initial investigations of COPS applied to a CVT were made by Anderson et al. [4] and Christiansen [5]. Both studies concluded that there is not enough understanding of COPS behavior while subjected to complex loads.

In order to better design COPS for complex load situations it is critical to better understand several of their characteristics such as, lateral stability and stiffness,

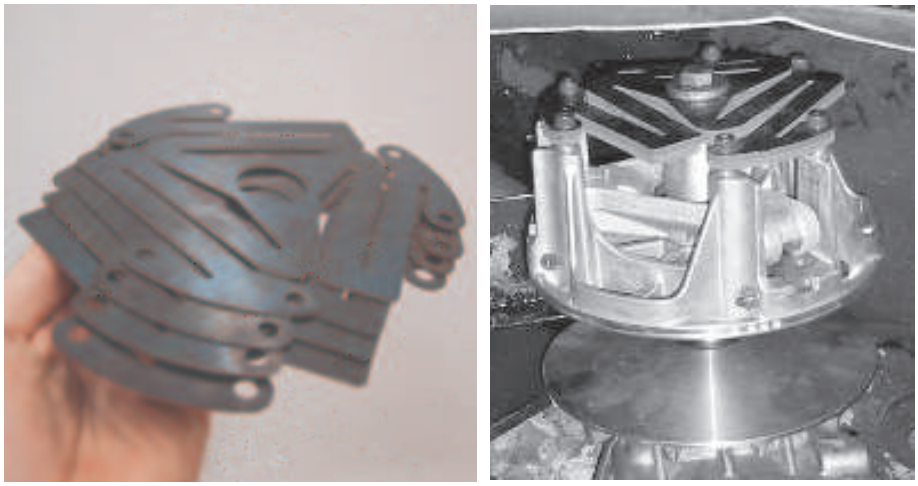

(a) (b)

Figure 1.3: COPS can be (a) stacked which is highly advantageous for a (b) CVT application.

the effects of stress stiffening, and how the various parameters affect COPS performance. New knowledge gained from this research will enhance the ability to design and analyze COPS for greater reliability when subjected to various load conditions.

1.2 Thesis Objectives

Thesis objectives will focus on the following.

- Summarize what has been done to date with COPS.
- Qualitative look at the design space and imposed limitations, spring geometry, loads, stresses and the applicability of current design tools.
- Investigate a 3D pseudo-rigid-body model for rectangular cross-section cantilever beams subjected to simple loads.
- Characterize parameter influence on output force in thin sheet COPS under static loads.

- Characterize parameter influence on output force in thin-sheet COPS under complex loads.
- Characterize limitations on design stability in leg design for rotational applications.
- Identify and analyze stress stiffening for COPS in rotational applications.
- Present a set of design steps for approaching COPS applications and the design tradeoffs associated with many of the design parameters.

1.3 Thesis Outline

Chapter 1 discusses the motivation for the research, states research objectives and a brief summary of each chapter.

Chapter 2 is a literature review of compliant mechanisms, analysis tools for compliant mechanisms, and a thorough review of what has been done with compliant ortho-planar springs to date.

Chapter 3 sets forth the limitations of the design space, the experimental setup, COPS loads and stresses, and finally current analysis tools and their limitations.

Chapter 4 covers the initial foray into deriving a pseudo-rigid-body model for 3-dimensional applications. Although the boundary conditions researched therein do not directly match those of a COPS leg segment, it does provide a foundation for future research on this subject.

Chapter 5 is an investigation of how each parameter in a COPS design affects the spring reaction force. An understanding of these factors will better help understanding of how the springs are affected by inertial loads.

Chapter 6 characterizes the lateral stability and stiffness of COPS legs. Two modes of lateral buckling are identified and the design space for lateral buckling is mapped out for the nominal COPS design. The results of this chapter are used to limit the design space exploration.

Chapter 7 quantifies stress stiffening for the nominal COPS design. The design tradeoffs between leg angle and the benefits of stress stiffening are discussed.

Chapter 8 presents some generalized steps that may be used to design COPS for a number of situations. A table of design tradeoffs between design parameters and design elements, such as stress stiffening, is presented with some discussion on those critical for rotational applications.

And finally, Chapter 9 presents the contributions and conclusions made by this research and recommendations made for further research.

Chapter 2

Background

2.1 Compliant Mechanisms

Compliant mechanisms have been around for a long time even though fundamental methods for synthesis and analysis have only recently been developed. The basic theory of compliant mechanisms has been well researched and there are numerous papers and books written on the subject. There is at least one resource book [1] which gives an in-depth overview of most topics related to compliant mechanisms. There are also other books which are more specialized in some aspects of compliant mechanisms [6, 7].

Mechanisms in general derive their usefulness from transferring or transforming motion, force or energy and have traditionally been composed of rigid links connected at movable joints. Compliant mechanisms, a sub class of mechanisms, differ from rigid body mechanisms in that they are composed of flexible members which transfer or transform motion, force, or energy [1]. Following are basic principles related to compliant mechanism classification, advantages and disadvantages, general design considerations, and methods of analysis.

2.1.1 Classification

Midha et. al. [8] separated compliant mechanisms into traditional classes such as linkages, lever systems, cam followers, gear trains, etc. Howell [1] broke compliant mechanisms into two main categories: fully and partially compliant. Fully compliant

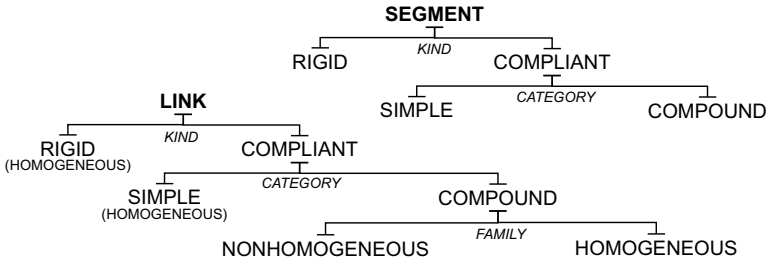

Figure 2.1: Characterization of segments and links.

mechanisms obtain all of their motion from compliant members and partially compliant mechanisms obtain only part. Compliant mechanisms can be divided further into links and segments. Figure 2.1 shows Howell's classification of links and segments. Parise [2] combined previous knowledge with his own in order to classify ortho-planar mechanisms of which ortho-planar springs (OPS) are a part. He also established the nomenclature for OPS and presented some design tools.

2.1.2 Advantages & Challenges

The advantages and disadvantages of compliant mechanisms in general were discussed by Sevak and Mclarnan [9] and can be found in many other works [10, 11, 2, 12]. The applicability of each advantage depends on the particular mechanism and its conditions. Advantages may include location in a single plane, reduced wear, increased precision, reduced maintenance, reduced weight, reduced size, reduced part count, and reduced cost in manufacture and assembly. Some of the challenges in designing and using compliant mechanism are problems with fatigue, creep, and stress relaxation.

2.1.3 General Design Considerations

Consider Equation 2.1 for the deflection of the rectangular fixed-guided beam shown in Figure 2.2.

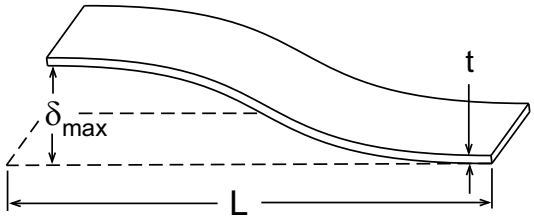

Figure 2.2: Fixed-guided beam simulating a leg segment in a COPS design.

It is important to note that deflection and force can be affected by both the material properties and geometry. The bracketed terms show how a designer might influence flexibility [1].

$$\delta_{max} = \frac{2}{3}\left\langle \frac{S_y}{E} \right\rangle \left\langle \frac{L^2}{t} \right\rangle \tag{2.1}$$

Material selection for CM's is primarily done to maximize flexibility. Deflection is maximized when the strength-to-modulus ratio is maximized. Picking out a material for a particular application should be done with this in mind. In some cases there will be a fine line between sufficient flexibility, so that the component does not break, and maximizing the force output. In such cases material selection may not be as simple as maximizing the strength-to-modulus ratio. Geometric design properties such as beam length, L, and thickness, t, will also heavily influence deflection and flexibility. With the addition of inertial loads, material selection will be even more difficult.

2.1.4 Methods of Analysis

As mentioned before, the history of compliant mechanisms began many centuries ago. However, the ability to accurately model and synthesize these mechanisms has come about only recently. The difficulty in modeling them lies in nonlinearities associated with large deflections. Foundation work for large deflection analysis of elastic rods began as early as the $17th$ century and contributions were made by the Bernoulli family, Euler, Lagrange and many others [13]. More recent developments include the

derivation of closed-form methods, numerical methods, topology design methods, and the pseudo-rigid-body model (PRBM). The later two have recently been developed and are being used quite successfully. They are both systematic design methods based on two different approaches. Topology methods are based on structural optimization whereas the PRBM is based on kinematics [14]. The PRBM has the most potential for quickly analyzing COPS in static situations but will be less advantageous for COPS in rotational applications. For a more complete discussion on these analysis methods and references see Appendix B.

2.2 Pseudo-Rigid-Body Models

The purpose of the pseudo-rigid-body model (PRBM) is to provide a simplified method of analyzing mechanical systems that undergo large, nonlinear deflections. Pseudo-rigid-body models have been used with great success in predicting force-deflection characteristics of compliant mechanisms [1].

A PRBM allows for rigid body replacement of the flexible segments of a compliant mechanism with rigid links, pin joints, and torsional springs. Doing this provides not only an analytical model, but also a visual representation of the replacement. These mechanism elements can then readily be analyzed using rigid-body kinematics.

The development of many PRBM's over the past decade has greatly simplified the design and analysis of compliant mechanisms. This includes a number of PRBM's for many different cases of geometries and load situations such as small length flexural pivots [15], fixed-pinned or cantilever beams with an end force on the free end [16], fixed-guided segments [1], beams with end-moment loads [1], initially curved cantilever beams [17], pinned-pinned segments [18], and fixed-fixed segments [1]. Small length flexural pivots and simple cantilever beams were among the first to be modeled and provided a foundation upon which other PRBM's were developed.

The key assumption upon which all PRBM's are based is that a near-circular path is followed by some part of the geometry on the mechanism-usually the end of a flexible segment. These PRBM's assume that the mechanism deflection occurs within a single plane.

There are other challenges associated with the application of the PRBM to rotational applications which will be discussed qualitatively in the next chapter. One important consideration is that planar deflections of compliant segments no longer exist under inertial loads. Deflection about more than one axis of rotation may occur due to combined orthogonal and inertial loads. The lateral component of the inertial loads may create instabilities in leg segments causing lateral buckling. Timoshenko [19] studied torsional and lateral buckling of thin rectangular cross-section beams subject to moments and loads in the direction of greatest flexural rigidity. He was able to find critical loads at which they buckled for cross sections of varying flexural rigidity. Timoshenko's research was done for a force applied only in the direction of greatest flexural rigidity. A COPS leg segment geometry is similar to the beams studied by Timoshenko but the loading conditions are different.

2.3 Manufacturing Compliant Mechanisms

The manufacture of macro-compliant mechanisms has not been a widely researched area. Herring et. al. [20, 21] investigated the high production manufacture of compliant mechanisms with long slender beams. Although his work did not consider the manufacture of ortho-planar mechanisms and COPS in particular, it does provide a framework for assessing processes which would be suitable for high volume production of COPS.

Herring noted the key characteristics of the mechanisms investigated. The two compliant mechanisms considered had geometry of both thick rigid and thin compliant out-of-plane segments as shown in Figure 2.3. Beam thicknesses of 0.508 mm or 0.02 inches were considered. Key characteristics included beam dimensions and ratios of each to the thin compliant beams. These key characteristics were useful for assessing the feasibility of each of the individual process capabilities for the mechanisms of interest.

There were two general areas of research within the shaping methods identified for manufacturing compliant mechanisms.

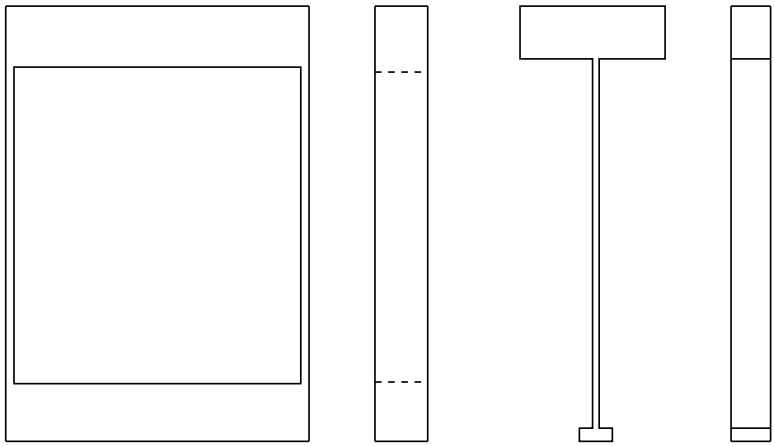

Figure 2.3: Generic complaint mechanisms used in Herring's manufacturing study: (a) with long thin fixed-guided beams and (b) with long thin cantilever beams.

- No assembly or one-piece processes, are those that are individually, or jointly used with other processes, capable of producing compliant mechanisms with long thin beams in one piece at high production rates.

- Assembly processes are those which are individually, or jointly used with other processes, capable of assembling compliant mechanisms.

Since COPS designs will only be made from a single flat sheet of material, assembly processes will most likely not be applicable.

A go-no go matrix was used as an initial method for excluding processes that would not be able to meet the two main criteria: ability to create the geometry and be able to meet high production rates. Because ortho-planar mechanisms were not of concern in Herring's work, many processes suitable for their manufacture were not considered.

Weight [22] considered a similar problem to that of COPS manufacturing with a multi-layer floating-opposing-arm clutch design. These clutch layers had similar dimensional characteristics to those of COPS designs and were made of similar materials. He added both the conventional and fine blanking processes to Herring's list of

potential processes. Both of these processes work great for single-piece thin-planar mechanisms and are capable of high production rates.

Herring collected process capabilities for each of the final processes. In comparing them with needed capabilities based on key characteristics, he found no process to be feasible for the designs he investigated. Although his approach resulted in no manufacturing methods capable of producing the desired geometry in a single process, his approach would be useful for evaluating the design for and manufacture of COPS. The planar nature of COPS make them suitable to high volume manufacturing because there are many rapid manufacturing processes which operate in two dimensions such as stamping and fine blanking and materials in sheet stock form are readily available.

2.4 Compliant-Ortho-Planar Springs

Compliant ortho-planar springs fall under the class of ortho-planar mechanisms. Parise combined all previous work done on ortho-planar mechanisms. Ortho-planar mechanisms consist of change-point mechanisms, metamorphic mechanisms, compliant mechanisms, and microelectromechanical systems or MEMS [2][1].

An ortho-planar mechanism is one in which all of its links can be simultaneously located in a single plane with motion out of that plane. When all of its links are located in that plane the mechanism is said to be in its in-line position [2].

All ortho-planar mechanisms have the advantages of being in a compact state and can be fabricated from a single work piece. Ortho-planar mechanism configurations are highly scalable making them ideal for a wide range of applications including MEMS [2]. The disadvantages of most ortho-planar mechanisms are associated with the change point. For most there needs to be some aid as it moves through the change point so that it does not change configurations and for other types it is a problem because there is no force at its in-line position. These disadvantages do not apply to ortho-planar springs because the mechanism configuration is fixed through its change point. It may also be desirable for a spring to have an undeflected state.

[1]The field of metamorphic mechanisms was researched by Carroll [12] while Lusk [23] explored spherical and spacial mechanisms some of which exhibit ortho-planar characteristics.

Parise [2] showed that the spring constants of each individual segment could be added to derive an overall spring constant. Christiansen [5] showed through experimentation that individual COPS spring constants can be added together with a great deal of accuracy to get an equivalent spring stack constant. This is a great advantage over traditional springs for any type of mechanism which requires tuning by changing a spring constant. Spring constants are easily changed by simply adding or subtracting layers of COPS. This idea is of particular interest in actuating a CVT [4].

2.4.1 Background

One of the major contributions made by Parise [2, 3] was the development of a new ortho-planar linear-motion spring. An ortho-planar spring is one which can be either fabricated in or compressed down to a single plane. Traditional ortho-planar springs include disc, volute, and spider springs. Parise's new ortho-planar linear-motion spring, referred to as COPS in this thesis, had several advantages over traditional ortho-planar springs. Spider and volute springs rotate as they move through their motion which creates torsion. Parise completed a qualitative analysis of the performance characteristics of COPS and spider springs. The rotation a spider spring experienced in the platform was considerable compared to that of COPS designs. Spider springs can also create friction between themselves and the object they are trying to displace if they are not secured. Disc springs require clearance to make deflection possible. The COPS design eliminates those disadvantages while maintaining the advantages of being compact and simple to manufacture [2, 3].

COPS exhibit linear motion output orthogonal to the plane of fabrication. They may consist of rigid, semi-rigid, and compliant segments or links. In general they can have as few as two legs and up to as many as is physically possible. The main parts of a typical COPS can be seen in Figure 2.4.

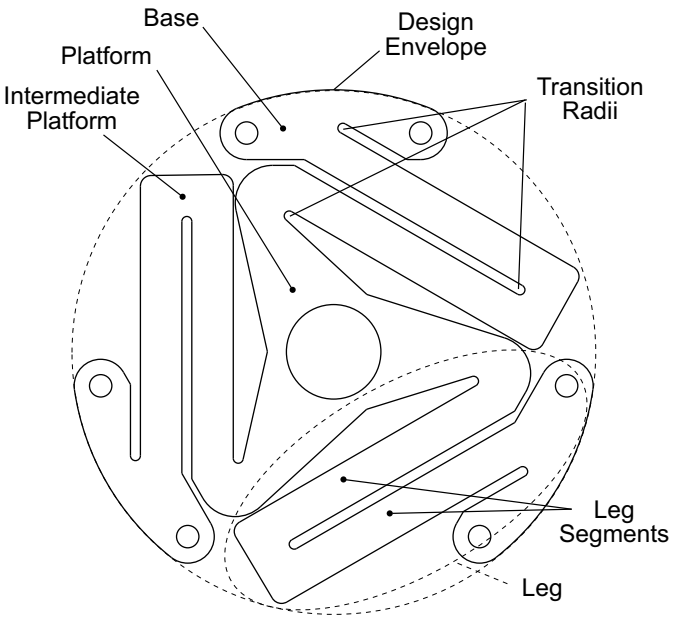

Figure 2.4: Main parts of a COPS.

2.4.2 Nomenclature

Parise also set forth the nomenclature of COPS designs. Parise's classification system is based on four elements of the design: number of legs, number of flexible segments per leg, leg style, and in some cases the leg angle.

The first term for a particular design consists of the number of legs used in the design: bi, tri, quad, pent, etc. A leg is defined as an unbroken connection of all of the segments between the base and the platform on a given side (i.e. the compliant segments and the intermediate platform(s)).

The second term tells how many flexible segments there are. First the number of segments connecting the base and the intermediate platform followed by a dash and the number of segments between the intermediate platform and the platform. It is possible to have more than two sets of segments in any one leg and if that is the case they are named in the same order and separated by dashes. If different leg geometries are in a single spring then each leg is declared with a full colon separating it from

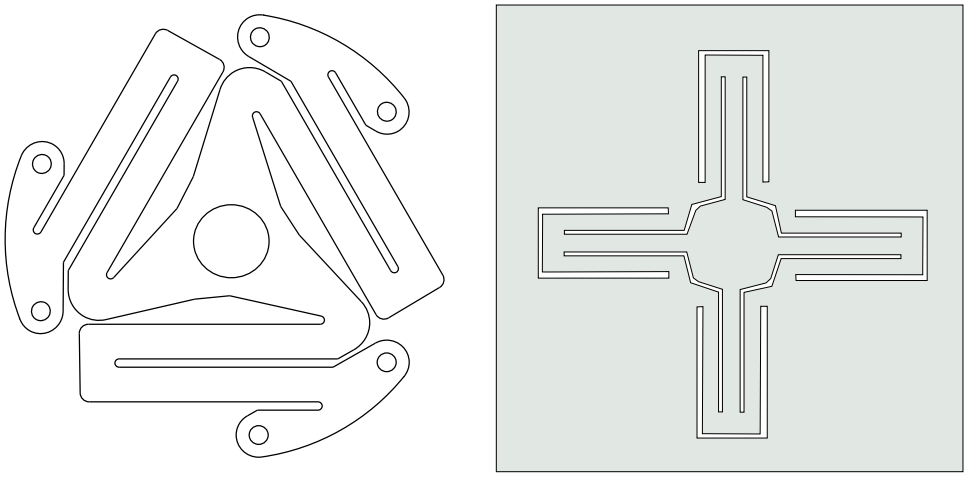

(a) (b)

Figure 2.5: (a) One and (b) two segments between the base and intermediate platform.

the next. Two typical leg designs with a different number of segments are shown in Figure 2.5.

The third element is the leg style. An S for side or an R for radial is appended. If it is a side leg position then it becomes necessary to distinguish them by the angle made between a radial line from the center of the platform to a line parallel to a leg segment as shown in Figure 2.6. The angle from which it deviates from the radial design should be appended to the S.

When combining these four elements a COPS design or class is adequately described. An example of the naming scheme can be seen in Figure 2.7. The spring shown in Figure 2.5 (a) is a $Tri\,1-1\,S135°$ while (b) is a $Quad\,2-1\,R$.

There are a few special cases that require additional nomenclature. If an extra set of segments is added to a leg then the nomenclature has an extra dash and number added to it (e.g. $Tri\,2-2-1\,R$ etc). It is also possible to nest one COPS inside of another. The nomenclature does not change for the individual springs but the two are joined with a + sign.

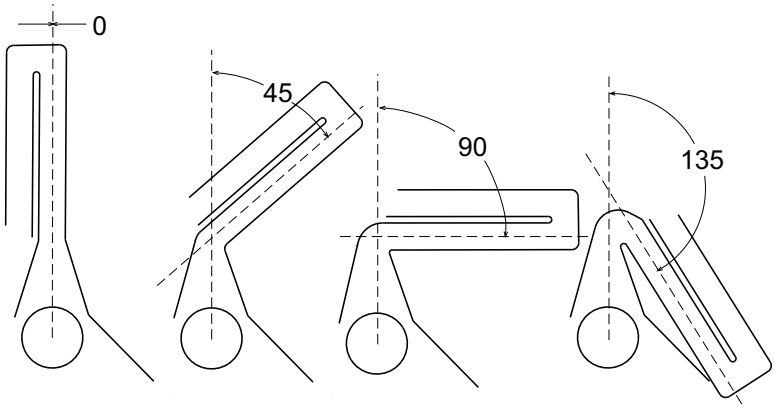

Figure 2.6: Various angles for side leg designs.

$$\overbrace{Tri}^{\#\text{ of legs}} \quad \overbrace{2-1}^{\text{Flexible Segments}} \quad \overbrace{S}^{\text{Leg Style}} \quad \overbrace{45^\circ}^{\text{Leg Angle}}$$

Figure 2.7: Nomenclature for COPS designs.

In addition to the straight-leg designs there are curved-leg designs. Curved flexible segments would have advantages of an even more compact design. Right angled leg designs were also mentioned although none were made or analyzed.

Unequal lengths in leg segments are possible if and only if the sum of the deflections in each leg is equal. If this is not the case then nonlinear motion will result and the platform deflection will not follow a straight line. Unequal length leg segments produce an uneven stress distribution in the legs. This is inefficient in that it decreases the maximum deflection while increasing the required force to achieve it. Recommendations were to stay away from unequal lengths because they are less efficient than those with equal length leg segments.

Inversions occur if an platform or intermediate platform is grounded to invert the motion. These could become structures depending on how the intermediate platforms are grounded or on the number of legs or segments.

The possible configurations of a COPS design are inexhaustible and can include multiple platforms, multiple flexible segments per leg, straight or curved or right angle flexible segments, unequal leg segments, various angles of attachment, and inversions.

A method for determining size envelope requirements for side and radial designs was developed by Parise [2] and a set of equations were derived.

2.4.3 Lateral Stability

Stability is defined as the property of a body that causes it, when disturbed from a condition of equilibrium or steady motion, to develop forces or moments that restore the original condition. Parise's [2, 3] definition of stability for a COPS design is the resistance the platform has to moving out of its prescribed motion. Using this definition he performed a qualitative stability analysis on various types of COPS designs. It is assumed his criteria for stability was strictly subjective because there were no metrics given for its measurement. The following list is a summary of his findings.

- Stability was shown to be dependent on the number of legs, leg segments/level, leg style, and leg angle.
- Each individual leg is unstable to rotations about the long axis of its flexible segments.
- In general, stability is proportional to the number of legs but all things being equal, the odd leg designs were more stable than the even leg designs. The pent design was the most stable of those tested but it is possible that designs with greater numbers of legs could produce as much or even greater stability. Multiple leg designs are more stable and theoretically have one degree of freedom [24] although there could still be some rotation of the platform due to compliance.
- Legs equally spaced around the platform produce the most stability in odd leg designs. Even leg designs have an unstable axis shared between legs opposite each other on the platform.

- Bi-leg designs are inherently unstable and are not recommended because they have more than one degree of freedom. Although side leg designs are unlikely, it is possible to create a $Bi2-2R$ design which is more stable but still experiences some rotation in the platform.

- Side leg designs are more compact than radial designs but are subject to more rotation in the platform. Curved-leg designs are even more compact but are not as easy to analyze yet. Side leg designs are subject to higher stresses because of the addition of torque around the intermediate platforms. This leads to possible torsion of a segment about its length and slight rotation of the platform.

- As the number of legs increases, the possibility of a single leg segment rotating about its long axis decreases.

- Multiple flexible segment levels per leg (i.e. two intermediate platforms per leg) and nested springs increase the possible deflection but decrease stability.

2.4.4 Lateral Stiffness

Stiffness is defined as the lack of suppleness or pliability. To this point there has been no research on the lateral stiffness of COPS. Stiffness will be related to the location of the platform relative to the base or a leg segment relative to the base. The leg segments themselves will need to be designed to resist lateral buckling due to inertial loads. Timoshenko [19] researched the lateral stability of thin rectangular cantilever beams subject to an end load. He derived equations for calculating the critical load at which the beam buckles laterally. Although loading conditions for a COPS leg do not have the same boundary conditions as Timoshenko's beams, the characterization of loading conditions still may be possible.

2.4.5 Stress Stiffening

Stress stiffening happens when the stiffness in a structure changes as a load is applied. An example is when a COPS leg has an orthogonal load, F_z, from platform displacement and an inertial load, F_i from an applied angular velocity, ω_z as shown

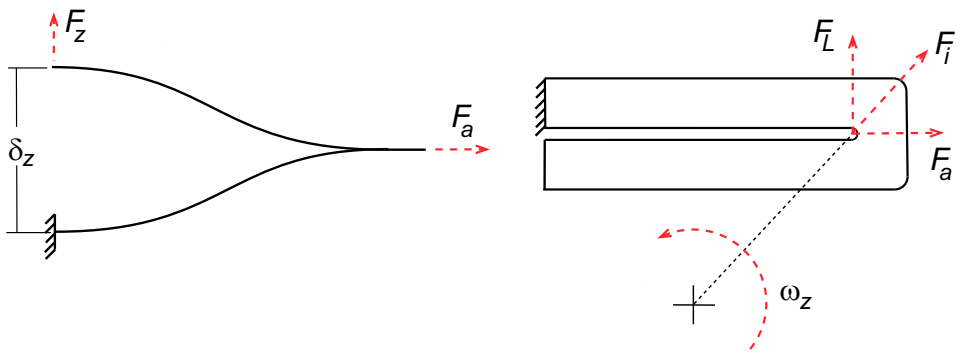

Figure 2.8: The axial component of inertial loads on leg segments increases the reaction force at a given displacement.

in Figure 2.8. For a given displacement, δ_z, there is a reaction force opposing that displacement. The addition of an axial component, F_a of an inertial load increases the reaction force by trying to pull the base and platform back into a single plane.

Because the stiffness changes as the load is applied, these types of problems are nonlinear. When solving them it is required to recalculate the stiffness matrix, applied forces, and moments a number of times while applying the loads.

Howell [1] states that tension should be reduced or eliminated if deflections are desired. For an application such as a CVT where the restoring force of the spring is desired, stress stiffening effects would seem to be desirable. It may increase the supplied spring force and return the sheaves together with greater ease. One would suppose that this additional force would enable the spring thickness to be reduced, reducing spring weight.

2.4.6 Applications

Parise [2] stated that COPS is one of the more promising applications of the developed theory on ortho-planar mechanisms. Recommendations suggest that more detailed analysis be done on COPS and that potential applications be explored.

One application in which a COPS design was successfully implemented was in an industrial control valve. Suggested applications include electrical contacts,

keyboards, compact space applications, positioning and centering, compact camping gear, speakers, circuit boards, damping devices, precision antennae, and touch probes. All of these applications are static or quasi-static in nature.

Chapter 3

Geometries, Loads, and Stresses

The objectives for this chapter are to narrow the research scope in the design space and discuss qualitatively the issues that arise when COPS are utilized in a rotational application.

3.1 Design Space Boundaries and Key Characteristics

Because the design space for COPS is quite large and the number of design parameters so many, it becomes necessary to focus on only the portion of the design space which is of most interest. The boundaries on the design space have been set specifically for a CVT application. The boundaries will include designs which are best suited for handling inertial loads, stress stiffening, are stable, and make the most economic sense with respect to manufacturing.

The complexity in design space is evident when a list of the possible parameters for COPS is considered. Material properties, design envelope, platform diameter, number of legs, leg style and/or angle, number of segments between intermediate platform and platform, number of segments between intermediate platform and base, spring thickness, leg segment length, leg segment width, base geometry, transition geometry, platform geometry, nested springs, multiple intermediate platforms, etc. all must be taken into consideration when designing COPS. COPS configurations considered undesirable for rotational applications would include multiple intermediate platforms and nested springs because of a significant reduction in stability.

The parameters which exhibit the most influence on force output under static loads are spring thickness, leg width, leg length, number of legs, and the modulus

of elasticity. With the addition of inertial loads the leg angle, platform diameter, and material density also become influential on force output. The parameters related to inertial loads determine the extent of stress stiffening in the leg segments. Stress stiffening, caused by an axial force applied at the ends of a leg segment, contributes to spring force.

The four parameters which have been limited to a specific configuration in this study are the number of legs, number of segments per leg, transition geometry, and material properties.

First, the number of legs were found to be critical in determining the stability of the spring [2]. The design space will be limited to COPS with an odd number of legs because they are more stable than those with an even number. Therefore the tri and pent leg designs are better candidates for rotational applications. The tri-leg design has additional advantages over the pent design such as more efficient use of space, lighter weight, and lower manufacturing costs. For a given design envelope, the greater the number of legs the more space taken up by leg attachment geometry such as the platform and base which means less available space for geometry like the leg segments which provide the spring force. This would lead to a decrease in maximum displacement and would possibly decrease the reaction force. Also, more legs would required a larger platform which could increase the spring weight. The greater the number of legs the more complex the COPS shape and the greater the spring perimeter. For a blanking operation, the tooling cost would increase with die complexity and the power consumption is significantly influenced by the total perimeter to be blanked. A Tri leg design would be a better parameter choice for number of legs because it can be made more compact, lighter weight, has a greater maximum displacement, more efficiently uses space, and is more economically manufactured than an equivalent pent design.

The number of leg segments per level in a leg can also be selected on the justification of geometry characterization and manufacturing. The size envelope required for the 2-1 and 1-2 leg designs is increased substantially when compared with the 1-1 design. A 1-1 leg design can much more easily be adapted to different leg angles as well making it ideal for compact situations. Manufacturing a 2-1 or 1-2

leg design has the same manufacturing cost implications as discussed previously. Multiple leg segments may add to the stability of the spring but for rotational applications this slight advantage would not outweigh its disadvantages. Therefore, a 1-1 leg design would be a better design choice for rotational applications.

The transition geometry also presents an opportunity to simplify the analysis. The simple arc shown in many of the figures could easily be scaled or replaced by other geometric configurations. For purposes of understanding operational characteristics and deriving simple design tools, the transition geometry will be limited to a 180° arc. An investigation of stress concentrations due to transition geometry will be qualitatively discussed later.

The material properties of greatest import in the analysis are Young's modulus and material density. The materials most likely to be used in rotating applications, specifically in CVT's, are spring steel and titanium. Although both materials are ideal for COPS designs, only spring steel will be investigated in this research.

In summary, the design space covered in this research will be focused on spring steel $Tri1-1$ designs. Although it is being limited to these designs, much of the analysis will be completed using a single leg with base and platform geometry truncated but retaining the intermediate platform. Doing this makes it possible to apply much of the analysis work to designs with more than three legs while maintaining a focus on $Tri1-1$ designs. Studies in this thesis will not consider platform-leg interference for more than three legs. With these general limitations in place, a nominal design is chosen which will be used for showing the effects each parameter has on spring force.

3.2 Nominal COPS Design

The number of design variables which influence the spring force is quite large. Because there are so many for a COPS design, it becomes necessary to choose a nominal or baseline design from which to work. This choice of nominal design dimensions and ranges was heavily influenced by the potential application of a COPS to a rubber V-belt CVT. Figure 3.1 shows each design parameter and Table 3.1 provides the nominal dimensions and their ranges for investigating.

Table 3.1: Baseline COPS nominal dimensions with limits of investigation.

Parameters	Nominal (in)	Range (in)	Nominal (mm)	Range (mm)
t	0.02	± 0.012	0.508	± 0.305
w_{leg}	0.50	± 0.125	12.7	± 3.175
L	2.75	± 0.25	69.85	± 6.35
r_{leg}	0.09375	± 0.03125	2.381	± 0.794
r_{plat}	2.0	± 0.50	50.8	± 12.7
ζ	$67.5°$	$\pm 67.5°$	$\frac{3\pi}{8} rad$	$\pm \frac{3\pi}{8} rad$
δ_z	low $\rightarrow$	3% of L	high $\rightarrow$	30% of L
ω_z	low $\rightarrow$	$0 \frac{rad}{sec}$	high $\rightarrow$	$650 \frac{rad}{sec}$

Table 3.2: Material properties for spring steel and titanium.

	Yield Strength	Young Modulus	Poisson Ratio	Density
Spring Steel	$1620 Mpa$	$207 Gpa$	0.30	$7850 kg/m^3$
Titanium	$1103 Mpa$	$110 Gpa$	0.33	$4480 kg/m^3$

The width of the intermediate platform,w_{ip}, and it's radius, r_{ip}, on the corners are dependent on leg width, w_{leg} where w_{ip} is equal to w_{leg} and the two r_{ip}'s are equal to half w_{leg}. The reason for this is because the outer material on the intermediate platform has been shown to have very low stress. To increase the w_{ip} greater than w_{leg} would be an inefficient use of space and to make w_{ip} less would compromise the structural integrity of the intermediate platform. For all experiments, parameters will be at their nominal value unless otherwise specified.

Important material properties for spring steel and titanium were found in Callister [25] and are summarized in Table 3.2.

The direction of rotation relative to the leg angle is one other parameter to clarify. Spring rotation, looking from the top of the COPS, will always be in a counterclockwise direction as shown in Figure 3.1.

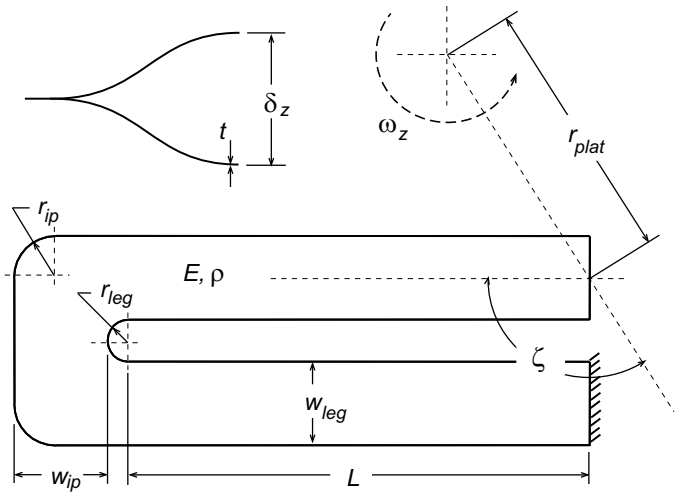

Parameter	Description
t	Spring Thickness
w_{leg}	Leg Segment Width
L	Leg Segment Length
r_{leg}	Transition Radius
w_{ip}	Intermediate Platform Width
r_{ip}	Corner Radii on Intermediate Platform
r_{plat}	Platform Radius
ζ	Leg Angle
ω_z	Angular Velocity
δ_z	Orthogonal Displacement
E	Modulus of Elasticity
ρ	Material Density

Figure 3.1: Design parameters for models and simulations.

Leg angle is one of the more interesting design parameters because of its ability to influence stress stiffening and stability while under inertial loads. At 0° the axial load in each leg segment is greatest for any given ω and stress stiffening is at its peak. When the leg angle is between 65° and 135°, depending on the platform diameter and other leg segment parameters, the lateral loads on leg segments are at a peak. At these angles, lateral stability may be compromised under certain conditions because of these lateral inertial loads.

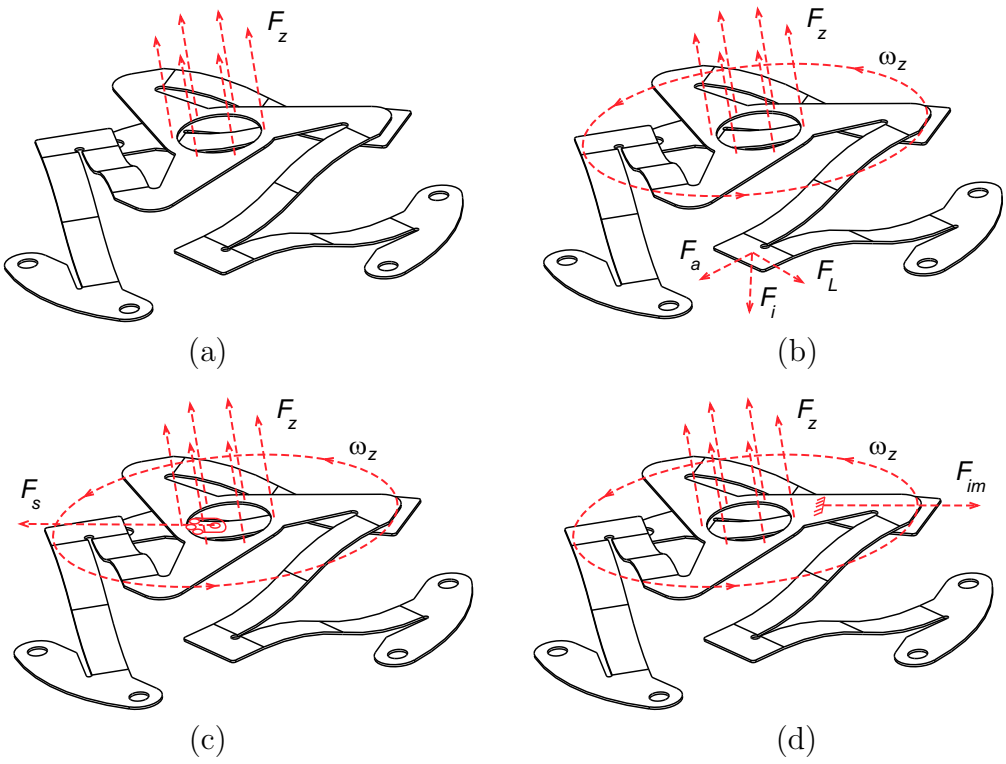

Figure 3.2: Identified load situations (a) orthogonal load (b) combined inertial and orthogonal load (c) lateral stationary load and (d) an imbalanced load.

3.3 COPS Loading

COPS design and analysis is dependent on the type of load situation. This section explores a number of the possible situations describing the loads and possible applications. The first four are derived from either existing applications or the possible load situations in a CVT while the rest are potential load situations.

3.3.1 CASE I: Orthogonal Loads

The type of load situation shown in Figure 3.2 (a) is the most fundamental. It is achieved by constraining the base and applying a load, F_z, to the platform orthogonal to the plane of fabrication. Applied loads may be either displacement or force. A COPS reaction force is the force that returns the platform to the in-line position after it has been displaced. The platform may be displaced to either side of

the base making a fully reversed loading condition possible. COPS subject only to orthogonal loads may be referred to as being under a static load.

3.3.2 CASE II: Combined Orthogonal and Inertial Loads

The addition of an angular velocity, ω_z, increases the load complexity experienced by a COPS. Refer to Figure 3.2 (b). It is really ω^2 which relates to inertial loads. As a mass rotates, its continual change in direction cause it to accelerate. For illustration purposes a single point load has been placed on one of the intermediate platforms. The inertial force can be broken into two components, an axial force, F_a, which creates tension in the leg segments counteracting F_z and a lateral force, F_L, which pulls the leg away from the platform. Holding the displacement, δ_z, constant an increase in angular velocity increases F_z. These components of inertial loading will be discussed shortly. Angular accelerations will also impact how the spring is loaded.

3.3.3 CASE III: Lateral Stationary Load

Figure 3.2 (c) shows combined loads with the addition of a stationary lateral load, F_s. This load may be caused by a shaft, through the center of the spring, which has a moment applied to it. This moment would cause the platform to rotate off axis. An example of this would be the CVT application where belt tension would create a load constant in direction but not necessarily constant in magnitude.

3.3.4 CASE IV: Imbalanced Load

Figure 3.2 (d) is similar to CASE II with the exception of an imbalance in the spring. This imbalance load, F_{im}, causes the spring platform to move out of its axis of rotation. An example may be a manufacturing defect or something such as grease adhering to the spring causing an imbalance.

3.3.5 CASE V: In-Plane Torsional Loads with Platform Rotation

Figure 3.3 shows a spring used for an application such as a drive coupler. The base is attached to one shaft and the other shaft would go through the center of

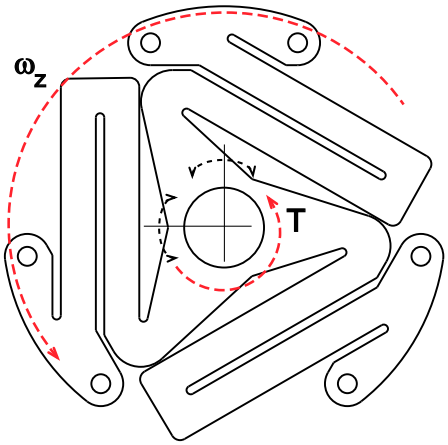

Figure 3.3: Lateral loads with platform rotation.

the platform. Both shafts rotate at the same speed but torque, T, would be transferred from one to the other. As the shafts rotate, the flexibility of the platform would allow compensation for misalignment. This type of a load situation would most likely use a different spring configuration than the one shown in the figure.

3.3.6 CASE VI: Six Degrees of Freedom, Platform

Refer to Figure 3.4 (a). This type of load would not fit in with the traditional applications other than it is quasi-static. Loads would fluctuate for a given region depending on the position of the platform-attached beam. An example of this type may be a joystick application. There may be a different spring style maximizing platform instability which would be ideal for a joystick type application.

3.3.7 CASE VII: Six Degrees of Freedom, Legs

Refer to Figure 3.4 (b). Another non-traditional load situation. Six degrees of freedom for each leg while the platform is fixed. Possible applications for this type of load situation are not yet known.

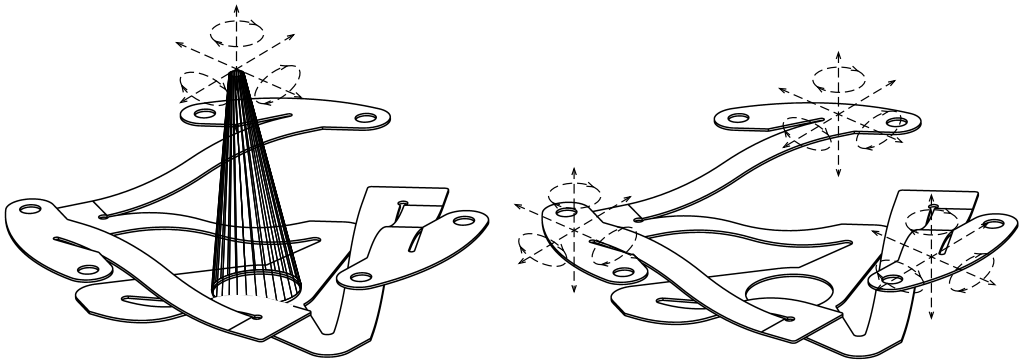

(a) (b)

Figure 3.4: Six degrees of freedom in (a) the platform and (b) in individual legs.

3.4 Inertial Load Components

The major focus in this research is on the interaction between leg angle and the inertial loads. A brief discussion of inertial loads will clarify why leg angle has such a significant effect on the performance of COPS.

Any rotating object will have a normal acceleration because of the change in direction as it rotates. Normal acceleration, a_n, depends on the square of the angular velocity, ω^2, and the distance from the center of rotation, r. Substituting that into the well known equation $F = ma$ results in

$$F = m\omega^2 r \tag{3.1}$$

This shows that there are three ways to influence the inertial load on a rotating object. First, the mass of the object can be altered by changing the volume or the material density. For a COPS leg this could entail changing the geometric parameters to alter the volume or by changing the material. Second, the angular velocity can be either decreased or increased resulting in a quadratic relationship to the inertial force. Third, the distance of the mass from the center of rotation may be altered. Figure 3.5 shows how the inertial loads and its components are altered as the leg angle and hence the distance of the mass to the center of rotation is changed.

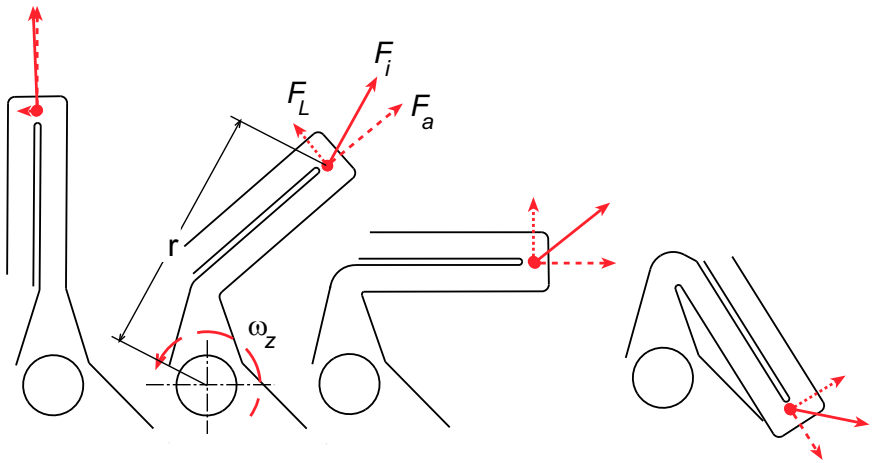

Figure 3.5: The two major components of inertial loads change in magnitude as the leg angle, ζ is changed.

For illustrative purposes the loads in Figure 3.5 are shown as point loads but in reality the load will be distributed throughout the COPS leg and the load magnitude will depend on the mass, distance from the center of rotation, and the angular velocity. From this Figure we can also see that for small leg angles, the axial force component is maximized and is fully utilized at $\zeta = 0$. The lateral force component is maximized somewhere between 60° and 135°. The axial component will be associated with stress stiffening of the leg segments and the lateral component will be associated with lateral buckling of the leg.

3.5 COPS Stresses

Although this research is not focused on understanding the nature of stresses in COPS, it is important to understand what stresses would occur from each type of load.

Bending stresses in COPS are caused by orthogonal loads, F_z and the lateral force component of the inertial loads, F_L. Bending stress from both loads will be the greatest at the ends of the leg segments near the base, intermediary platform or platform. Bending stress in the leg segments in the z direction will increase as

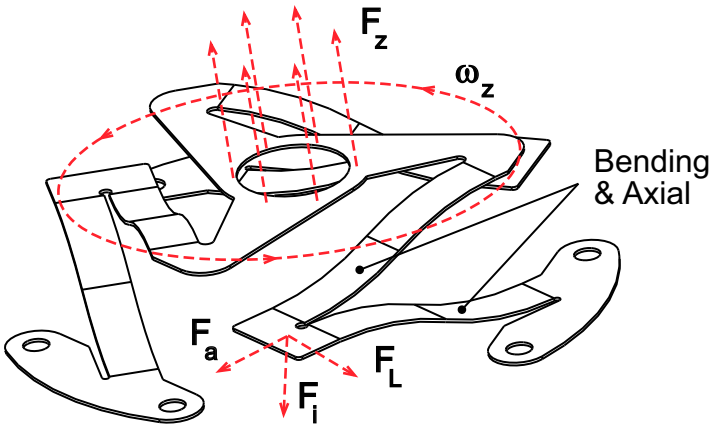

Figure 3.6: Bending and axial stresses in COPS.

orthogonal loads increase and in the lateral direction will increase with increased angular velocity and an increase in leg angle.

Axial stress may be present in leg segments when COPS are subject to inertial loads. Angular velocities and angular accelerations of COPS would cause either an increase or decrease in F_z creating tension or compression in the leg segments. The amount of axial stress will be highly dependent on the angular velocity, angular acceleration, and the leg angle. Axial stresses in leg segments will increase with an increase in angular velocity and small leg angles.

Torsional stress is a third type of stress that will be present in leg segments of COPS. As shown in Figure 3.7 (a), the eccentric nature of the leg design turns the intermediate platform into a moment arm which creates torsion along the leg segments. These stresses may be more prevalent in the 1-1 type than in other leg designs. Torsion may also be present in the intermediate platforms. Torsional stress in the leg segments will increase as r_{leg} increases. Torsion in the intermediate platform will increase with the orthogonal load.

Shear stress will be present near the transition geometry due to a tearing phenomena created by orthogonal loads. See Figure 3.7 (b). This type of stress will

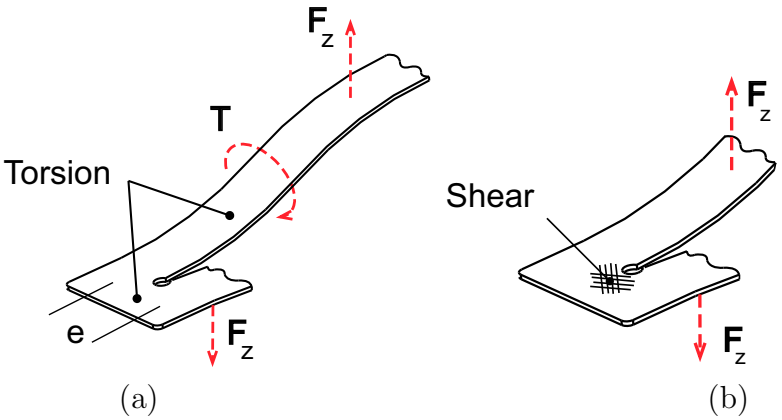

Figure 3.7: (a) Torsional stresses in leg segments and intermediate platform from eccentricity of 1-1 leg design (b) shear stresses in intermediate platform.

produce a stress concentration found at the transition radii. Shear stress increases with a decrease in r_{leg} and an increase in orthogonal loads.

This shear area in the intermediate platform has the highest stress while subject to only orthogonal loads. This stress concentration, with the tearing phenomena, will need to be better understood. An in depth study of stress concentrations will be left for future research. A short qualitative analysis of stress concentrations follows.

3.6 Stress Concentrations

The presence of stress concentrations in COPS will be one of the more challenging elements in their design. Stress concentrations in COPS have not previously been examined. The shear or tearing phenomena in the transition geometry may be an opportunity to create a new stress concentration table. There were no similar loading situations in any machine design books including Roark's [26].

In order to understand the stress concentrations like the one shown in Figure 3.8, it is important to understand what the stress flow looks like around a transition radii such as r_{leg}. For one side of the leg the stresses in one segment are highly compressive and in the other are tensile. As these two opposing stresses flow around the transition geometry they create a shear zone through the intermediate

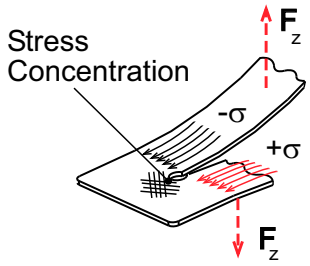

Figure 3.8: Shear stress in non-leg segment geometry creates stress concentrations.

platform. This stress flow tends to hug the transition geometry and the outer material in the intermediate platform is under utilized.

The approach taken to better understand the stress concentrations was to first see if a minor change in transition geometry would disrupt the stress flow and decrease the stress. A number of geometries were tried in order to disrupt the stress flow through the intermediate platform in an attempt to decrease stress. FEA was used to evaluate each type of geometry. All experimental design parameters were held constant while the transition geometry was changed. Only two geometry changes had a slight decrease in stress but it was not significant enough to separate it from model noise. The geometries which were experimented with can be seen in Figure 3.9. Although some geometry configurations may have appeared to compromise other aspects of COPS designs such as the force output, they were ignored.

Because no simple change in geometry decreased the stress concentration the only other option was to increase r_{leg}. One thing to note about making r_{leg} larger is that this will increase the mass of the intermediate platform. Inertial loads will then have a greater affect on the leg which may increase the stresses at the base and platform transition radii and make lateral buckling more probable.

While stresses are very important in designing a COPS for adequate fatigue life, especially for rotational applications, they have been left for future research when simplified methods for predicting forces are better understood. The final word on stress concentrations is that they should be considered by the designer.

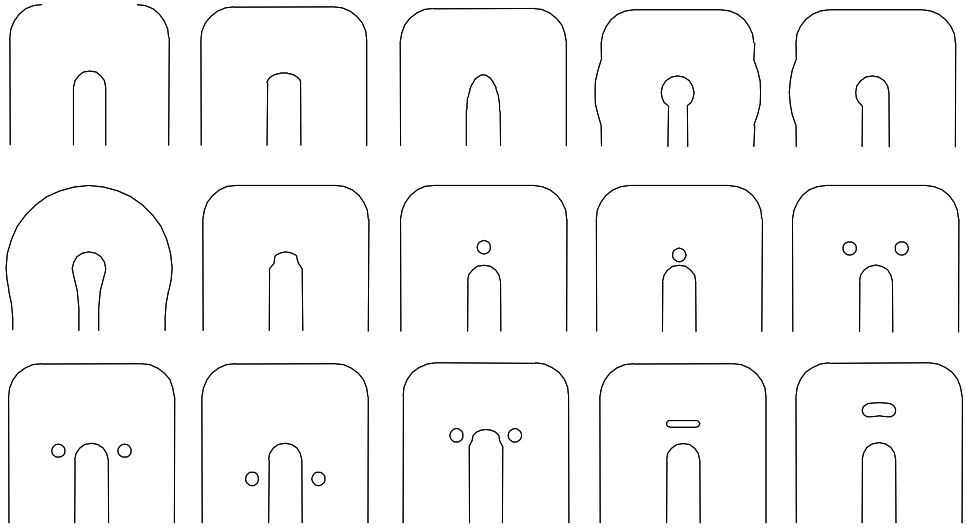

Figure 3.9: Transition geometry changes investigated to decrease stress.

3.7 Analysis Tools

Parise's [3] discussion and analysis was centered on understanding some of the fundamental relationships between spring parameters for static applications and to qualitatively evaluate issues such as stability. His prototype COPS were made of polypropylene and were fabricated with the use of a milling machine. Doing this allowed him to maintain rigid ends for each segment by leaving the platform, intermediate platform, and base as thick as the original stock. By building the boundary conditions into the prototypes, the ability to accurately model them with a PRBM for fixed-guided segments was maintained. While a non-uniform thick spring design was useful for a qualitative study it would not be the best applicant for high volume manufacturing. This notion is confirmed by the case study presented in [3] where a COPS was designed and manufactured from a single thin sheet of metal for an industrial valve control. A thin sheet COPS design has the advantages of being easily manufactured and can easily be stacked while a non-uniform thick COPS design forfeits these advantages.

Traditionally, research on ortho-planar springs has used the PRBM for fixed-guided segments as a simple design tool for predicting force and stress under orthogonal loads. The problem in applying the PRBM to fixed-guided leg segments in thin

sheet COPS is that the boundary conditions are not met. These boundary conditions are semi-rigid end end effects on leg segment ends, high axial loads, and distributed inertial loads.

First, the semi-rigid effects in the base, platform, and intermediate platform add additional flexibility to the ends of a leg segment. This challenges the assumption of infinite rigidity attachment at the ends.

The other fundamental assumption of the PRBM for fixed-guided segments is that the segment remains in a single plane. As inertial loads are applied to a COPS design, lateral loads on legs may cause bending to occur out of that plane.

In the case of a radial design, lateral loads will be minimal but the amount of stress stiffening seen in the legs may be large enough to cause a problem if there are high negative load factors where $n < 0$. This load factor is inversely proportional to the inertial loads which cause stress stiffening or negative load factors. As the inertial forces increase the constraint on Θ_{max} decreases. Accuracy becomes an issue for pseudo-rigid-body angles greater than Θ_{max}.

One other condition which will have to be researched is a PRBM for distributed loads. The inertial loads for a COPS cannot easily be reduced to point loads on the ends of the segments or into convenient lumps of mass for simplified analysis.

Even though there are many obstacles for developing a PRBM suitable for analyzing a rotating COPS, an initial foray investigating the feasibility of a 3-dimensional PRBM will be done. Until new PRBM's are developed, finite element analysis will be the best way to analyze loads, stresses, and behavior of COPS designs under complex load situation.

Chapter 4

3D Pseudo-Rigid-Body Model

4.1 Introduction to 3D PRBM

Because the PRBM has been a very effective analysis tool for compliant mechanisms, an investigation of a 3D PRBM for analyzing the complex loads a COPS leg segment might be subject to is a natural compliment to understanding COPS for rotational applications. As discussed previously, a COPS leg may experience deflections in multiple directions.

The key assumption upon which all PRBM's are based is that a near-circular path is followed by some part of the geometry on the mechanism - usually the end of a flexible segment. These PRBM's assume that the mechanism deflection is constrained within a single plane and that all axis of rotation are parallel to one another and orthogonal to the plane in which motion occurs. This motion will be referred to as 2D.

A 3D PRBM models deflections of beams that occur in 3D space where the two principle axes of rotation are orthogonal to one another and motion does not occur in a single plane. Flexible segments in COPS generally have cross-sections with large aspect ratios, (AR). An aspect ratio is the cross-section width divided by the thickness. As a starting point, a beam with a circular cross section deflected in 3D could easily be transformed into a 2D PRBM through a transformation of the coordinate system. A circular cross-section would then be a trivial case where there is no variation in the flexural rigidity between the y and z axes. In addition, the free end of the beam would

always follow a near-circular path. This being the case, its clear that a circular cross-section beam tip would follow a spherical shell within some specified limit. The investigation of interest then becomes that of non-circular cross-section beams. How closely do they follow a spherical shell when deflected in more than a single direction? What are the limits for each aspect ratio (AR)?

This chapter explores the possibility of deriving a 3D PRBM for non-follower, end loaded, rectangular cross-section cantilever beams. Building on what has previously been done in the field, a 3D PRBM will be based on the hypothesis that a beam end deflected about two orthogonal principle axes will follow a near-spherical shell.

4.2 Model Setup

Table 4.1: Nomenclature for 3D PRBM investigation.

Parameter	Description
L	Compliant beam length.
t_z	Beam width.
t_y	Beam thickness.
AR	Aspect ratio $\frac{t_z}{t_y}$ of the beam cross-section
γ	Characteristic length factor.
Θ	Angle deflection around the w axis.
Φ	Angle deflection around the v' axis.
Ψ	Torsional angle about the beam.
(x_i, y_i, z_i)	ANSYS beam tip data
(x, y, z)	Theoretical spherical shell.
(x_c, y_c, z_c)	Characteristic pivot location.
δ_y	nondimensional Y displacement.
δ_z	nondimensional Z displacement.

Figure 4.1 (a) shows a schematic for a rectangular compliant beam used in the FEA model. The beam is setup in a Cartesian coordinate system. The beam cross-section orientation is chosen such that the beam thickness is in the y direction

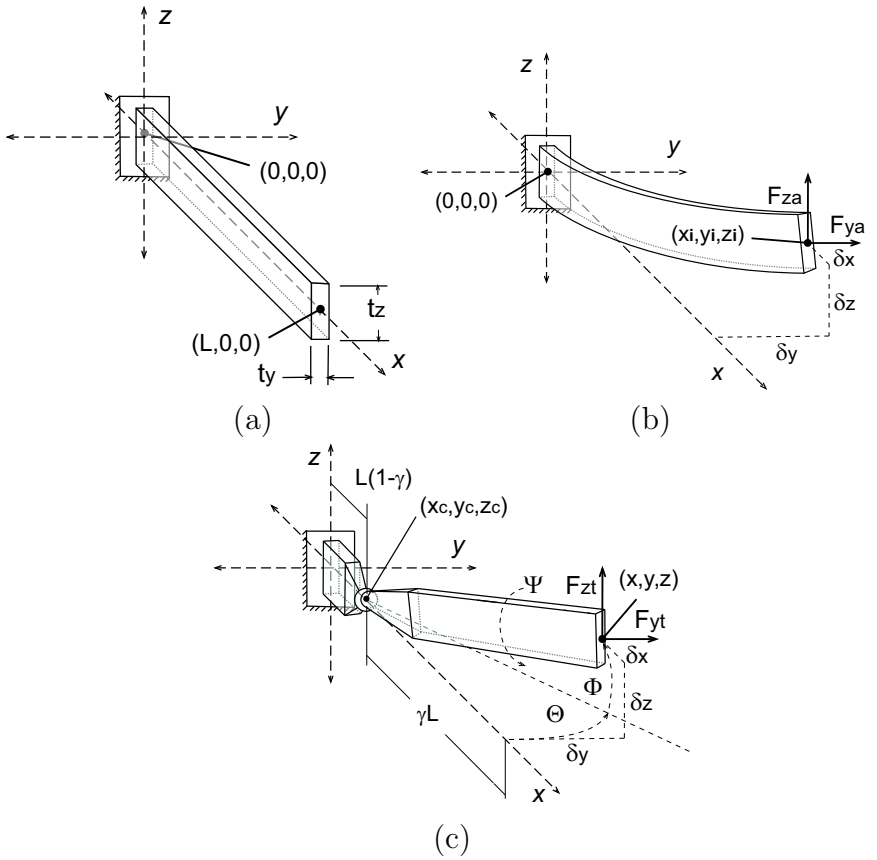

Figure 4.1: (a) Compliant cantilever beam setup (b) deflected beam (c) and 3D pseudo-rigid-body model replacement of beam with a spherical joint.

and the beam width is in the z. The aspect ratio of the beam is a significant factor and will be one of the key nondimensional parameters upon which the model is based.

Figure 4.1 (b) shows the beam deflected due to an applied vertical and horizontal end load. A cartesian coordinate system is used for specifying the displacement loads to create radial deflection paths. The load conditions are such that a displacement is placed orthogonal to the beam tip in both the y and z directions. The free end of the beam moves as if there were a spherical joint on the beam tip to which the loads are applied yet allows the beam tip to rotate freely. There are no applied moments or follower loads to the beam tip but as the beam is deflected about multiple axes, the end twists due to the aspect ratio and there is a resultant moment. The location of the

deflected beam tip is specified as (x_i, y_i, z_i). Inputs into the FEA model are y_i and z_i whereas x_i is an output.

Figure 4.1 (c) shows a replacement of the compliant beam in (b) with rigid-body components such as links, joints, and springs. Because the model is based on the beam tip following a near-spherical shell, spherical coordinates will be used. The characteristic length factor, γ, will heavily influence sizing of the rigid-body components. The characteristic pivot, located at (x_c, y_c, z_c) is the center of the spherical shell. The angles Θ and Φ are associated with the displacement of the beam tip in the y and z directions and originate from the characteristic pivot. Ψ accounts for the rotation in the beam tip as it is deflected. Analysis of the key components for this model will be discussed in the next sections.

Because the path of the beam tip is a near-spherical shell, all that is needed to describe it is a radius and the location of the sphere center. Gamma is an important nondimensional parameter used to determine the rigid link length, γL, and the location of the characteristic pivot, $L(1-\gamma)$. The determination of γ is the key to developing the 3D PRBM.

Once γ has been selected for a particular model, the PRBM components can be developed and used for analysis. The characteristic pivot is located on the x-axis and in order for it to lie at the center of the beam cross section, y_c and z_c are set to zero. It is at this location that joints and torsional springs will be located.

There are several options for setting up the three degrees of freedom for this particular model. The use of a single spherical joint or three revolute joints were evaluated. The revolute joints make the most sense for a model predicting both deflection and force because torsional spring constants are more easily equated to a respective joint. A spherical joint provides another solution although it is not as simple to equate three torsional springs to a single joint. There may yet be a spring element developed which would resist in all three directions. This spring might be called a global or spherical spring. A spherical joint does however provide a simple solution to deflection alone because spherical coordinates can be used with it. Because this research is mainly focused on predicting displacements, a spherical joint will be used.

The reason accurately modeling the three DOF's is important is because they will play a key role in calculating the forces. Although force prediction is not the main focus of this portion of the research, recommendations for research on predicting the force will be presented later.

4.2.1 FEA Setup

The FEA model used 20 node solid elements for all experiments. Inputs into the model were beam dimensions and the displacement load in the y and z directions. Model outputs were deflection in the x direction and forces in the y and z directions. An ANSYS script file for this model is in Appendix C.1. ANSYS was driven by MatLab to facilitate large batches of runs. A typical MatLab script for these design simulations can be found in Appendix D.2.

Mesh density was analyzed and an adequate density for these types of experiments was established. Beam elements with a cross-section type were also tested but were found to show discrepancies in the force output compared with the solid elements. These simulations also showed that deflection remained within 0.25% accuracy between all element types and mesh densities but the force varied by as much as 35%. Solid elements were used so output could be reused in a study to derive the force prediction equations.

4.3 Model Derivation

The derivation of γ begins by selecting beam geometry and the limits of deflection. These limits are δ_y and δ_z and are non-dimensionalized through division by the beam length, L. For an acceptable magnitude of error in the deflection, bending in the direction of greater flexural rigidity will have a smaller deflection limit while the direction of lesser flexural rigidity will have a larger deflection limit. In the following section two sets of boundaries are presented; first, the nondimensional deflection limits for the y and z directions are set equal to each other and second, the limit in the z direction is set to equal half the limit in the y direction.

Because of symmetry, the model only needs to be evaluated for a quarter of the quadrant in the yz plane. The quadrant is divided up into a number of vectors separated by equal angles. Their respective lengths, l_i, are established as a function of the angle and the nondimensional deflection limits. Vector length is determined by

$$l_i(\theta, \delta_y, \delta_z) = \sqrt{\left[\left(\frac{cos\theta}{\delta_y}\right)^2 + \left(\frac{sin\theta}{\delta_z}\right)^2\right]^{-1}} \tag{4.1}$$

This allows the deflection limits to be specified by either a circle or ellipse. An elliptical section of the spherical shell will be advantageous because it is possible to get a larger area of deflection for the same amount of error. This will be more apparent after reading the next section.

The FEA model evaluates a specified number of points along each vector and records the output for each distinct set of inputs. From the radial contours shown in Figure 4.2 a regression model was setup to determine a γ which minimizes the error between the collected beam end location and a theoretical spherical shell. The following regression model parallels that found in Wittwer *et al.* [27]. Figure 4.2 shows a visual representation of the beam end location and the spherical shell.

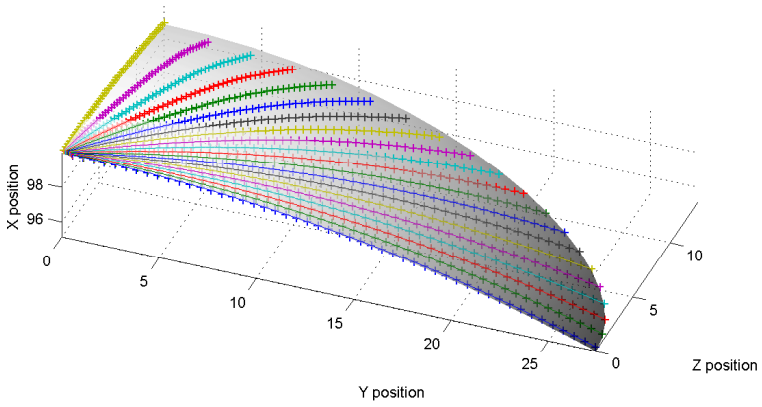

Figure 4.2: The theoretical spherical shell (surface) and beam end locations (points).

The theoretical spherical shell and the actual shell traced by the beam end locations are represented by

$$r_t{}^2 = (x - x_c)^2 + (y - y_c)^2 + (z - z_c)^2 \tag{4.2}$$

$$r_a{}^2 = (x_i - x_c)^2 + (y_i - y_c)^2 + (z_i - z_c)^2 \tag{4.3}$$

where r_t is the radius of the theoretical shell and r_a is the distance from the characteristic pivot location to the actual beam tip location found through FEA. If the right side of each equation is set equal to one another and if we desire the characteristic pivot to lie at the center of the beam cross section, where y_c and z_c both equal zero, the result is

$$\frac{x^2 - x_i^2 + y^2 - y_i^2 + z^2 - z_i^2}{2} = x_c(x - x_i) \tag{4.4}$$

In this form, x_c, or the distance from the origin to the characteristic pivot can easily be solved using polynomial regression where x_c is the regression coefficient. Equation 4.4 is represented as

$$\mathbf{v} = b\mathbf{u} \tag{4.5}$$

where

$$\mathbf{v} = \frac{x^2 - x_i^2 + y^2 - y_i^2 + z^2 - z_i^2}{2}$$

$$\mathbf{u} = (x - x_i)$$

$$b = x_c \tag{4.6}$$

and can be solved using the following approach

$$b = (\mathbf{u}^T\mathbf{u})^{-1}\mathbf{u}^T\mathbf{v} \tag{4.7}$$

With x_c known, the characteristic length factor, γ, can be found by

$$\gamma = 1 - \frac{x_c}{L} \tag{4.8}$$

The radius of the theoretical shell is equal to γL and will be such that the error between the beam tip data and the fitted shell is minimized. The equation for the theoretical shell then becomes

$$(\gamma L)^2 = (\delta x)^2 + (\delta y)^2 + (\delta z)^2 \tag{4.9}$$

where $r_t = \gamma L$.

The deflection prediction is a simple calculation when γ is known. Rearranging Equation 4.9 and adding x_c gives the theoretical x coordinate for any given y and z displacement and is represented by

$$x = \sqrt{(\gamma L)^2 - (\delta y)^2 - (\delta z)^2} + x_c \tag{4.10}$$

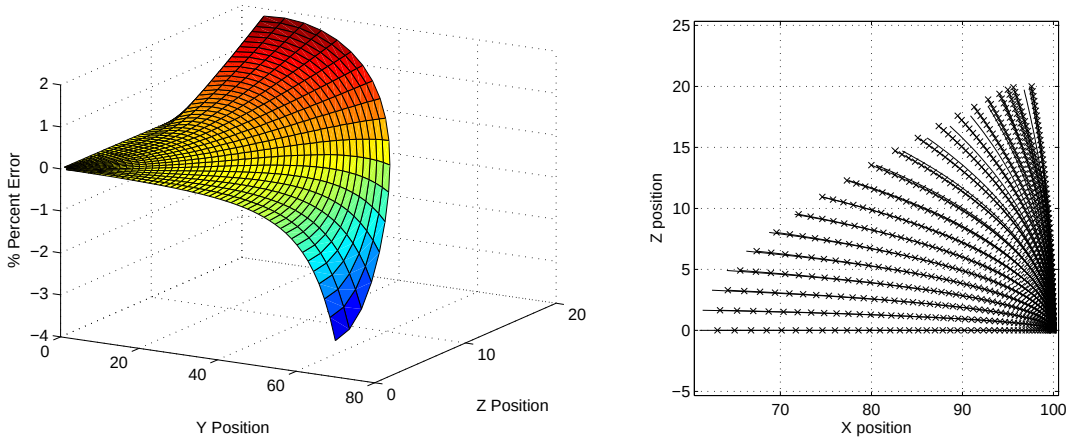

(a) (b)

Figure 4.3: Graph (a) shows the error between the two sets of data in the x direction and (b) shows that deflections mostly in the direction of greatest flexural rigidity, z, are instable.

Nondimensionalized parameters in Tables 4.2 and 4.3 should be used for specific beam geometries.

The error between the PRBM and beam end location data then becomes

$$\epsilon_i = 100 \cdot \frac{x - x_i}{x_i} \tag{4.11}$$

This error could be plotted against deflections in the y and z directions for a visual representation of the deviations between the theoretical shell and the deflected beam end locations. Figure 4.3 (a) shows the percent error, ϵ_i, in the x direction between the two surfaces. Note that contours along the outer edge result in the largest errors.

A more accurate method for quantifying the error would be the difference normal to the surfaces. Although this would be more accurate, the outlined method is a simpler and more conservative method for representing the deflection error.

One other thing to notice in Figure 4.3 is that there is a degree of instability when the beam is deflected in the plane of greatest flexural rigidity. As the deflection increases, the beam cross-section twists in order to compensate for the difference in flexural rigidity between the two directions. Twisting in the beam allows it to reach an equilibrium state [19]. Figure 4.4 shows a typical beam from an FEA simulation as an example of how the beam end rotates an angle, Ψ to find equilibrium.

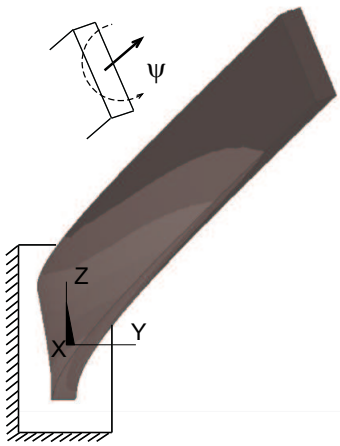

Figure 4.4: The beam end rotates as it is deflected around two orthogonal cross-section axis with different flexural rigidity.

Beam end rotation is caused by the difference in flexural rigidity between the two planes of symmetry in the cross-section. Beam twisting increases proportional to AR and does not significantly effect the ability to predict beam tip location but it does present challenges for accurately predicting the forces at the beam tip.

4.4 Model Limits

The deflection limits influence the value of γ and are uniquely associated to a specific aspect ratio (AR). As the aspect ratio becomes larger so does the deflection error for a given set of limits. Because of the interdependency between the AR and

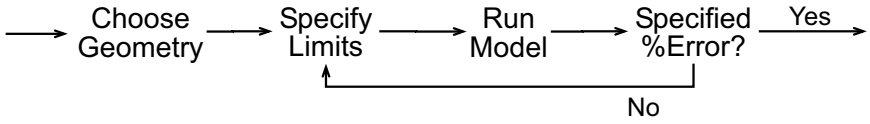

Figure 4.5: Model for calculating nondimensional parameters in Tables 4.2 and 4.3.

deflection limits, it is necessary to choose deflection limits for a specific AR that result in a specified percent error. This process is iterative as shown in Figure 4.5.

To some extent, the deflection error is dependent on the product of inertia. The product of inertia is a result of uneven flexural rigidity in the two directions. This difference in flexural rigidity is better described by the square of the aspect ratio, AR^2, which results from dividing I_z by I_y. Both deflection limits and γ are represented as functions of AR^2. Each set of limits for any given AR will have a unique solution for fitting a spherical shell. This unique solution will have its own particular γ which in turn will influence the rest of the model.

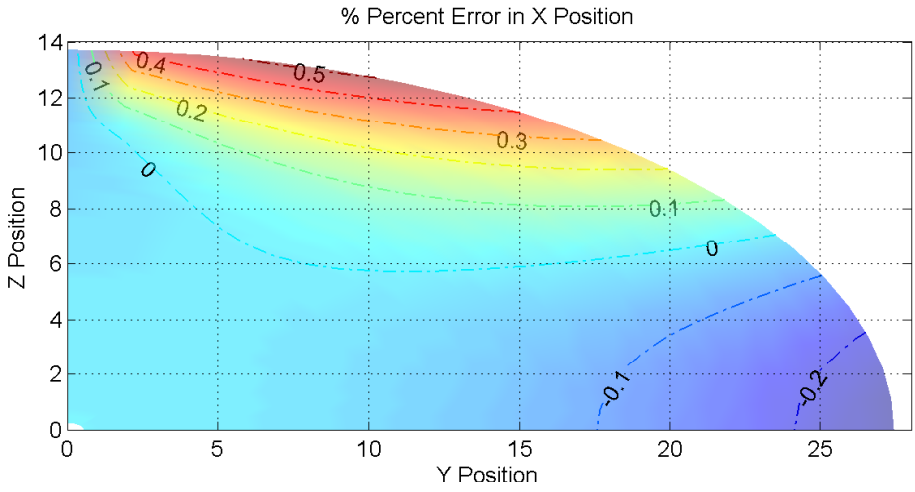

Figure 4.6: %Error contours for $AR = 5$. Note that 0.5% is the maximum.

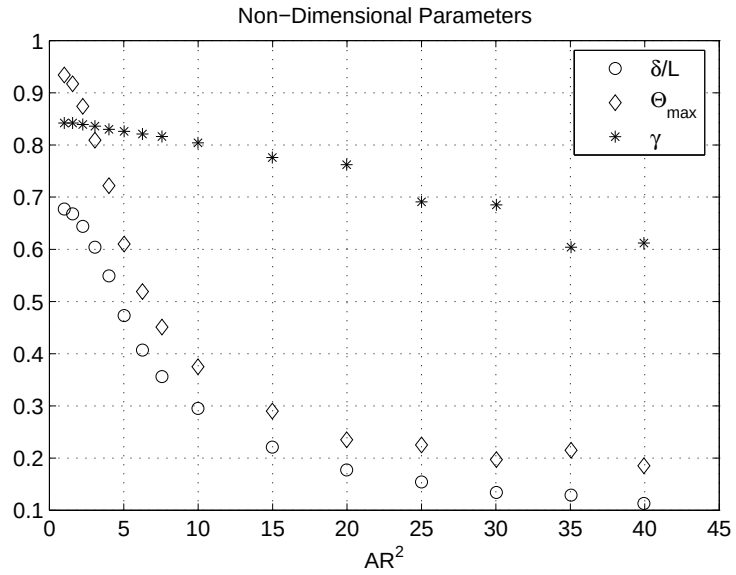

Figure 4.7: Gammas and deflection limits for an error of 0.5% where $\frac{\delta_y}{L} = \frac{\delta_z}{L}$.

Each AR produces a unique error field because of the variation in flexural rigidity. Any effort to maximize the deflection limits for an AR based soley upon a fixed error would not be effective because there are multiple solutions. For example, both sets of results in Tables 4.2 and 4.3 are for an approximate error of 0.5% yet the limit boundaries are different for any given AR. Figure 4.6 shows the % error in deflection for a beam with an $AR = 5$ and $L = 100$ mm, and deflection limits described by Table 4.3. Note that the maximum error in the figure is 0.5%.

Two sets of data were generated: one where $\frac{\delta_y}{L} = \frac{\delta_z}{L}$ and the other where $\frac{\delta_y}{L} = 2\frac{\delta_z}{L}$. Both sets had a target error of 0.5%. An optimization routine was set up and each AR was used to determine the deflection limits that would achieve the desired accuracy. Figure 4.7 shows a graphical representation of the nondimensional parameters as a function of AR^2. Table 4.2 shows a list of AR's with their nondimensional parameters. AR as opposed to AR^2 is used in the tables for convenience. Figure 4.8 and Table 4.3 provide the second set of limits.

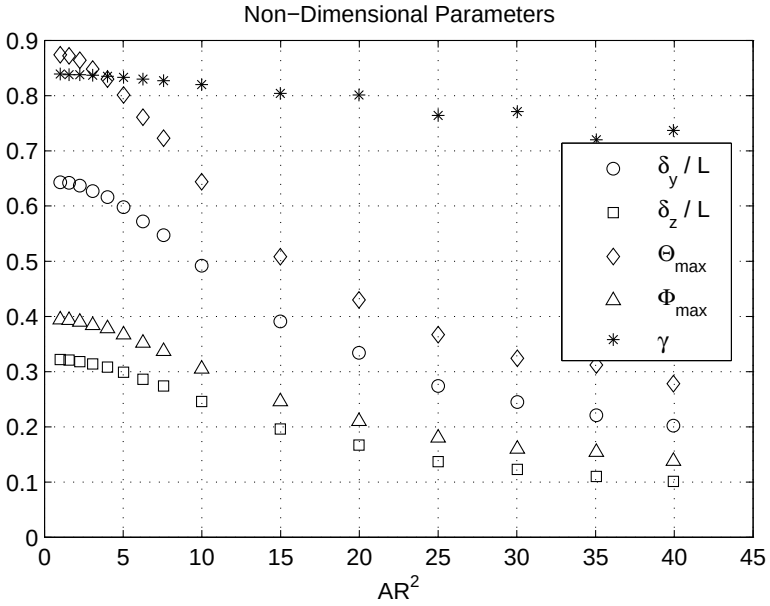

Figure 4.8: Gammas and deflection limits for an error of 0.5% where $\frac{\delta_y}{L} = 2\frac{\delta_z}{L}$.

One thing to note in Figures 4.7 and 4.8 is that for an AR^2 of 1, γ is approximately 0.85 which corresponds well with the γ's of 2D pseudo-rigid-body models. As the AR^2 increases both γ and the deflection limits decrease.

In order to test the results of this study several ARs (with their respective parameters) were simulated to validate the resulting error of 0.5%. Table 4.4 and 4.5 show the results as recorded. All calculated γ's and ϵ_{max} were reasonably close to those calculated previously.

Another analysis was performed to check the accuracy based on the length of the beam and the non-dimensional limits. Table 4.6 contains the results. The error, ϵ_{max}, was somewhat dependent on beam length but is still fairly accurate. The calculated γ was also fairly accurate for all beam lengths tested. Although this test is just a snapshot of the error associated with changing the beam length for a single set of geometry, it does provide insight on the accuracy of the model.

Table 4.2: Nondimensional parameters for $\frac{\delta_y}{L} = \frac{\delta_z}{L}$ and 0.5% error.

AR	$\frac{\delta}{L}$	Θ_{max}, Φ_{max}	γ
1.00	0.677	0.934	0.842
1.25	0.667	0.917	0.842
1.50	0.644	0.874	0.839
1.75	0.604	0.809	0.836
2.00	0.549	0.722	0.830
2.24	0.473	0.610	0.826
2.50	0.407	0.519	0.821
2.75	0.356	0.451	0.816
3.16	0.295	0.375	0.804
3.87	0.221	0.290	0.776
4.47	0.177	0.235	0.762
5.00	0.154	0.225	0.691
5.48	0.134	0.197	0.685
5.92	0.129	0.215	0.604
6.32	0.113	0.185	0.612
6.71	0.106	0.185	0.578

4.5 Conclusions

This investigation proves that a rectangular cross-section beam tip does follow a near-spherical path for the specified load conditions and within the specified limits. The key parameter of the 3D PRBM, γ, is dependent upon the deflection limits and the aspect ratio of the cross-section of the beam. For a given aspect ratio, a γ was recommended along with the deflection limits for a position prediction with an error of approximately 0.5%. 3D path prediction of a rectangular cross-sectioned beam end is possible with the use of this 3D PRBM under the specified load conditions.

Although a 3D PRBM was derived, the direct applicability of this model to the movements in a COPS leg is rather limited for several reasons. First, the geometric boundary conditions for the 3D PRBM model and a COPS leg segment are incompatible as shown in Figure 4.9. In a COPS leg, deflection from an orthogonal load, F_z, induces a fixed guided motion while deflection from inertial loads, F_L, produces motion like that of a cantilever beam. This research investigated only the motion that

Table 4.3: Nondimensional parameters for $\frac{\delta_y}{L} = 2\frac{\delta_z}{L}$ and 0.5% error.

AR	$\frac{\delta_y}{L}$	$\frac{\delta_z}{L}$	Θ_{max}	Φ_{max}	γ
1.00	0.643	0.322	0.874	0.394	0.839
1.25	0.642	0.321	0.872	0.393	0.838
1.50	0.637	0.318	0.864	0.390	0.838
1.75	0.627	0.314	0.848	0.384	0.837
2.00	0.616	0.308	0.830	0.378	0.835
2.24	0.598	0.299	0.801	0.367	0.833
2.50	0.572	0.286	0.761	0.352	0.830
2.75	0.547	0.274	0.723	0.337	0.827
3.16	0.492	0.246	0.644	0.305	0.820
3.87	0.391	0.196	0.508	0.246	0.804
4.47	0.334	0.167	0.430	0.210	0.801
5.00	0.274	0.137	0.367	0.180	0.764
5.48	0.245	0.123	0.324	0.160	0.771
5.92	0.221	0.110	0.312	0.154	0.720
6.32	0.202	0.101	0.278	0.138	0.737
6.71	0.178	0.095	0.254	0.134	0.708

a simple cantilever beam would experience. A COPS leg is not a simple beam but has two attached beams, leg segments, in parallel which further complicates the analysis.

Second, the derived 3D PRBM is for point loads applied at the end of a cantilever beam. A COPS leg has a mix of loading conditions. Deflections from orthogonal loads are essentially applied at a point or at the ends of the leg segments. However, lateral deflections are a result from the lateral component of the inertial load which is a distributed load condition as shown in Figure 4.10. Distributed loads on the COPS legs cannot easily be transformed into point loads at the end of the intermediate platform because of the many parameters which effect the load distribution.

Third, because of its simple load condition, this 3D PRBM makes no concession for stress stiffening and relaxing like many of the 2D PRBM's do. The axial component of the distributed inertial loads must be accounted for concurrent with the lateral component of which the 3D PRBM is attempting to analyze.

Table 4.4: Results from testing select AR's and their limits for $\frac{\delta_y}{L} = \frac{\delta_z}{L}$.

AR	$\frac{\delta}{L}$	Calculated γ	ϵ_{max}
1.00	0.677	0.842	0.533%
2.00	0.549	0.830	0.508%
2.75	0.356	0.817	0.450%
5.00	0.154	0.710	0.529%
6.32	0.113	0.592	0.474%

Table 4.5: Results from testing select AR's and their limits for $\frac{\delta_y}{L} = 2\frac{\delta_z}{L}$.

AR	$\frac{\delta_y}{L}$	$\frac{\delta_z}{L}$	Calculated γ	ϵ_{max}
1.00	0.643	0.322	0.839	0.454%
2.00	0.616	0.308	0.836	0.441%
2.50	0.572	0.286	0.832	0.417%
3.16	0.492	0.246	0.824	0.492%
5.00	0.274	0.137	0.792	0.513%

Fourth, a thin-sheet COPS subject to an angular velocity will have the challenge of semi-rigid attachments at the leg segment ends. This semi-rigidness of the leg segment ends does not comply with the boundary condition of infinitely-rigid ends assumed by the 3D pseudo-rigid-body model.

This particular 3D pseudo-rigid-body model may also be used for the analysis of other compliant mechanisms which do comply with the boundary conditions. Even though there is little applicability to analyzing COPS for rotational systems with this 3D PRBM, this research provides a starting point for the derivation of many more 3D PRBM's, some of which may be more applicable to this type of problem in the future.

Table 4.6: Sensitivity to L for $t_y = 2$, $AR = 5$, $\frac{\delta}{L} = 0.15394$, and $\gamma = 0.710$.

L	γ	ϵ_{max}
70	0.713	0.490%
100	0.710	0.529%
130	0.706	0.537%
150	0.705	0.539%
200	0.704	0.543%
250	0.703	0.544%

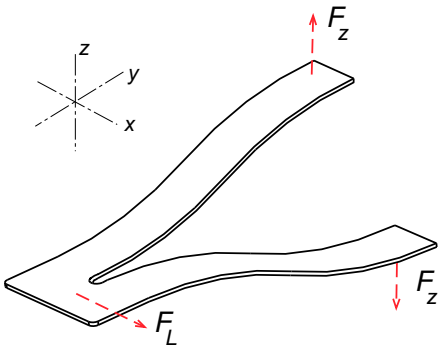

Figure 4.9: The geometric boundary conditions of the 3D pseudo-rigid-body model and a COPS leg are incompatible.

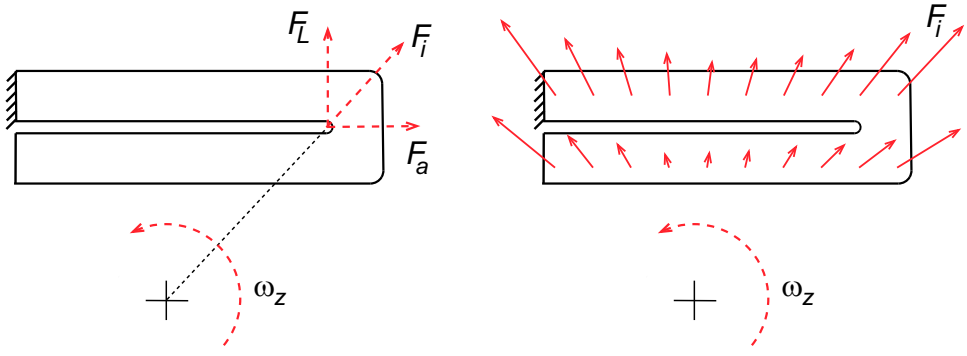

Figure 4.10: The distributed loading condition from an inertial load is different from the point load condition of the 3D pseudo-rigid-body model.

Chapter 5

Thin Sheet COPS - Orthogonal Loads

The objective of this chapter is to present the effects of semi-rigid ends on the force output of a COPS in an orthogonal loading condition. The two main parameters which may affect how the intermediate platform behaves are the transition radius, r_{leg}, and the intermediate platform width, w_{ip}. Both of these parameters may influence the rigidity of the intermediate platform. A better understanding of how each parameter affects the reaction force in an orthogonal loading condition may provide a foundation for understanding how to predict the reaction force for a COPS subjected to inertial loads.

Because the 3D pseudo-rigid-body model cannot be directly applied to the analysis of COPS subject to rotation and because there are no other simple analysis tools to use we turn to more complicated methods of analysis. Finite element analysis will be used to better understand how the reaction force due to orthogonal loads is effected by the design parameters. The finite element model setup will be discussed followed by a study on the effects of two design parameters on semi-rigidity in the intermediate platform and then a more general study of the relationship and sensitivity of the reaction force to each parameter.

5.1 FEA Model Setup

A parametric model of a COPS leg was created using ANSYS parametric design language (APDL). Doing this allowed for quickly changing COPS configurations within the specified model boundaries outlined in Chapter 3. For convenience

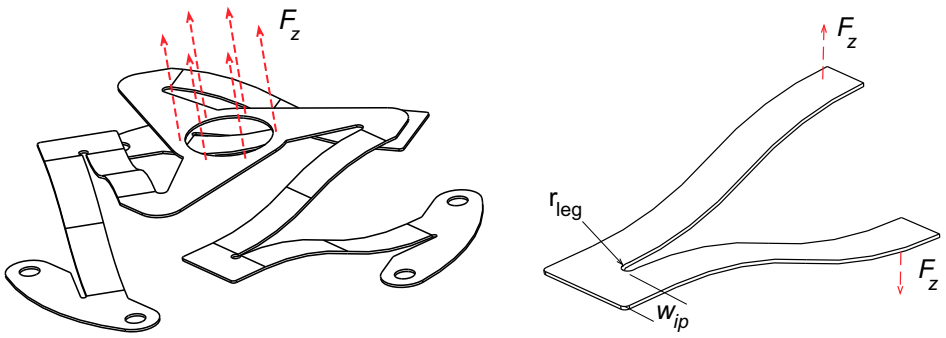

(a) (b)

Figure 5.1: (a) Static loading conditions (b) and the two parameters which influence the semi-rigid effects.

Table 3.1 and Figure 3.1 describing model parameters are reproduced here. All deterministic computer simulations of a COPS leg using FEA were accomplished with the same parametric model.

All nodes on the free end (base) farthest from the center of rotation are constrained in all degrees of freedom. The nodes on the other free end (platform) are also constrained to zero displacement in the x and y directions and zero rotation about x and y, however it is allowed to rotate about the z axis. This end also has a point in the center which is used for applying displacement loads in the z direction. It is from this same point that the reaction force in the z direction is recorded.

The two element types investigated for the FEA model were SOLID186 and SHELL181. ANSYS literature recommended 18x elements for nonlinear large deflection analysis. A comparison of the two elements was performed to check accuracy. Although there was a large disparity, of approximately 35% between the stress levels for the two different types of elements, the difference in force in the z direction was within .26%. The run time difference between the solid and shell elements was significant with the solid element model taking approximately two hours while the shell element

Table 5.1: Baseline COPS nominal dimensions and ranges defining the design space.

Parameters	Nominal (in)	Range (in)	Nominal (mm)	Range (mm)
t	0.02	± 0.012	0.508	± 0.305
w_{leg}	0.50	± 0.125	12.7	± 3.175
L	2.75	± 0.25	69.85	± 6.35
r_{leg}	0.09375	± 0.03125	2.381	± 0.794
r_{plat}	2.0	± 0.50	50.8	± 12.7
ζ	67.5°	$\pm 67.5^\circ$	$\frac{3\pi}{8} rad$	$\pm \frac{3\pi}{8} rad$
δ_z	low $\rightarrow$	3% of L	high $\rightarrow$	30% of L
ω_z	low $\rightarrow$	$0 \frac{rad}{sec}$	high $\rightarrow$	$650 \frac{rad}{sec}$

model took around 40 seconds. With the very minor discrepancy in resulting force between the two elements, the large gap in run time, and because stresses are not a major focus of this thesis, shell elements were chosen over solid elements for all simulations.

When using SHELL181 elements there are a few recommendations by ANSYS. First, degenerate elements are not recommended for non-linear analysis therefor the element type control, or ETCONTROL, was turned to off. Second, the equation predictor, or PRED, in the solution control panel was also turned off or set to 0 as recommended. Third, for analysis with a single thin layer of elements it was recommended that full integration with incompatible modes, KEYOPT(3)=2, be used for nonlinear problems involving large rotations and in-plane bending.

Mesh density for all COPS legs was driven by the leg width, w_{leg}. The area around the transition radii had a much denser mesh than the legs for accuracy. A typical meshed leg can be seen in Figure 5.3

Appendix C.2 shows the parametric ANSYS script used for most simulations. Only minor variations were made for some of the experiments in order to collect different data. Matlab was used for its ability to automate ANSYS. Figure 5.4 shows a schematic of how MatLab and ANSYS were set up to communicate with each other. The heart of the communication is in the EVAL file, Appendix D.1, which was created

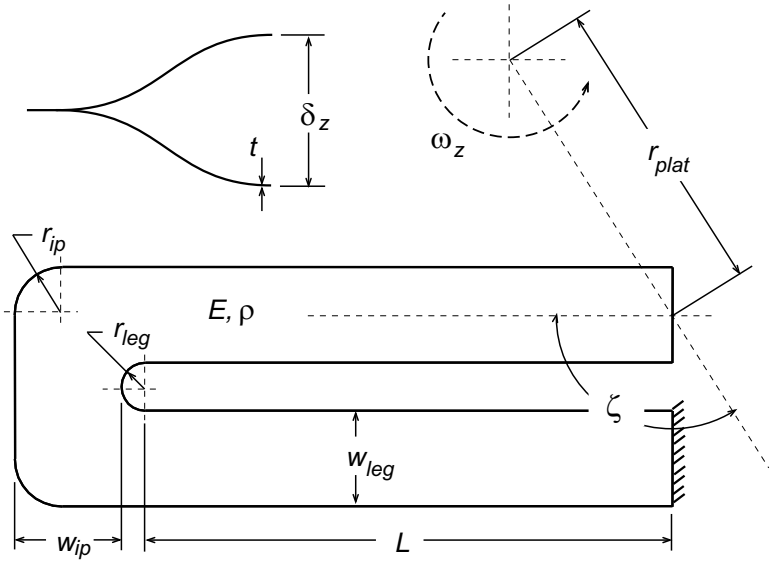

Figure 5.2: Design parameters for experiments.

by Jon Wittwer and modified for this research. Matlab script files were created for each simulation and can be found in Appendix D.

5.2 Analysis of r_{leg} and w_{ip} Under Orthogonal Loads

For an orthogonal load situation not all design parameters influence the reaction force. Leg angle, ζ, material density, ρ, and platform radius, r_{plat} will not significantly impact the force output in static load situations. For a full COPS,

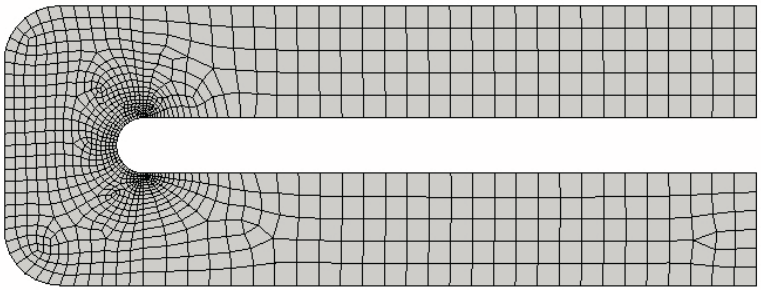

Figure 5.3: Typical meshed COPS leg used in simulations.

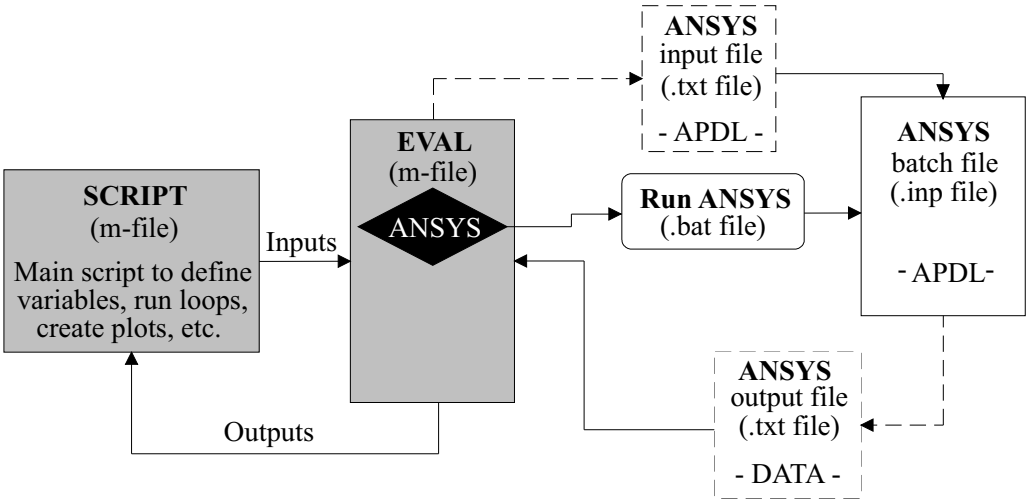

Figure 5.4: Communication between MatLab and ANSYS.

ζ and ρ will have no impact on the reaction force for orthogonal situations but r_{plat} may because of its contribution to semi-rigid effects. Because the base and platform geometry have been truncated for these simulations these affects will be ignored. The addition of both will cause a decrease in spring force similar to that caused by the intermediate platform because of their semi-rigid nature. All other parameters will have some effect on the spring force.

There is a good understanding of how leg thickness, leg width, leg length, and modulus of elasticity affect the force and displacement through PRBM analysis on a single leg segment even though PRBM boundary conditions are not entirely met. The understanding now needed is how significant the transition radius, r_{leg}, and the intermediate platform width, w_{ip}, affect the reaction force for a single leg.

While holding spring thickness constant, r_{leg} and δ_z were divided into 10 intervals each. Refer to Figure 5.2. MatLab was used to create a design matrix as a simple way of organizing the simulations. Each set of inputs was fed into ANSYS and the results recorded back into MatLab for analysis. The results of r_{leg} on the reaction force can be seen in Figure 5.5. First it is important to note that the relationship between δ_z and F_z is very linear for any given r_{leg}. The force is inversely proportional to r_{leg}. For

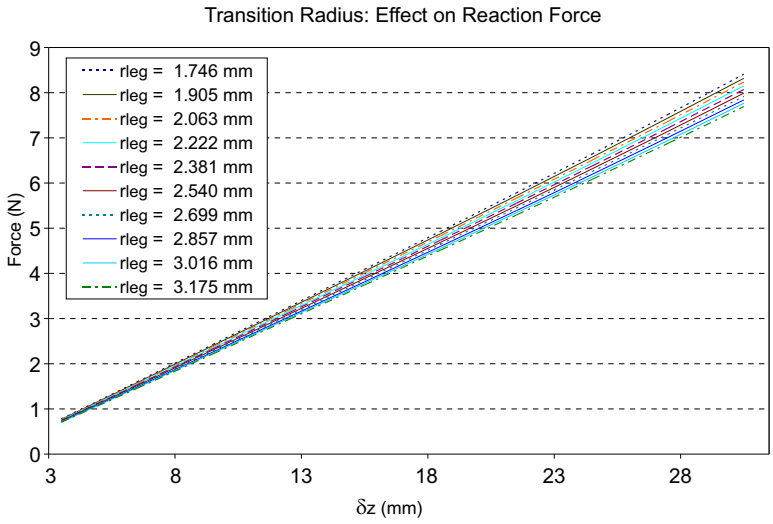

Figure 5.5: Relationship of r_{leg} to force/deflection.

any given displacement of the nominal COPS there is an approximate 9% increase in the reaction force, F_z from the largest radii to the smallest over the specified range.

The effects of the w_{ip} on the reaction force are shown in Figure 5.6. This parameter proved to have a lesser effect on the force than r_{leg}. The width of the intermediate platform for the nominal design was held equal to the width of the leg segments. To see if the semi-rigidity of the intermediate platform could be influenced by w_{ip}, increments of $1/12^{th}$ its width were added until it was 1.5 times wider than the leg segment. Increasing the intermediate platform width by 50% produced a meager 1% increase in reaction force. In reference to the inset in Figure 5.6 the increasing line density shows that as w_{ip} increases it will eventually have no effect on the reaction force. Decreasing w_{ip} to less than w_{leg}, which results are not shown in Figure 5.6, would result in a significant drop in the reaction force. There would be an increase in torsion in the intermediate platform, allowing the leg segments to rotate more before they actually start bending.

In summary of these two parameters, r_{leg} should be held to the upper limit of its range because the drop in reaction force with a larger value of r_{leg} is not that significant and there will be a reduction in the stress concentration around the

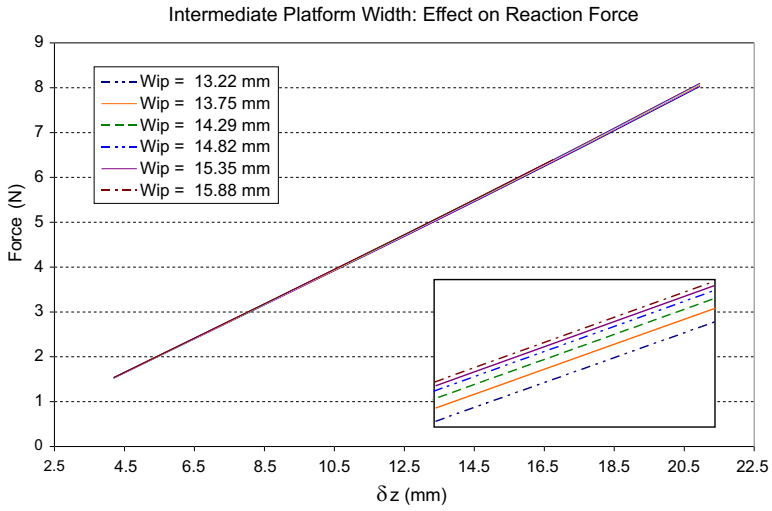

Figure 5.6: Relationship of w_{ip} to deflection/force.

transition radius. For w_{ip}, if its value were less than w_{leg} its structural integrity would be compromised and increasing w_{ip} to greater than w_{leg} has no significant effect on the output force. Because of this it is recommended that w_{ip} be held constant to w_{leg}.

5.3 Parameter Trends Under Orthogonal Loads

With the effects of these two design parameters better understood, we now shift the focus of the rest of the chapter to understanding the relationships and sensitivities of each of the individual design parameters to static loads. One way to show the relationship each design parameter has to reaction force is to change one parameter at a time over its respective range and compare the results with the nominal reaction force. Figure 5.7 shows a spider graph representing the relationship each parameter has to the reaction force over its respective range. The x-axis represents the range in limits with the lower limit indicated by a negative one, the nominal by a zero, and the upper limit indicated by a positive one.

Spring thickness has a cubic relationship to the force output. Modulus, width, and displacement have a near proportional linear relationship to the output force

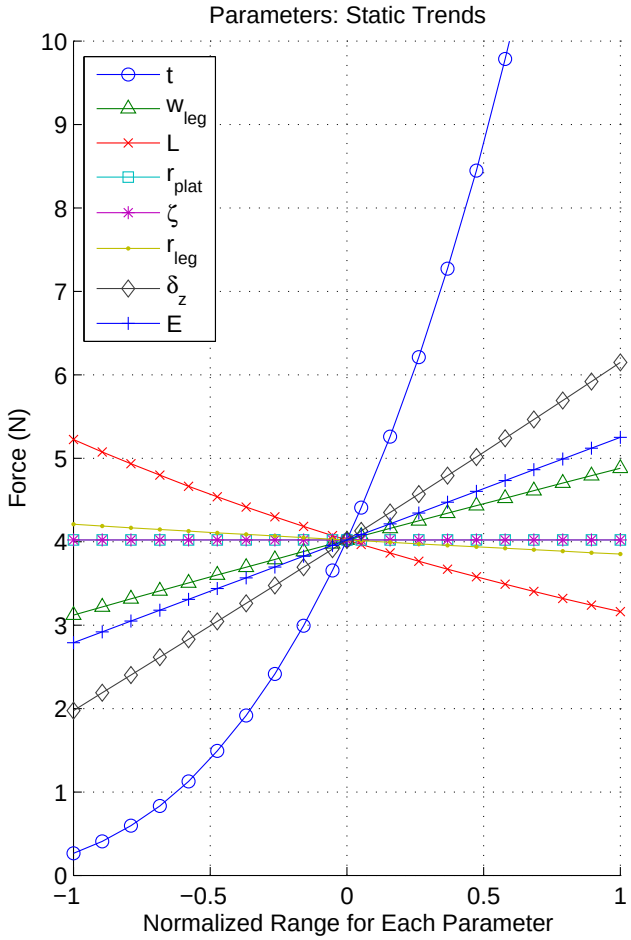

Figure 5.7: Individual parameter relationship to deviation from the nominal.

while transition radius and leg length are inversely proportional. Leg segment length's relationship to the reaction force appears to be non-linear as well as inverse. Notice that platform diameter and leg angle have no relationship to the reaction force while $\omega = 0$ and if density were included it would also have no effect on the reaction force.

A full factorial design was performed to understand the relative sensitivity the reaction force has to each of the design parameters and their two-way interactions. Each parameter was changed by 5% of its range, both above and below the nominal dimension, in order to show the relative effect each had on the reaction force. The results help us understand how a change in a design parameter will affect the reaction force and its relative significance. Figure 5.8 shows the results of the sensitivity

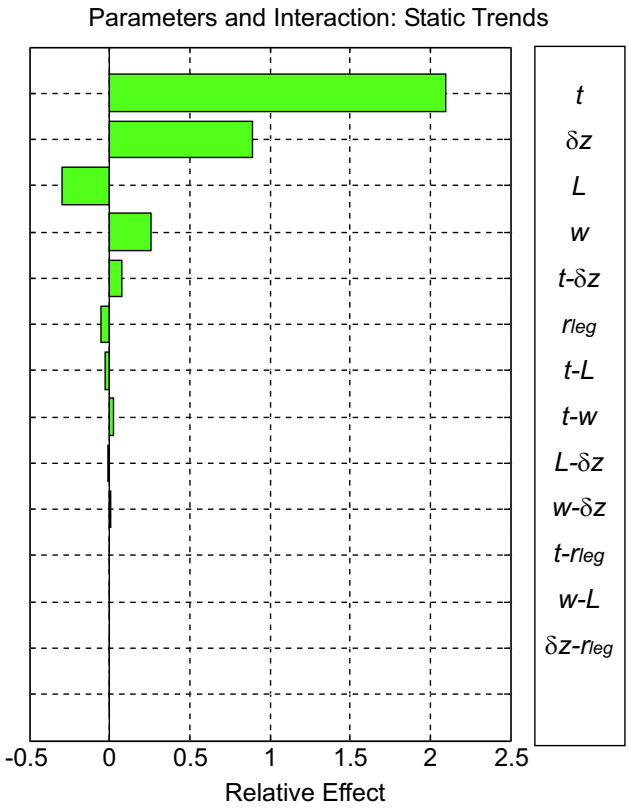

Figure 5.8: Full factorial design shows relative significance of design parameters and their interactions. Parameters are listed in order of importance to reaction force.

analysis. The reaction force is most sensitive to COPS thickness, then platform displacement, etc. The proportional or inverse relationship can also be seen in the sensitivity analysis as shown by the leg segment length. Interactions of significance occur between leg segment dimensions and platform displacement.

In summary, there are many ways to change the reaction force for a COPS subjected to orthogonal loads. For example, the reaction force can be increased by either decreasing the leg length or increasing spring thickness. There are however tradeoffs in using each approach. A decrease in leg length, would decrease the design envelope and make it incompatible for stacking with the original design. Increasing the thickness slightly would not create incompatibility with the original spring design yet would achieve the same results in increasing the reaction force. Once a final

design is settled on, COPS of varying thicknesses can be used to customize the spring constant.

Chapter 6

Lateral Stability & Stiffness

While Parise described stability as the resistance a COPS platform has to moving outside its path or prescribed motion while subject to orthogonal loads, the addition of angular velocity and inertial loads will affect the stability of the legs and not so much the platform. If the lateral inertial loads on the legs are significant enough to cause lateral buckling the COPS will fail. What design parameters influence lateral buckling of the legs and what parameter settings will ensure a COPS design free from this type of failure?

The objective of this chapter is to introduce the issues of lateral stability and stiffness as they relate to COPS for rotational applications. The motivating factor for this chapter is the inertial loads which a side leg design would see while subject to angular velocities as shown in Figure 6.1. There may also be some concern for lateral loads pushing or pulling on the platform of a rotating COPS. These loads may have a constant direction but not constant in magnitude like the CVT application.

6.1 Lateral Stability in COPS Legs

A new definition of lateral stability would be the ability of a COPS to maintain proper function and structural integrity when subjected to angular velocities. Lateral stiffness on the other hand would be the ability of a COPS to resist lateral loads placed on the platform. It is important to design for both of these to make sure the COPS design will avoid buckling. By carefully choosing the parameters for a COPS design, lateral buckling in the legs may be avoided. This issue of buckling will be more critical for applications involving high rpm such as would occur using a COPS in a CVT.

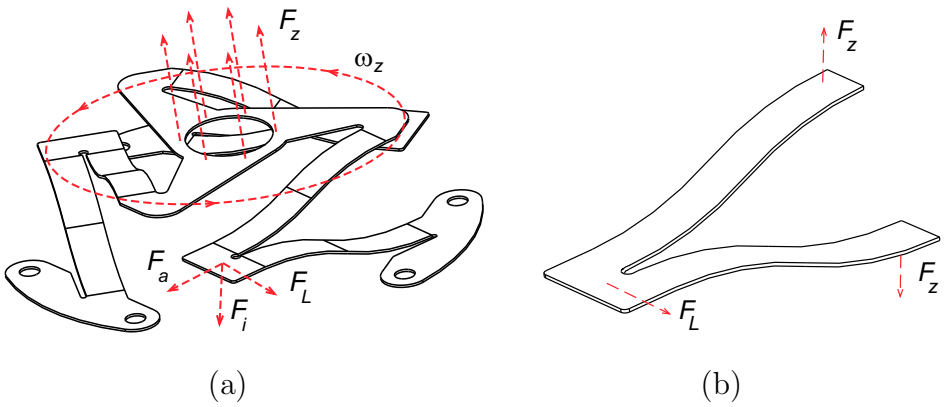

(a) (b)

Figure 6.1: (a) Inertial loading conditions (b) and loads associated with lateral buckling.

So the question then is what design features, parameters and their respective settings will cause instability in a COPS design? Many design features have been qualitatively identified in previous chapters such as even leg designs, multiple intermediate platforms and nested springs. The individual parameters which are most likely to contribute to COPS instability are very thin springs, long leg lengths, and large leg angles, all of which require the presence of a critical angular velocity. Of particular interest is the interaction or relationship between leg angle, spring thickness, and angular velocity.

The same model of a single COPS leg discussed previously will be used to analyze the design space to find which parameter settings are most likely to contribute to COPS instability. The interactions of most concern are between spring thickness, leg length, leg angle, displacement, and angular velocity. Many of the findings are presented in terms of ω^2 because of the relationship this term has to inertial loads.

Leg angle will contribute heavily to COPS stability. When the leg is at an angle of 0°, stress stiffening will be at its peak and will actually enhance stability. For leg angles between 60° and 135°, the lateral loads on spring legs will be at their peak dependent on the dimensions of the platform radius and leg length. At these angles the

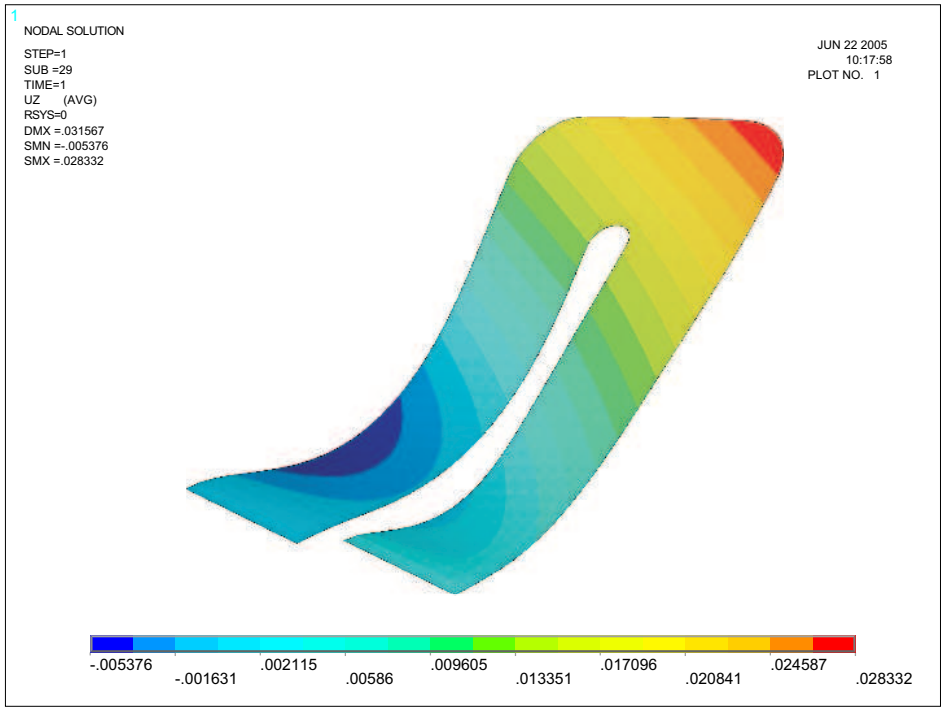

Figure 6.2: Deformation characteristic in small t & δ with large ζ and ω.

lateral inertial loads will pull the leg segments away from the platform causing them to buckle out of plane.

6.2 Two Modes of Lateral Buckling in COPS Legs

Two modes of lateral buckling were identified in a preliminary analysis. Mode I occurs when there is a small displacement in the platform, leg angles are high, and the spring is subjected to large angular velocities. As the leg spins, a lateral inertial load on the leg pulls the intermediate platform out of plane and causes the leg segments to buckle. This type of buckling occurs only when displacements are small. An FEA model depicting this type of buckling mode can be seen in Figure 6.2.

Mode II occurs when there is a large displacement and the lateral inertial load is sufficient enough to begin pulling the intermediate platform away from the center

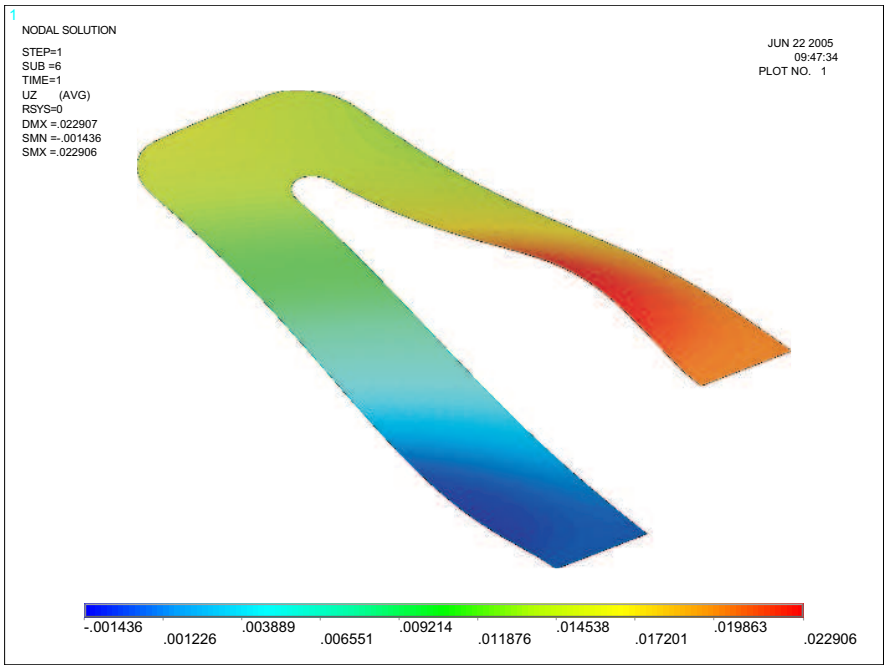

Figure 6.3: Deformation characteristic in medium to large t & δ for large ω and ζ.

of the COPS. As this motion occurs a portion of both leg segments begins to buckle as the leading edges are forced away from the the intermediate platform plane as shown in Figure 6.3. This mode occurs under the conditions of large displacements, large leg angles, and high angular velocities.

Both Modes I & II were more dependent on the platform displacement, δ_z, than on spring thickness. Under transient loads like in a CVT, the occurrence of Mode I would require a small platform displacement with a high angular velocity. This is not that likely because platform displacement be larger for high angular velocities and small for lower angular velocities. Mode II is more likely to occur in an application like the CVT because the COPS platform should be fully displaced by the time the CVT reaches peak rpm.

As a check on the FEA model, a physical test involving an actual COPS leg close to the nominal design was used to recreate both failure modes. The test leg

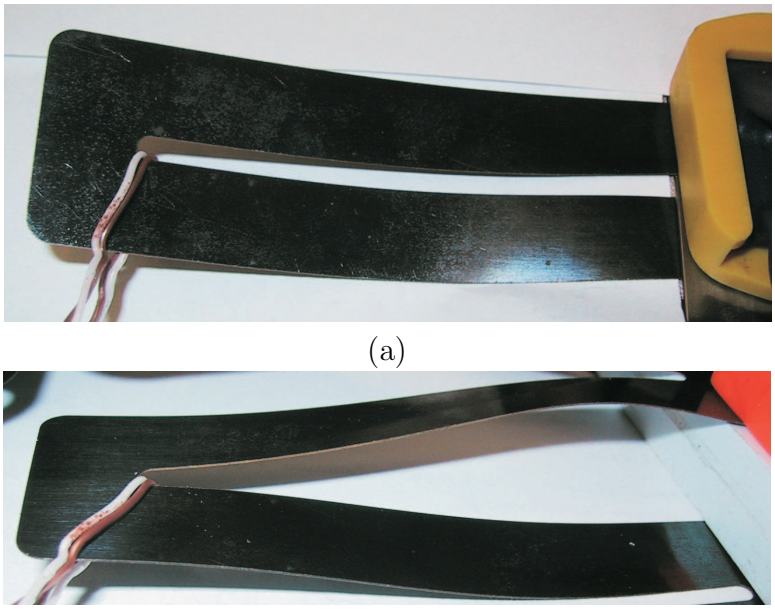

(a)

(b)

Figure 6.4: (a) Mode I and (b) Mode II buckling experiments.

was constrained to a small displacement and a simulated lateral load was placed near the intermediate platform using a small cable. The test for small displacements proved that Mode I buckling does occur if the lateral load is significant enough. The same test was performed for larger displacements and the results were also positive in confirming the buckling mode. Figure 6.4 shows the COPS leg in Mode I buckling (a) and Mode II buckling (b). Both modes match those found through FEA analysis.

6.3 Lateral Buckling Metrics for COPS Legs

There are two possible metrics for quantifying lateral buckling. The first comes from monitoring the spring geometry enabling a pinpointing of when buckling will occur. Because displacements are used to supply the load, the platform distance from the base is known. If Mode I occurs then the maximum displacement will occur in the intermediate platform which can then be compared to the input displacement to check for buckling. Likewise, Mode II can be monitored by tracking the maximum displacement along the leg segments and again comparing it to the input displacement.

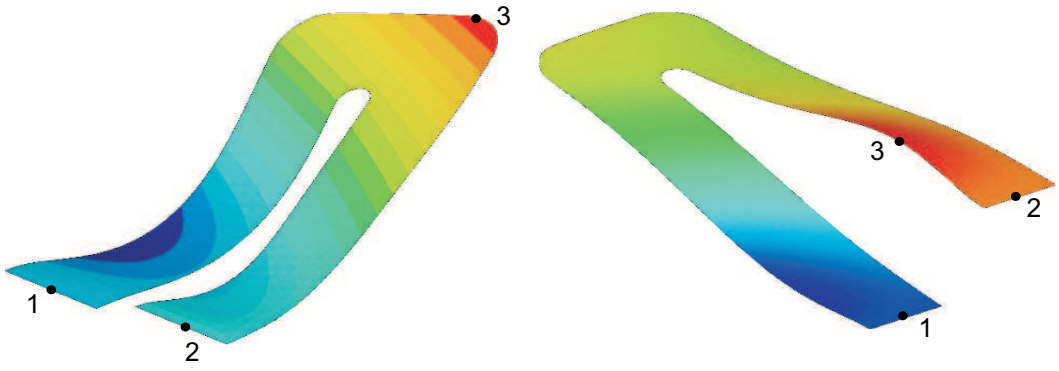

(a) (b)

Figure 6.5: Metric monitoring the distance between the base (1) and either the input displacement (2) or the maximum displacement (3) for (a) Mode I and (b) Mode II.

By finding a predetermined percent change between the input and maximum displacements, buckling failure can be pinpointed. An illustration of this can be seen for both modes in Figure 6.5. The input displacement is the distance from the base (1) to the platform (2) and the maximum displacement is from the base (1) to some extremity (3) of the geometry caused by lateral buckling. The only difference between the two Modes is that for Mode I the buckling will occur in the intermediate platform, which is located at half the platform displacement. Mode II buckling, on the other hand, will occur on the leading edges of the leg segments, one of which is located at the displacement of the platform. This means that for Mode I half the input displacement (2) should be compared with the maximum displacement (3) to show when it buckles.

The second possible metric to identify lateral buckling is the change that occurs in reaction force as the angular velocity is increased. Because displacement is used as the input for loading the platform, it will be held at a constant state while inertial loads are applied. Under normal operating conditions, when the loads are removed the spring should have a positive force which will return the platform to its undeflected state and its structural integrity will be maintained. If there is any type of buckling present in the spring, the buckling forces will cause the legs to move apart opposing the reaction force because of the fixed displacement. The force should have a positive

rate of change with the increase of inertial loads because of stress stiffening. If the rate of change in reaction force is equal to zero then the lateral inertial loads have induced a negative reaction force in the leg equal in magnitude to the positive reaction force from orthogonal loads. It is at this point that the COPS leg will buckle laterally.

Several cases of each buckling mode, using a thick and thin COPS leg, were simulated and the % change in displacement and the reaction force were recorded as the angular velocity was increased. In Figure 6.6 one can see that for both buckling modes the reaction force does have a local maximum. For the four examples in Figure 6.6 in the two lower graphs, lateral buckling does not occur at the same % change in reaction force. The % change in displacement metric is not as clear cut as the force metric because a global critical % change in displacement would need to be established in order for it to be useful. Although these two methods do not agree exactly on the critical angular velocity, ω_{cr}^2, every time, they are in the ballpark with each other.

Using the reaction force to identify lateral buckling was chosen because it avoids establishing a subjective criteria for lateral buckling. The point at which lateral loads begin to overcome orthogonal loads is a very distinct point and is unique to each spring geometry.

6.4 Lateral Stability Boundaries for Nominal COPS Model

The following simulations are an exploration of the design space involving spring thickness, leg angle, displacements, angular velocities, and leg lengths. An initial study was set up to investigate 20 spring thicknesses, 20 angular velocities, and 10 displacements over each parameters design space. This simulation was run for $\zeta = 0$, 45, 67.5, 90, and 135 degrees. Each simulation required 4000 individual runs which were set up in a design matrix inside of MatLab. Each thickness and displacement had a respective curve created by changing the angular velocity. A reaction force curve for a given spring thickness and displacement was produced by changing the angular velocity. A 5^{th} order polynomial was fit to each curve, then by taking the derivative,

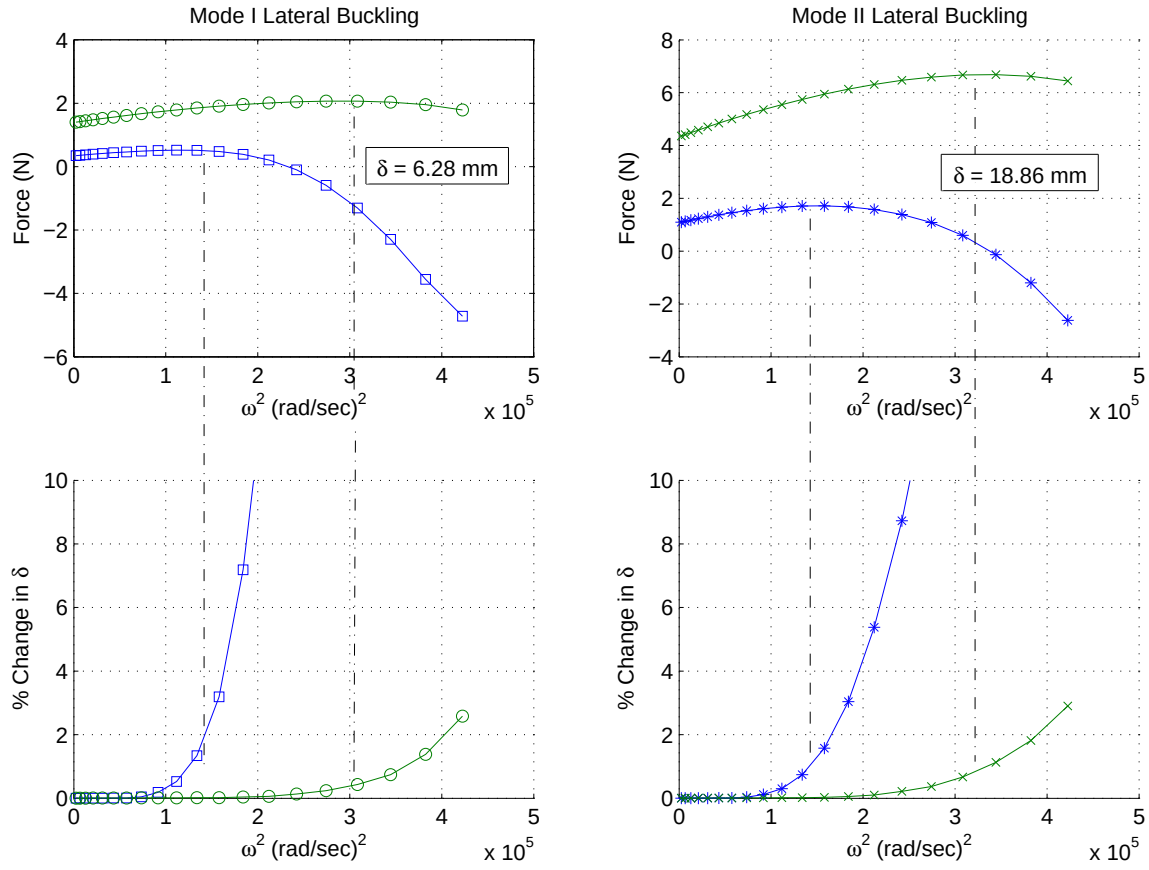

Figure 6.6: The relationships buckling has to displacement and reaction force.

setting it equal to zero and solving for the roots, an ω_{cr}^2 could then be characterized for each combination of δ_z and t at a specific leg angle, ζ.

For $\zeta = 0°$ there was no lateral buckling for any combinations of δ_z and t. This result was expected as there is no lateral inertial load on a leg at $\zeta = 0$. Each of the other four angles showed some type of buckling occurring mostly in thinner springs. Figure 6.7 shows the results of the other four angles tested. After each simulation the data was examined. Some of the data for very thin springs, large angular velocities, large leg angles, and small displacements resulted in ANSYS having some problems with convergence. One possible reason for this is the proximity the platform has to the change point or in-line position of the spring (very small displacements) and the

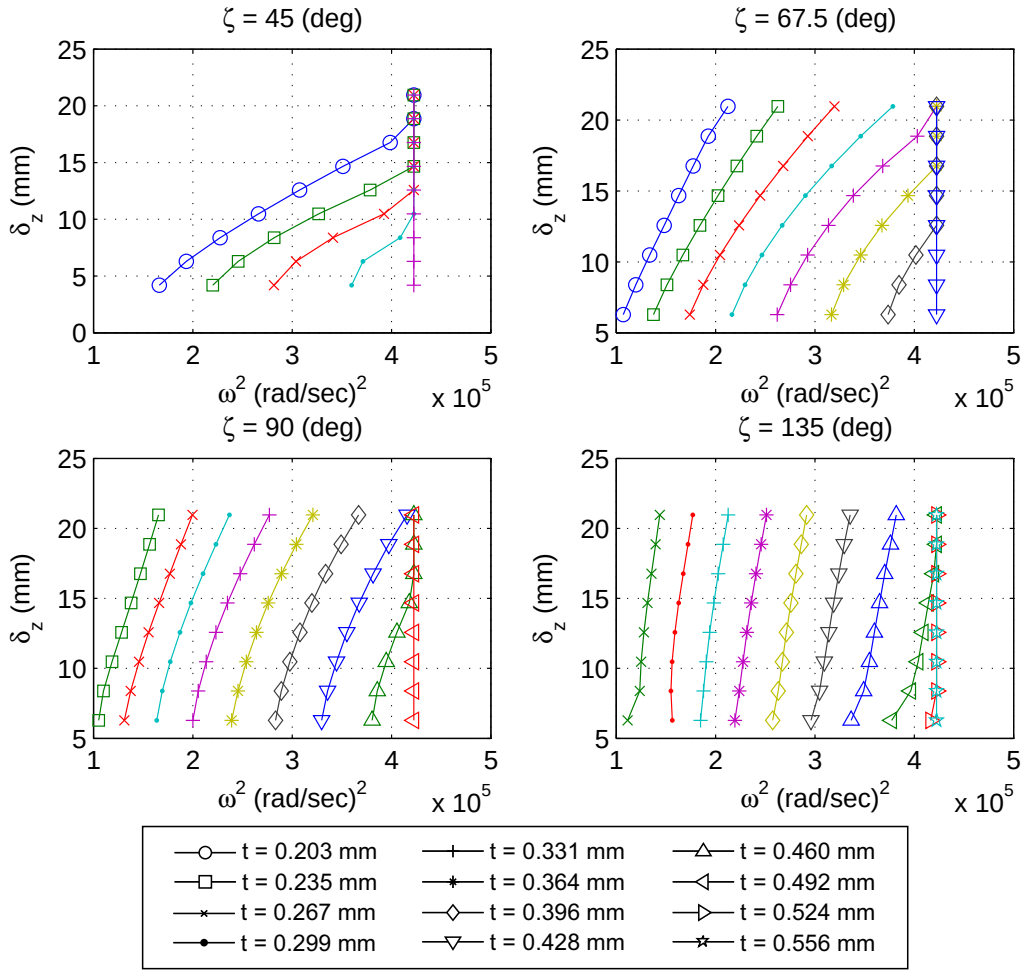

Figure 6.7: ω_{cr}^2 for various δ_z and spring thicknesses.

combination of the other three variables. All data that showed signs of convergence problems has been removed from the results.

The data in Figure 6.7 was useful for understanding the relationship between spring thickness and displacement. A preliminary graph with lines of stability was created by taking the thinnest spring which did not cross to the right of a given ω^2. Three ω^2 were used to create the lateral stability lines shown in Figure 6.8. The coarseness of the resulting graph inhibited the ability to see what was happening for thinner springs between 0 and 45 degrees.

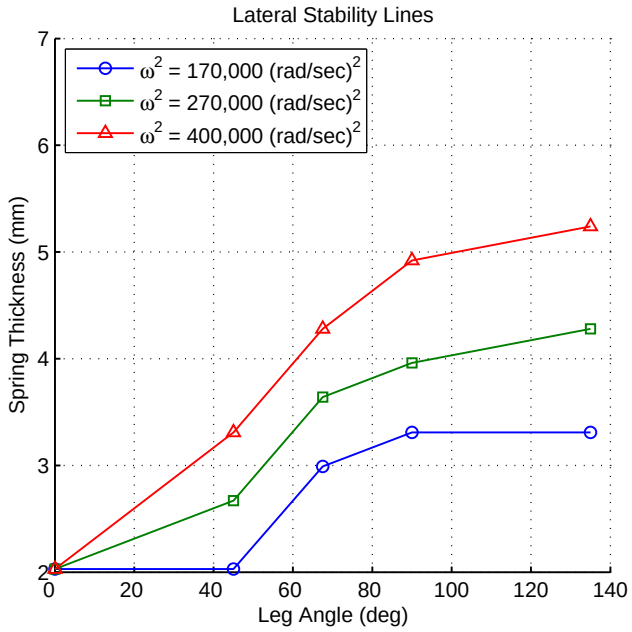

Figure 6.8: Stability boundaries for various ω^2 derived from Figure 6.7 design space simulation.

Returning to the data in Figure 6.7 we can see that as a spring's displacement increases so does its ω_{cr}^2 for buckling. With the knowledge that a spring will buckle first at a smaller displacement, displacement can then be fixed in order to investigate the effects of other design variables. The boundary for displacement was chosen to be at $\delta_z = 6$ mm because it seemed to be the threshold for which the model is well behaved. A new study was completed which involved studying the relationship between leg angle and spring thickness with the new fixed displacement. This study involved the entire range of ζ and ω but narrowed the range for t to an upper limit of 0.508 mm or the nominal design. Each parameter was divided into 20 intervals and combinations of each were simulated for a total of 8000 runs. The same technique for finding a critical angular velocity, ω_{cr}^2, from a reaction force curve generated by changing ω was used for each unique set of a ζ and t. Leg angle and spring thickness were plotted against each other with ω_{cr}^2 as contour levels.

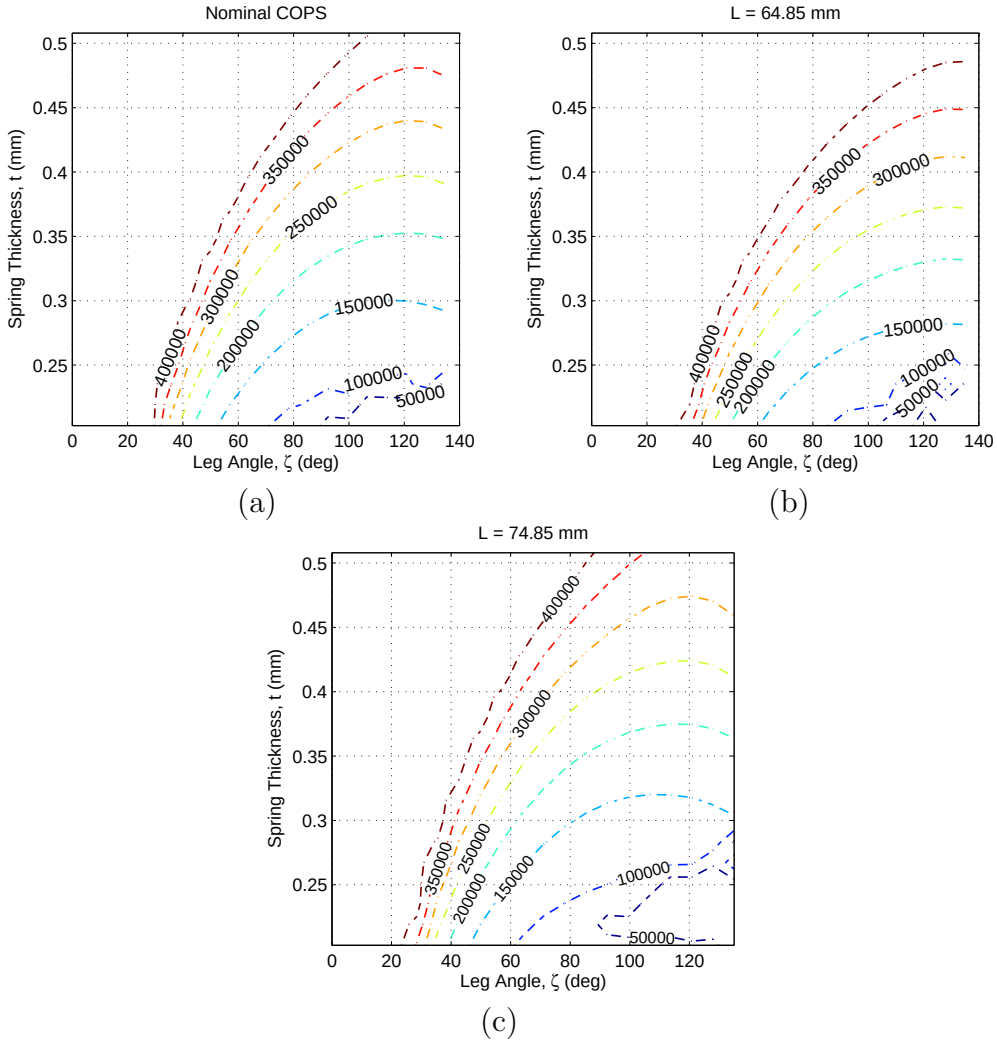

Figure 6.9: ω_{cr}^2 contours for lateral buckling (a) of the nominal case leg (b) of a slightly shorter leg and (c) of a slightly longer leg.

Figure 6.9 (a) is a contour plot of the nominal COPS design with the exception of the variables being changed. It is in good agreement with the curves shown in Figure 6.8 but in finer resolution. Note that there is a specific leg angle in which the spring thickness is no longer a factor in lateral buckling. To give some idea of how these curves might shift with a parameter change, leg length, L, was changed in both directions. Figure 6.9 (b) shows lateral buckling contours for a COPS leg with a slightly shorter length while (c) shows lateral buckling contours for a COPS leg with a slightly

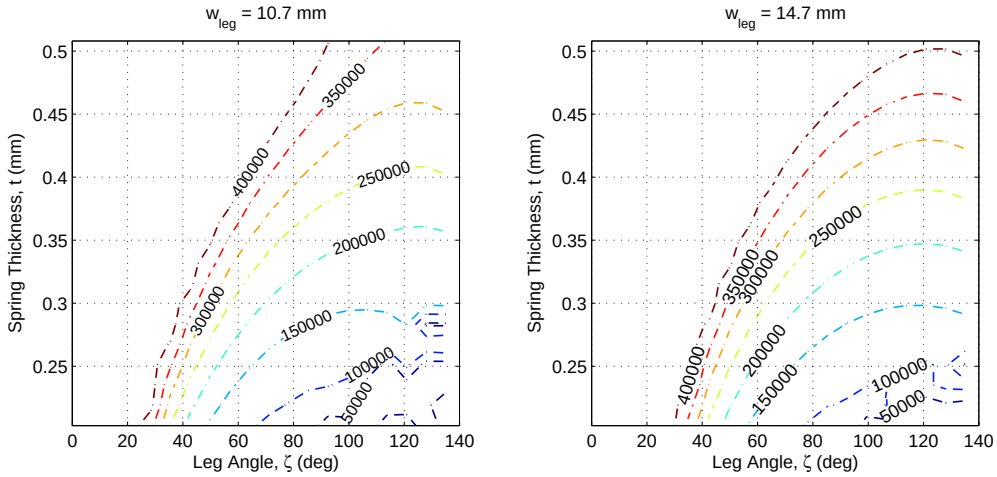

Figure 6.10: ω_{cr}^2 contours for lateral buckling (a) of the nominal with a narrower leg and (b) of a wider leg.

longer length. Note the lower left corner of each of the three graphs. For all three leg lengths there was some instability in the data for very thin springs with large leg angles signifying locations in the design space to be avoided. Also, one can see that the longer a leg is the easier it will be to buckle.

Two more sets of simulations involving a change in the leg width were performed. Figure 6.10 shows the ω_{cr}^2 contours for (a) a slightly narrower leg and (b) a slightly wider leg. As the leg segment width is decreased the leg will buckle at a lower ω_{cr}^2 and as it is increased the ω_{cr}^2 will increase.

For an example take the location where $\zeta = 80°$ and $t = 0.35$ mm. For the nominal design $\omega_{cr}^2 \approx 250,000\,(rad/sec)^2$. By changing the length of the COPS leg by 5 mm in either direction, ω_{cr}^2 changes by approximately $50,000\,(rad/sec)^2$.

6.5 Conclusions on Lateral Stability

Although much of what has been done in this chapter is for a specific COPS design, it does give an understanding of how design parameters affect lateral stability of COPS legs. A number of inferences can be drawn from this research on lateral

stability. First it is possible to create lateral buckling curves for individual COPS geometry based on spring thickness, angular velocity, and leg angle. Creating preliminary design graphs such as the ones in Figure 6.9 will help a designer determine which areas in the design space to avoid.

It is hard to say exactly how the curves in Figure 6.9 would shift with a change in each of the other design parameters not already involved. Parameters which would be interesting to research with regards to lateral buckling include the platform radius, material density and the leg width.

Leg length has an inverse relationship to lateral buckling. As the leg length is decreased the ω_{cr}^2 is increased and vice versa. This is because the mass of the leg will increase as well as the distance of the mass from the center of rotation. Both will increase the lateral inertial loads on the spring leg.

One of the most profound conclusions drawn from this chapter is the fact that the leg angle, ζ, has the most significant influence on the lateral stability of a COPS. The five graphs in Figures 6.9 and 6.10 show that for that particular COPS design there is no chance of lateral buckling for leg angles of approximately 20° and lower independent of spring thickness. If the design is to avoid all possibilities of lateral buckling then the COPS design should have a very small leg angle. This same approach could be used to understand safe design space for other COPS designs.

Two things should be considered when doing future research on this subject. First, consider the effects angular acceleration and deceleration may have on the spring. The rate of change in angular velocity may have a more significant impact on lateral stability than angular velocity alone. Second, the results of this simulation will change with the addition of base and platform geometry. The addition of both will tend to increase flexibility which will decrease stability. For the given spring geometry analyzed, base and platform geometry will increase the effective length of the leg segments and a similar trend to that seen in Figure 6.9 would possibly result.

There are a few things which can be done to increase lateral stability of COPS legs. The smaller the ζ and the thicker the COPS the less likely it is to buckle laterally. Shortening the leg segments as much as possible and keeping the platform radius to a

minimum will also increase lateral stability. Lateral stability may also be enhanced by stacking springs together. Placing thicker springs on the outside faces of a COPS stack may keep thinner springs in the middle from buckling laterally.

Lateral stability will be crucial to the proper operation of a rotating COPS. For this purpose it may be wise to test the design space for lateral buckling before moving on to the finer details. Doing this first would put the designer in a safe design space as far as lateral buckling is concerned. This refined design space could be refined further to eliminate high stresses and fatigue.

One more issue which has not been addressed is the overall lateral stiffness of a COPS design. Thoughts on testing this are to create a parametric model of a COPS and put a lateral displacement load on the platform at various angles through 120 degrees (for a Tri leg design) and record the reaction force opposing the lateral displacement. In this way both the amplitude and the mean of this reaction force could be used to categorize the lateral stiffness of COPS with various leg angles, thicknesses, etc. Doing this would show which combinations of parameters produce the stiffest COPS design. For the drive coupler and possibly the CVT mentioned in Section 3.3, this would be a necessary step to make sure the legs would not buckle under a load placed on the platform.

Chapter 7

Thin Sheet COPS - Axial Inertial Loads

The primary motivation for this chapter is to present the effects that stress stiffening has on the reaction force in a COPS subjected to inertial loads. The main advantage of stress stiffening is that it increases the reaction force of a COPS. This means that a COPS may be thinner if subjected to angular velocities and yet still provide an adequate restoring force. The implications of this would lead to lighter and more compact designs not only in COPS but also the mechanisms that utilize them. With regard to the CVT application, not only could a thin sheet COPS provide superior tunability but also a reduced overall weight and space, and an enhanced reaction force through stress stiffening. Figure 7.1 shows the axial component of the inertial loads, F_a, which causes stress stiffening.

The relationship and sensitivity of the reaction force to each of the design parameters of a COPS subjected to inertial loads will first be discussed followed by an investigation of stress stiffening.

7.1 Parameter Trends Under Combined Loads

The same model discussed in Chapter 3 is used for all simulations in this Chapter. The last Chapter took an in depth look at lateral buckling caused mainly by the lateral inertial loads, F_L. The loads of interest to us in this Chapter are axial inertial loads, F_a. Under combined loads, what relationship does each design parameter have to the reaction force? How sensitive, relative to each other, is the reaction force to each of these design parameters and are there any important interactions a designer

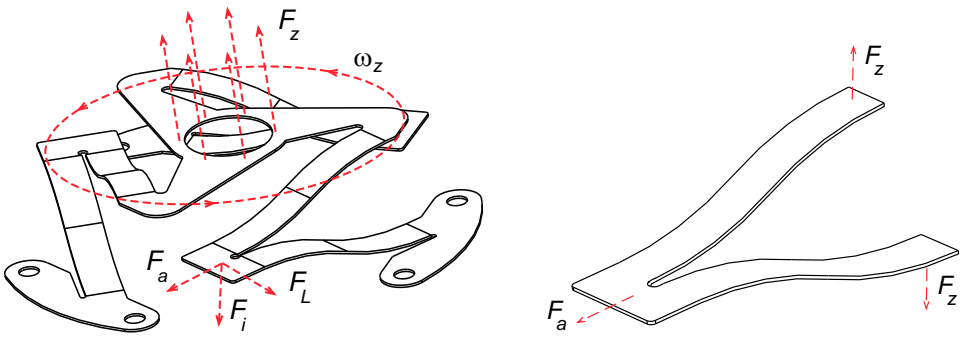

Figure 7.1: (a) Inertial loading conditions (b) and loads associated with stress stiffening.

must be aware of when designing COPS for rotational applications? How does stress stiffening affect the spring reaction force?

Figure 7.2 is a spider plot much like the one in Figure 5.7 but shows the relationship each parameter has to the reaction force with the addition of inertial loads. The nominal design, located at the center of the plot shows the reaction force at that point. All other points on the plot show the reaction force as a result of changing a particular parameter over its range. Spring thickness continues to have the greatest impact on the reaction force.

Parameters found in both the orthogonal and combined loading spider plots maintain their relationships to the reaction force with the exception of leg angle, ζ, density, ρ, and platform radius, r_{plat}.

The relationship that leg angle, ζ, has to the reaction force is dependent on the presence of an angular velocity, ω. The spider plot covers the range from 0° to 135° and has an inverse "s-shape" relationship with the reaction force. As ζ gets larger the axial component of the inertial load decreases and the stress stiffening effects drop off. The platform radius, r_{plat}, has a positive relationship with the reaction force although it is much more subtle. As it increases so does the reaction force slightly. This is because mass is being moved farther away from the center of rotation which increases

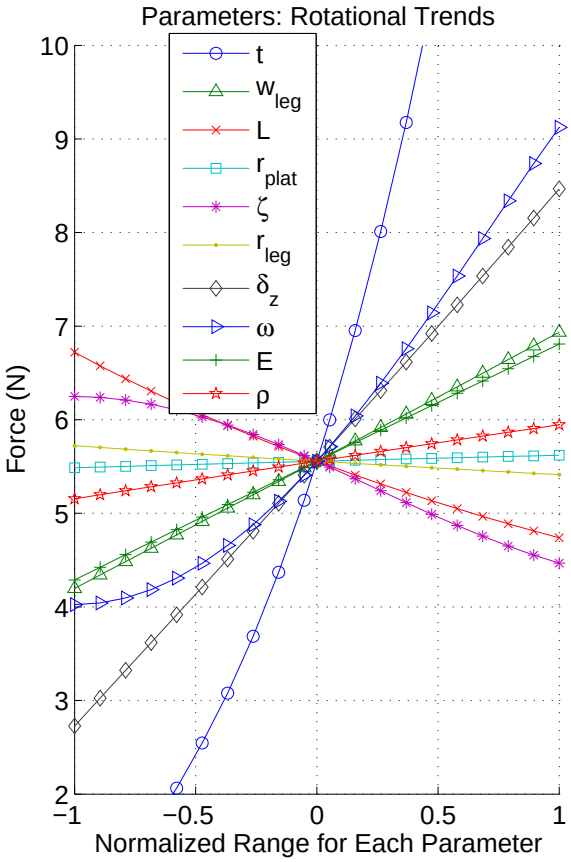

Figure 7.2: Spider plot depicting the relationships of each parameter to the reaction force.

its acceleration as it rotates. Density, ρ, also has a positive relationship to the reaction force. An increase in density, increases the mass of the leg upon which the acceleration acts.

Another sensitivity analysis was done with the inclusion of all the design parameters. Parameter settings for the full factorial design study were small enough that the assumption of linearity would hold true, again set to 5% of each parameters range. Material properties were changed only to show the relationships and sensitivities each has on the reaction force. All other simulations were done using spring steel properties. Figure 7.3 shows similar results to those found in the orthogonal load case with the exception that there are now many more parameters which are significant

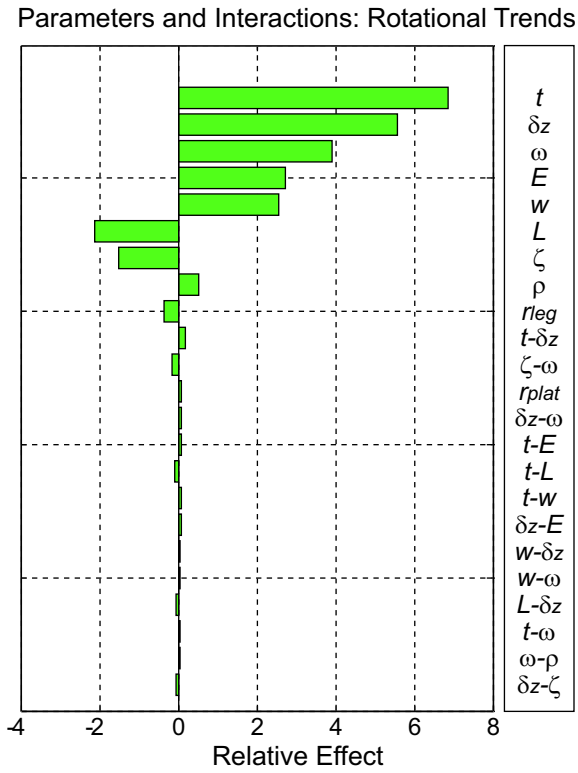

Figure 7.3: Individual parameter relationship to deviation from the nominal in presence of angular velocity.

and many more significant interactions. The reaction force is still the most sensitive to thickness, width, the thickness-width interaction, displacement, and now angular velocity.

Because there was some lateral buckling between smaller springs and high angular velocities in the last chapter it was necessary to make sure that any studies in this chapter were not influenced by lateral buckling. For this reason all springs under $t = 0.5$ mm are not included in the remainder of the studies involving inertial loads. The previous simulations are ok because the nominal spring was $t = 0.508$ mm.

7.2 Stress Stiffening Analysis of Nominal COPS

In order to better understand stress stiffening, a simulation involving leg angle, ζ, angular velocity, ω_z, and displacement, δ_z was performed. Leg angle was divided

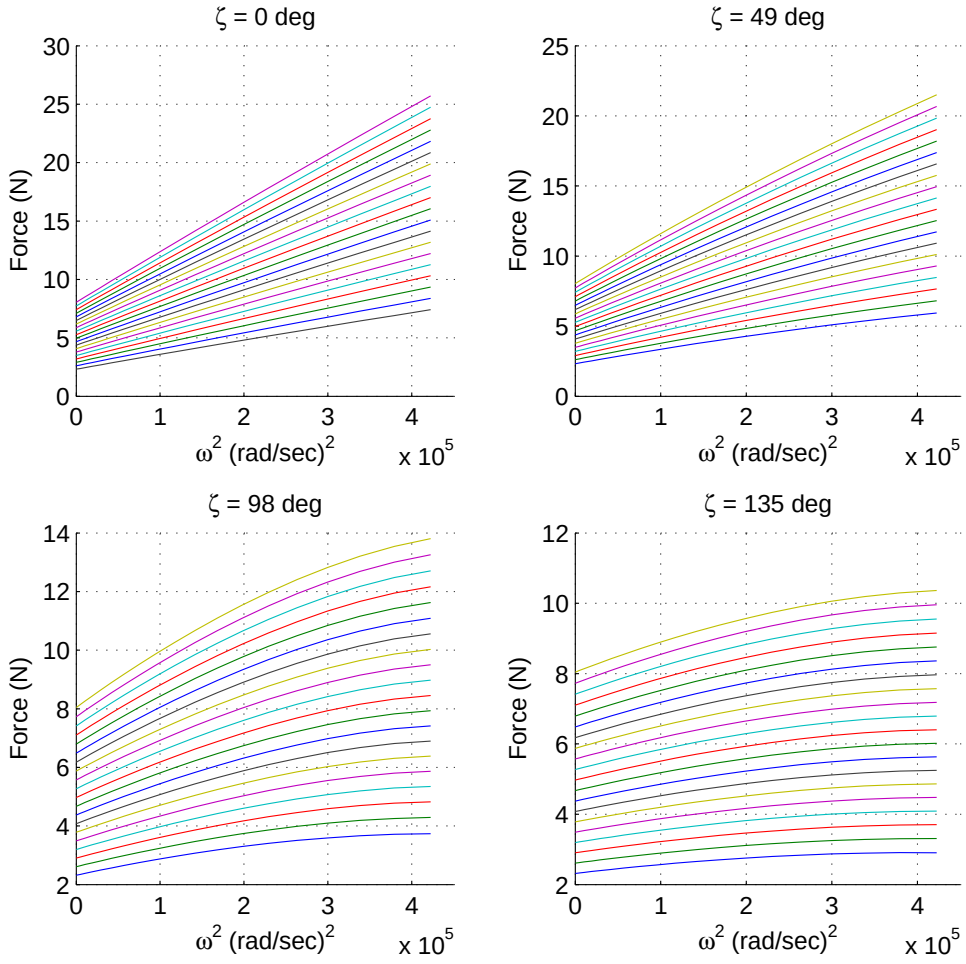

Figure 7.4: Reaction force curves over range of ω^2 for several different leg angles. Each contour line in a given graph is a different platform displacement.

into 12 intervals over its range while the other two were divided into 20 intervals over their ranges and all other parameters were held at their nominal values. A set of 4800 simulations was run and analyzed. Each set of simulations required approximately three days to run.

First we look at the reaction force and its relationship to ω^2 for various displacements. Figure 7.4 shows that when $\zeta = 0°$ the relationship between the reaction force and ω^2 is fairly linear. Looking at a an angle of $\zeta = 98°$ the relationship is no longer linear. As ζ increases, the axial component of the inertial loads decreases and likewise the effects of stress stiffening decrease.

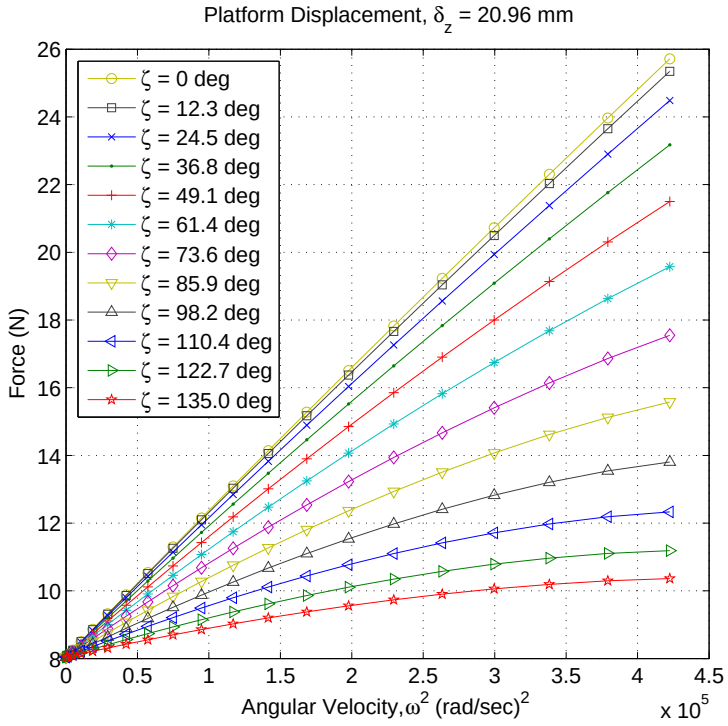

Figure 7.5: Maximum displacement curve for each of the 12 studied leg angles.

Figure 7.5 is a compilation of curves for each leg angle, ζ, at the largest displacement, δ_z. Doing this shows how the relationship is linear for small angles and as ζ gets larger the reaction force decreases along with the decrease of the axial component of the inertial loads. Also note that they all converge to the orthogonal load condition as would all curves for a given displacement.

Note that the contours for each leg angle are similar in shape and that the very left data point for each contour is at $\omega^2 = 0°$ representing the orthogonal load condition. This point may be used for characterizing the contribution of stress stiffening by the equation

$$\%Increase\ In\ F_z = 100 \cdot \frac{F_{\omega^2} - F_{(\omega^2=0)}}{F_{(\omega^2=0)}} \tag{7.1}$$

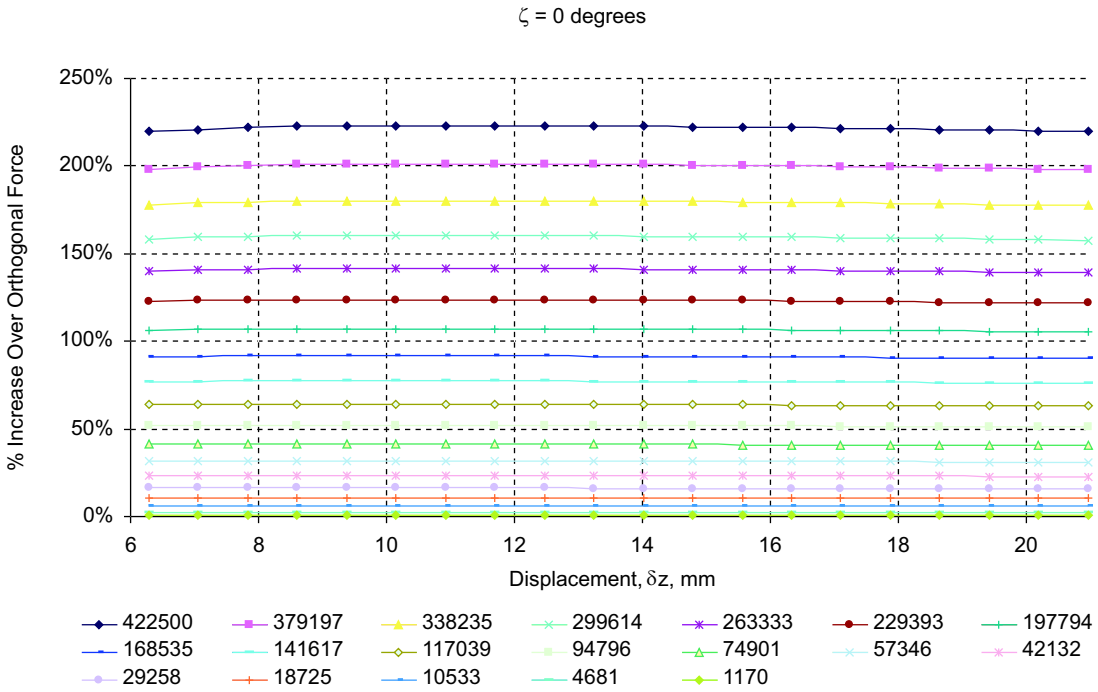

Figure 7.6: % increase in force over orthogonal load is independent of displacement.

By choosing an ω^2 and using Equation 7.1 for each of the displacement contours for a given angle, an average % increase in the reaction force can be determined. An example of this can be seen in Figure **??** for $\zeta = 0$. Note that for the largest ω^2 the average increase in reaction force is around 220%. This shows that the % increase in reaction force due to stress stiffening is independent of the displacement for a given ω^2 and ζ. Doing this over the range for each shows how stress stiffening's contribution to reaction force is affected by the leg angle.

Use the legend in Figure 7.7 for interpreting the contours found in Figures 7.8 to 7.12.

Figure 7.8 (a) shows the average % increase in the reaction force due to stress stiffening for the nominal COPS. The % increase in force due to stress stiffening is relatively independent of displacement and can be averaged for a given leg angle and angular velocity. All points in the remainder of the graphs are average values.

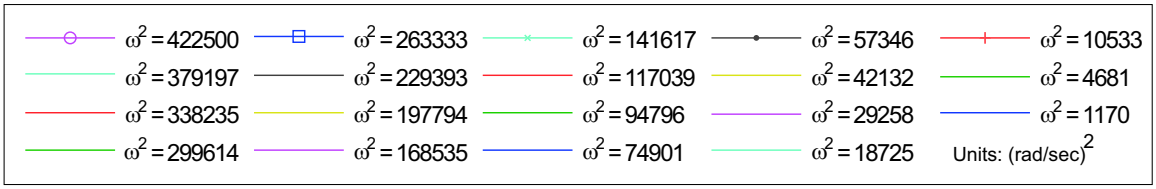

Figure 7.7: Legend for % increase in force over static load curves.

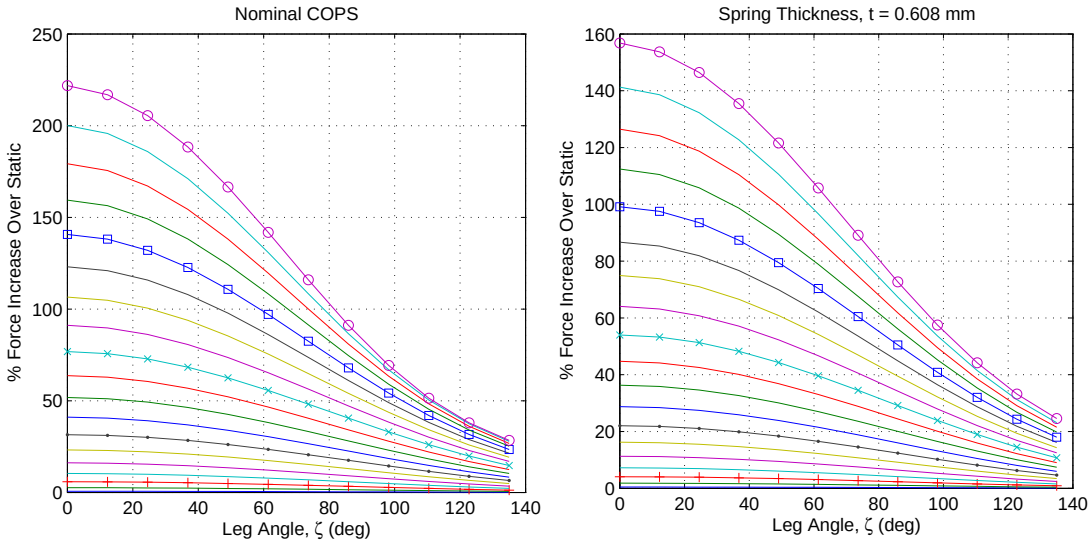

(a) (b)

Figure 7.8: The % increase in reaction force over orthogonal loading between ω^2 and leg angle, ζ for (a) the nominal COPS and (b) for a thicker COPS.

The % increase is greatest for small values of ζ and larger ω^2 with the full effects of stress stiffening occurring at $\zeta = 0°$. Figure 7.8 can be useful in deciding what the right balance is between keeping a compact design and the amount of stress stiffening a COPS design utilizes.

Figure 7.8 (b) shows the average % increase in the reaction force for a slightly thicker COPS leg. A noticeable drop in the % increase can be seen. This is due to the sensitive nature the reaction force has to the spring thickness. A small increase in COPS thickness has a greater affect on increasing the orthogonal reaction force than it has on the contribution to reaction force made by an increase in stress stiffening due to a larger leg mass.

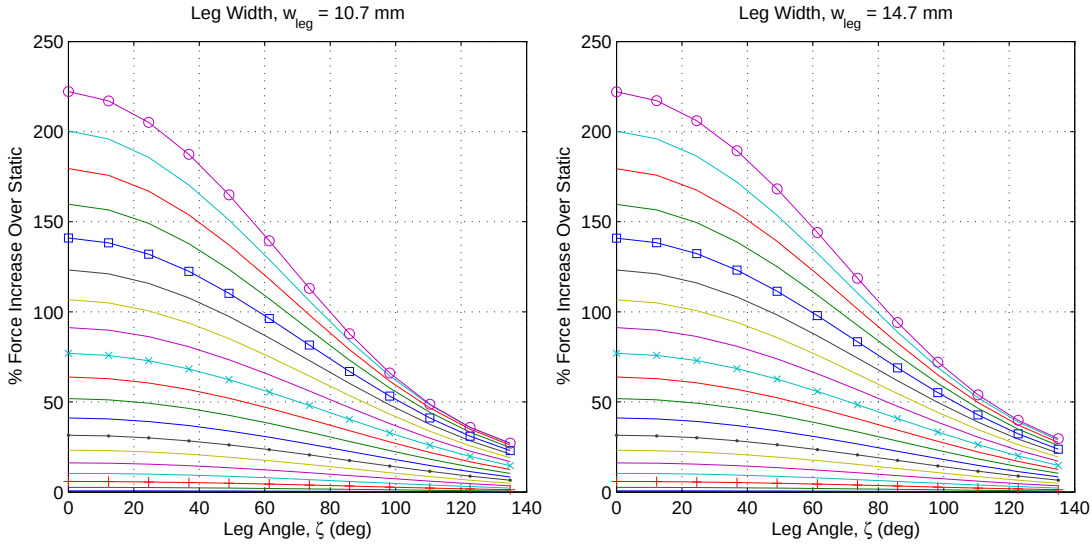

Figure 7.9: The % increase in reaction force in (a) a narrower leg and (b) a wider leg.

Figure 7.9 results from (a) increasing the leg width and (b) decreasing the leg width. It is interesting to note that while the magnitude in reaction force changes, the % increase in force over the static load seems to be independent of leg width. One plausible explanation for this is that the intermediate platform width, w_{ip}, and the intermediate platform radii, r_{ip}, were constrained to change with w_{leg}. If w_{ip} were increased alone the leg would see an increase in stress stiffening without an increase in reaction force due to the orthogonal load.

Figure 7.10 (a) shows the effects of stress stiffening on the reaction force by decreasing the platform radius, r_{plat}. Decreasing the platform radius has opposite effects for small and large leg angles. For small leg angles the effect on the % increase in stress stiffening over the nominal COPS design is decreased, but when leg angles are large it actually has a positive impact on stress stiffening. If the semi-rigid effects of the platform were present in this study, shortening r_{plat} would also increase the orthogonal reaction force and further decrease the contribution of stress stiffening to the reaction force.

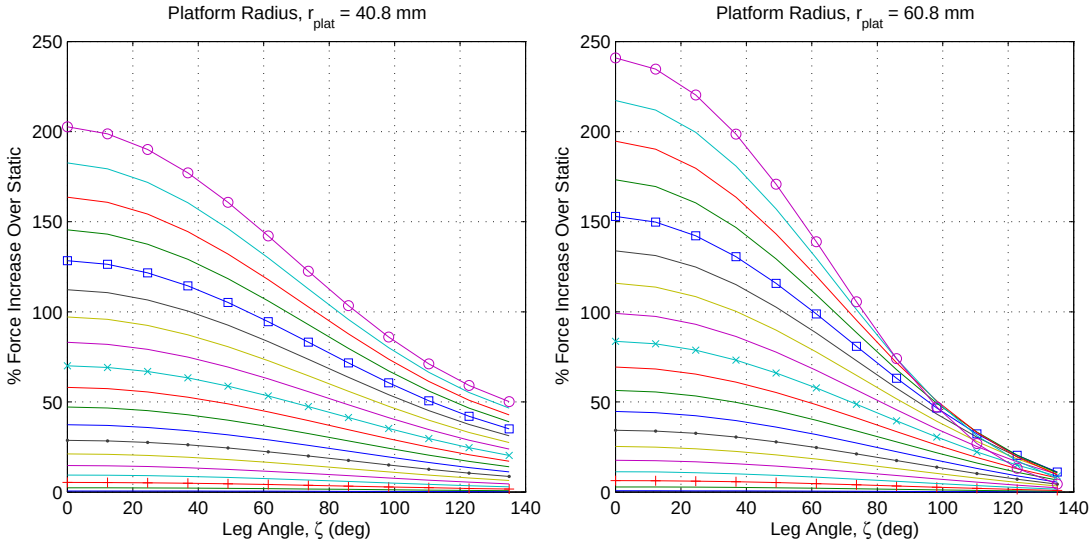

(a) (b)

Figure 7.10: Depending on the leg angle, ζ, (a) decreasing and (b) increasing r_{plat} have opposite effects on the % increase in reaction force due to stress stiffening.

Figure 7.10 (b) shows the effects of stress stiffening on the reaction force by increasing the platform radius, r_{plat}.a Increasing the platform radius increases the stress stiffening effects for small leg angles but for large leg angles it decreases stress stiffening while increasing the possibility of lateral buckling. This can be seen in Figure 7.11 where contours of greater ω^2 appear to have a % decrease in reaction force over the orthogonal load case for larger leg angles. Note that the two largest ω^2 contours dip below some of the others. This is most likely caused by lateral buckling of the legs.

Figure 7.12 shows the effect of changing the leg length on the contribution of stress stiffening to the reaction force. A shorter leg length, shown in (a), results in a decrease in stress stiffening for smaller leg angles. A longer leg length results in an increase in stress stiffening. Neither decreasing or increasing the leg length significantly affects stress stiffening for larger leg angles.

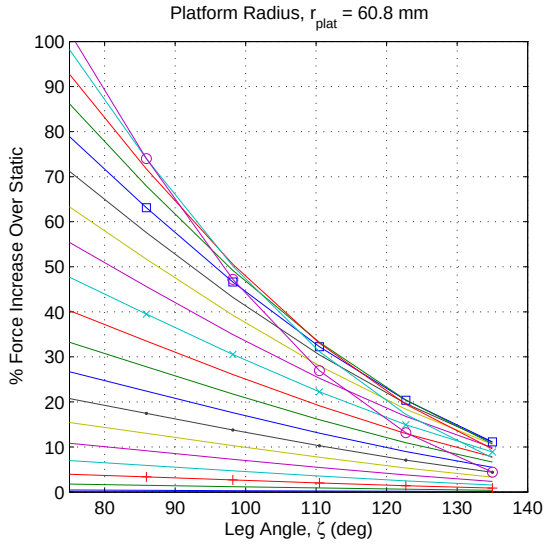

Figure 7.11: Decreasing r_{plat}, decreases the % increase in reaction force over the nominal COPS design.

7.3 Conclusions on Stress Stiffening

There are four important conclusions from the research in this chapter. First, the orthogonal load for any COPS can be used to quantify the % increase in reaction force due to stress stiffening. Second, the % increase in reaction force due to stress stiffening for a particular design is relatively independent of the platform displacement. This allows for a more concise way of interpreting the effect leg angle has on the reaction force of a COPS subject to an angular velocity. Third, the % increase in reaction force is greatest when leg angles are small and is fully utilized when $\zeta = 0$. The opposite is true, that larger leg angles are not as desirable if the effect of stress stiffening is to be utilized. Fourth, the reaction force for a COPS can be more than tripled by stress stiffening depending on the COPS configuration. This is an attractive characteristic of the radial leg design that may be advantageously used.

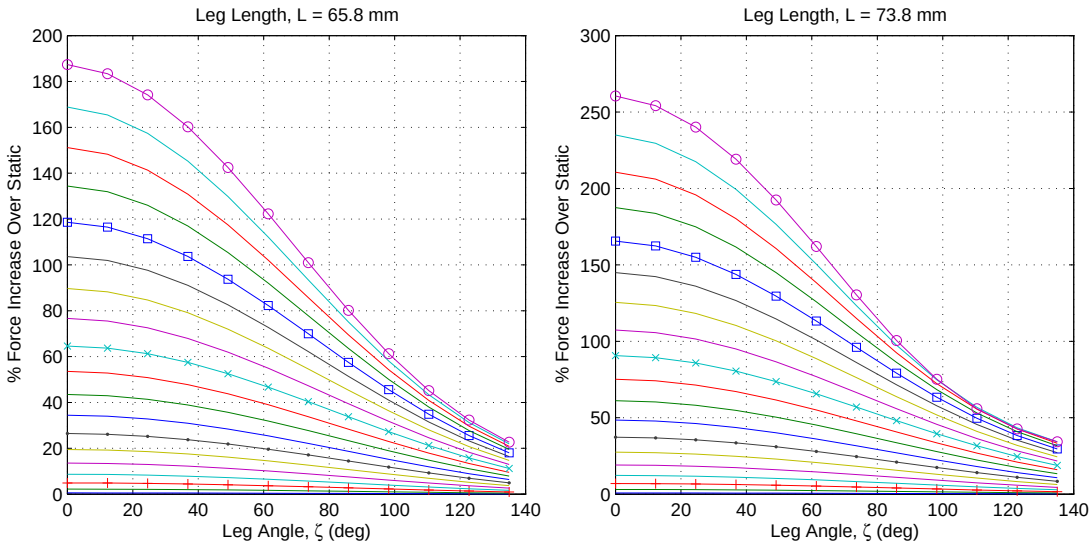

(a) (b)

Figure 7.12: Depending on the leg angle, ζ, increasing r_{plat} has different effects on the % increase in reaction force due to stress stiffening.

Chapter 8

COPS Application Design Steps and Important Tradeoffs

8.1 COPS Design Steps

The following design steps are merely a suggestion for approaching the design of COPS. These design steps are intended to be useful for the design of both orthogonal and inertial loaded COPS so not all steps may apply to any one application.

1. Understand Design Constraints
   (a) Physical constraints - space, weight, and shape
   (b) Loading constraints - forces, deflections, angular velocities and accelerations
   (c) Material constraints - types, stresses, and characteristics
   (d) Miscellaneous constraints - adverse conditions such as corrosion, application, and stackability
2. Investigate Initial Design Space
   (a) Choose number of legs
   (b) Choose leg segment parameters of t, w, and L based on design constraints
   (c) Use fixed-guided PRBM to analyze forces and stresses
   (d) Remember that these will change due to:
      i. Semi-rigid effects of base, platform and intermediate platform
      ii. ω and α if COPS are subject to rotation

3. Create CAD Models

   (a) Watch leg angle, number of legs, plat radius, etc. for interference

   (b) Consider manufacturing issues (i.e. complexity and intricate detail will be more expensive)

   (c) Choose other geometric parameters to fit within the design constraints

4. Finite Element Analysis

   (a) Choose material

   (b) Check for lateral buckling in legs for rotational applications

   (c) Check stress levels especially around tight radii

   (d) Fine tune the model

   (e) Alter the reaction force for the final design by changing thickness, thus maintaining stackability

5. Testing

   (a) Validate the design

   (b) Simulate run environment to test for fatigue, stress relaxation etc.

8.2 Design Tradeoffs for COPS

When designing COPS there are a number of design tradeoff decisions to make. The reaction force, stresses, stress stiffening effects, lateral buckling, and a number of other important elements to design can be influenced in multiple ways. Table 8.1 is useful for understanding how to influence design elements through design parameter changes. An $\uparrow$, $\downarrow$, or $\updownarrow$ indicates what would happen to the element in the left column if the parameter is increased. The converse would happen if the parameter were to be decreased. A $-$ or ? indicates that it is either not applicable or it is not certain how it would affect the design element. Those with double arrows indicate that the design element change may be dependent on other parameter settings.

Table 8.1: Parameter influence on design elements.

	t	w_{leg}	L	w_{ip}	r_{leg}	r_{plat}	ζ	δ_z	ω_z	E	ρ
F_{static}	$\uparrow$	$\uparrow$	$\downarrow$	$\uparrow$	$\downarrow$	$\downarrow$	$-$	$\uparrow$	$-$	$\uparrow$	$-$
σ_{static}	$\uparrow$	$\uparrow$	$\downarrow$	$\uparrow$	$\downarrow$	$-$	$-$	$\uparrow$	$-$	$\uparrow$	$-$
$F_{dynamic}$	$\uparrow$	$\uparrow$	$\downarrow$	$-$	$\downarrow$	$\uparrow$	$\downarrow$	$\uparrow$	$\uparrow$	$\uparrow$	$\uparrow$
$\sigma_{dynamic}$	$\uparrow$	$\uparrow$	$\downarrow$	$-$	$\downarrow$	$\uparrow$	$\updownarrow$	$\uparrow$	$\uparrow$	$\uparrow$	$\uparrow$
Leg Stability	$\updownarrow$	$\updownarrow$	$\updownarrow$	$\updownarrow$	$\updownarrow$	$\updownarrow$	$\downarrow$	$\downarrow$	$\uparrow$	$\updownarrow$	$\updownarrow$
Stress Stiffening	$\downarrow$	$-$	$\updownarrow$	$\uparrow$	$\uparrow$	$\updownarrow$	$\downarrow$	$-$	$\uparrow$	?	$\uparrow$
Semi-Rigid Ends	$\downarrow$	$\uparrow$	$\downarrow$	$\downarrow$	$\uparrow$	$\uparrow$	$-$	$-$	?	$\downarrow$	?
Compactness	$-$	$\downarrow$	$\downarrow$	$\downarrow$	$\downarrow$	$\downarrow$	$\uparrow$	$-$	$-$	$-$	$-$

Among the many design tradeoffs, the one parameter in this research that seems to be at the heart of most of them is the leg angle, ζ. A radial design is the best candidate for minimizing the possibility of lateral buckling and maximizing the effects of stress stiffening. However, the design tradeoff is lack of compactness which, for the CVT application, would be important. It would be unattractive and dangerous to have thin objects protruding out of a high rpm rotating mass. At the same time though, a radial leg design may be a rather attractive option if the CVT were to be redesigned specifically for accommodating COPS.

Chapter 9

Conclusions & Recommendations

9.1 Conclusions and Contributions

The purpose of this thesis has been to investigate the behavior of compliant ortho-planar springs subjected to complex loads, specifically their behavior for lateral stability, the effects of stress stiffening, and the effects of inertial loading for potential use in a CVT. While investigating COPS, the possibilities of a new type of pseudo-rigid-body model for 3-dimensional applications was also investigated. A parametric FEA model was developed for understanding COPS behavior under different load situations. This same approach was used for investigating the possibility of a 3D PRBM.

Qualitative Analysis

General observations and issues related to COPS designs were discussed in Chapter 3. The design space was narrowed to a spring steel $Tri\,1-1$ design because it has a good combination of stability, compactness, efficient use of space, and is less costly to manufacture than other COPS designs. Each parameter was given a specific range most likely to be used in a CVT application. Four load conditions a COPS in a CVT might see were identified. Other load conditions for COPS, some of which may be promising, were also identified.

A brief analysis of stresses and stress concentrations was also discussed. Stresses were found to be highest in and around the transition geometry in the intermediate

platform for static loads and at the base and platform for high inertial loads. Geometric modifications to the transition radii were found to have little to no effect on stress levels. It was found that the most effective way to bring down the stress in the transition geometry was to increase the transition radius.

For non-uniform thick COPS under orhtogonal loads it is possible to use the fixed-guided PRBM with some degree of accuracy. For thin sheet COPS however, there is a need to develop analysis tools which would allow a designer to quickly iterate COPS configurations. The 3D PRBM was an investigation of such a tool.

3D Pseudo-Rigid-Body Model

The research in Chapter 4 proved that a rectangular cross-section beam end does follow a near-spherical path for the specified load conditions when deflected in 3-dimensions. The key parameter in the 3D PRBM is the characteristic length factor, γ, which is dependent upon the deflection limits, δ_y and δ_z, and the aspect ratio, AR, of the rectangular beam cross-section. For a given AR, a γ was recommended along with the deflection limits for a maximum x position prediction error of approximately 0.5%.

When finding a γ for a 3D PRBM of a rectangular beam with an aspect ratio, AR, there are multiple solutions for finding nondimensional limits with a specific maximum % error in deflection. Limits can be found using optimization by choosing a desired % error in deflection and a ratio of the limits (i.e. $\frac{\delta_y}{L} = 2\frac{\delta_z}{L}$) as objective functions. Once the limits are established, the resulting γ can be used to predict deflections within the approximate maximum % error.

Force prediction at the deflected beam end proved to be more complicated than predicting the path of the beam end. The complications arose because the reaction of a rectangular beam deflected in two directions of differing flexural rigidity was to twist. This twisting brought the beam to an equilibrium state but also complicated predicting the forces through use of a 3D PRBM.

Even though force prediction is not yet possible, it was proved that path prediction of a rectangular cross-sectioned beam end, while under the specified load conditions, is possible with the use of this 3D PRBM.

Orthogonal Loaded Thin Sheet COPS

The reaction force for orthogonal load conditions was researched in Chapter 5. The two design parameters, r_{leg}, and w_{ip}, were studied and found to have very little effect on the reaction force within their specified ranges. It is recommended that future studies consider holding them constant in order to better understand the more important design parameters. Parameters of more significance to the reaction force from static loads are leg segment dimensions and platform displacement. Relationships of parameters to the reaction force were qualitatively characterized.

Lateral Stability

The effects that inertial loads had on COPS stability were studied in Chapter 6. Using FEA on COPS was not feasible for certain cases inside the design space. When a COPS is close to its in-line position, meaning the displacements of the platform are very small, the COPS is subjected to a high angular velocity, and its leg angles are relatively large, ANSYS has convergence problems. This problem was evident in Figure 6.9 where the lower right portion of the design space was not well behaved.

For COPS stability in the legs, two modes of lateral buckling were identified. Mode I occurred while there were small platform displacements and Mode II occurred for moderate to large platform displacements. For both Modes to occur, a design must have larger leg angles and large inertial loads. Lateral buckling was more likely to occur in thinner legs and was highly dependent on ω^2. It was found that lateral buckling in the legs could be pinpointed, as to when it occurs, by monitoring change in the reaction force. This approach was used in several studies on lateral buckling.

One study involved looking at displacement, leg angle, and angular velocity. From this it was evident that for a given set of design parameters there is a specific critical angular velocity, ω_{cr}^2, at which point the leg will buckle. As displacement increased, so did ω_{cr}^2. So for any given COPS design, lateral buckling will occur at smaller displacements before it will at larger ones. Knowing this, the displacement could be fixed while the effects of other variables on leg stability were observed. Critical lateral buckling curves were created for spring thickness and leg angle. In

reference to Figure 6.9 the design area to the right of the $400,000(\frac{rad}{s})^2$ is safe design space for that particular COPS design. It is possible to understand thresholds for lateral buckling by creating such graphs for specific designs.

Stress Stiffening

Stress stiffening was the topic of Chapter 7. Stress stiffening has often been looked at as a less desirable phenomena, however, for a COPS it can be positive when the objective is to have greater spring force. The effects of stress stiffening for the nominal COPS design had the potential to increase the orthogonal reaction force by as much as 220%. Such increases in stress stiffening may allow for thinner and lighter COPS designs. The effects of stress stiffening were maximum for small leg angles and minimum with larger leg angles due to a decrease in magnitude of the axial force component of the inertial loads. There are also many design tradeoffs between stress stiffening and the leg angle. While the full effects of stress stiffening may be utilized for $\zeta = 0$, the radial leg design is not as compact as a side leg design. Radial leg designs may require that the mechanism have a larger profile to enclose it.

The % increase in reaction force for a given leg angle and angular velocity was found to be relatively independent of the displacement. Finding other relationships and experimenting with non-dimensional parameters may lead to useful design tools.

Implications for CVT Application

Although many of the findings are generalizations and to date there is a lack of useful design tools for designing a specific COPS, much of the work contained herein is useful for laying the foundation for others to follow. This research provides a step closer to solving the design of a COPS for a CVT application.

Results of this research clearly lean toward a redesign of the CVT system to accommodate a radial leg design. A radial COPS configuration would be a great candidate for a CVT because of the avoidance of lateral buckling and the advantages of stress stiffening.

Even though we are closer to designing a COPS adequate for a CVT application, there are still some key issues which must be investigated and better understood. Stresses comprise a great deal of concern because of their complexity in rotating COPS. Stresses can currently be understood only through finite element analysis and full spring models may take a great deal of time and computing power to better understand. Fatigue is another issue which may only be better understood after studying actual COPS prototypes subjected to physical testing.

We are several steps closer to solving this but there is yet much to be researched and understood.

9.2 Recommendations for Further Research

3D PRBM Force Prediction

Force prediction for 3D PRBM's will be possible with a better understanding of how the flexural rigidity in the two directions relates to the induced torsion in the beam. Also an understanding of how much the beam end rotates and what the true beam end angles are relative to its undeflected state may also be necessary and helpful in predicting the forces.

Applicability of 3D PRBM to COPS Design

In order to directly apply 3D PRBM's to COPS for rotational applications, four boundary conditions must be satisfied. First, orthogonal loads induce a fixed-guided motion in the leg segments while lateral inertial loads induce bending like that of a cantilever beam. The current 3D PRBM only accounts for a cantilever beam bending about two orthogonal axes. Second, a COPS leg acts as two parallel beams rigidly fixed at one end with motion parallel to the plane of fabrication. Concessions for this odd boundary condition must be made. Third, the complex loads acting on a rotating COPS leg segment are a mix of point loading (displacement loads) and distributed loading (lateral inertial loads). Currently there does not exist even a 2D PRBM considering a distributed loading condition. Finally, the effects of stress stiffening would

need to be accounted for in a 3D PRBM because of the presence of an axial component from the inertial loads.

Semi-Rigid Effects and the Fixed-Guided PRBM

The semi-rigid effects in thin sheet COPS under orthogonal loading presents an opportunity for research. Several attempts to create an empirical model of the outlined COPS design space yielded some encouragement. The semi-rigid effects may be quantified by using an angle associated with the torsion of the intermediate platform or by developing an effective leg length. Both methods allowed for accurate orthogonal force prediction within 10%. With more research it may be possible to derive a design equation which more accurately predicts the force for orthogonal load situations.

Stress Concentration Table

One other opportunity for research is the unique stress concentration created by the eccentric loading of the $1-1$ leg design. A literature review revealed no documentation concerning this type of stress concentration. This stress concentration is different from all others in that loading does not occur in the same plane as the stress concentration but orthogonal to it. In other stress concentrations, the thickness of the work piece is nondimensionalized or not given whereas with a COPS stress concentration, the workpiece thickness may have a great deal of influence on it. The creation of this table would be a valuable design tool for estimating the true stress at the stress concentration from knowing the spring thickness, and the width and length of the leg segments. A study of this may be of benefit to more than COPS as this type of stress concentration is common in other compliant mechanisms.

Base and Platform Geometry

The truncation of base and platform geometry was done to simplify the analysis. It may be beneficial in the future to include both geometries in order to better understand how they affect performance characteristics of COPS such as the reaction

force, lateral stability, and stress stiffening. The addition of both will likely increase the semi-rigid effects decrease both the force and the stress levels and may also lower the ω_{cr}^2 for any given spring.

COPS Overall Lateral Stiffness

Lateral stiffness was defined as a COPS resistance to lateral loads on the platform. It may be possible to quantify lateral stiffness in COPS by laterally displacing the platform a specified amount over the range of 0° through a 120° (for a Tri leg design) and recording the reaction force. By plotting this vs the angle at which the displacement was applied, a mean and amplitude reaction force may be used to characterize lateral stability. Doing so and changing only a single parameter such as the leg angle, will provide more insight into the relationship between overall lateral stiffness and each design parameter.

Non-dimensional COPS Design Parameters

Non-dimensional parameters for modeling the behavior of COPS legs under complex loads was researched and their proved to be to many parameters to create a simple design tool. By narrowing the number to only those parameters which have the most effect on spring force, and using some of the trends noted in this research, it may be possible to come up with some simple analysis tools for helping a designer get an initial design much quicker.

Bibliography

[1] L. L. Howell, *Compliant Mechanisms*. New York: John Wiley & Sons, Inc., 2001.

[2] J. J. Parise, "Ortho-planar mechanisms," Master's thesis, Brigham Young University, Provo, Utah, 1999.

[3] J. J. Parise, L. L. Howell, and S. P. Magleby, "Ortho-planar linear-motion springs," *Mechanism and Machine Theory*, vol. 36, pp. 1281–1299, 2001.

[4] M. C. Anderson, N. O. Rasmussen, and M. Whiting, "Design of an ortho-planar spring for a continuously variable transmission." Brigham Young University, Provo, Utah, 2002.

[5] M. P. Christiansen, "Behavior of stacked ortho-planar springs in cvt's." Brigham Young University, Provo, Utah, 2003.

[6] S. T. Smith, *Flexures: Elements of Elastic Mechanisms*. The Netherlands: Gordon and Breach Science Publisher, 2000.

[7] N. Lobontiu, *Compliant Mechanisms: Design of Flexure Hinges*. New York: CRC Press, 2003.

[8] A. Midha, I. Her, and B. A. Salamon, "A methodology for compliant mechanisms design: Part i - introduction and large-deflection analysis," in *Advances in Design Automation* (D. A. Hoeltzel, ed.), vol. 2 of *18th Annual ASME Advances in Design Automation Conference*, pp. 29–38, ASME, 1992.

[9] N. M. Sevak and C. W. McLarnan, "Optimal synthesis of flexible link mechanisms with large static deflections," *Journal of Engineering for Industry*, vol. 74-DET-83, 1974.

[10] L. L. Howell, "The design and analysis of large-deflection members in compliant mechanisms," Master's thesis, Purdue University, West Lafayette, Indiana, 1991.

[11] G. K. Ananthasuresh and S. Kota, "Designing compliant mechanisms," *Mechanical Engineering*, vol. 117, pp. 93–96, 1995.

[12] D. W. Carroll, "Metamorphic process for compliant ortho-planar mechanism design," Master's thesis, Brigham Young University, Provo, Utah, 2002.

[13] S. P. Timoshenko, *History of Strength of Materials*. New York: McGraw-Hill, 1953.

[14] M. I. Frecker, S. Kota, and N. Kikuchi, "Optimal design of compliant mechanisms for smart sturctures applications," *SPIE*, vol. 3323, pp. 234–242, 1998.

[15] L. L. Howell and A. Midha, "A method for the design of compliant mechanisms with small-length flexural pivots," *Journal of Mechanical Design, Trans. ASME*, vol. 116, no. 1, pp. 280–290, 1994.

[16] L. L. Howell and A. Midha, "Parametric deflection approximations for end-loaded, large-deflection beams in compliant mechanisms," *Journal of Mechanical Design*, vol. 117, no. 1, pp. 156–165, 1995.

[17] L. L. Howell and A. Midha, "Parametric deflection approximations for initially curved, large-deflection beams in compliant mechanisms," in *Proceedings of the 1996 ASME Design Engineering Techinical Conferences*, 96-DETC/MECH-1215, 1996.

[18] B. J. Edwards, "A pseudo-rigid-body model for functionally binary pinned-pinned segments used in compliant mechanisms," in *Proceedings of the 25th Design Automation Conference*, DETC99/DAC-8619, 1999.

[19] S. P. Timoshenko and J. M. Gere, *Theory of Elastic Stability*. New York: McGraw-Hill, second ed., 1961.

[20] A. L. Herring, "High production manufacturing considerations for metallic compliant mechanisms with long thin beams," Master's thesis, Brigham Young University, Provo, Utah, 2001.

[21] A. Herring, L. L. Howell, S. P. Magleby, and R. H. Todd, "High production manufacturing considerations for metallic compliant mechanisms with long thin beams," in *DETC 2001/DFM-21184*, 2001.

[22] R. G. Weight, "High-torque capacity compliant centrifugal clutches," Master's thesis, Brigham Young University, Provo, Utah, 2004.

[23] C. Lusk, *Ortho-Planar Mechanisms for Microelectromechanical Systems.* PhD thesis, Brigham Young University, Provo, Utah, 2005.

[24] L. L. Howell and A. Midha, "Determination of the degrees of freedom of compliant mechanisms using the pseudo-rigid-body model concept," in *Proceedings of the 9th World Congress on the Theory of Machines and Mechanisms*, vol. 2, (Milano, Italy), pp. 1537–1541, 1995.

[25] W. D. Callister, *Materials science and engineering: an introduction.* John Wiley & Sons, Inc., fifth ed., 2000.

[26] W. C. Young and R. G. Budynas, *Roark's Formulas for Stress and Strain.* New York: McGraw-Hill, seventh ed., 2002.

[27] J. W. Wittwer and L. L. Howell, "Design of a functionally binary pinned-pinned segment for use as a tension-compression spring in compliant micro mechanisms," ASME International Mechanical Engineering Congress and Exposition, pp. 1–8, ASME, 2002.

[28] F. R. Stieg and W. S. Worley, "A rubber belt cvt for front-wheel drive cars," in *SAE Transaction 820746*, (Troy, Michigan), SAE, 1982.

[29] C. R. Mortensen, "Behavior models for compliant continuously variable transmissions," Master's thesis, Brigham Young University, Provo, Utah, 2000.

[30] N. H. Beachley and A. A. Frank, "Continuously variable transmissions: Theory and practice," tech. rep., Lawrence Livermore Laboratory, Livermore, California, 1979.

[31] W. S. Worley, "Designing adjustable-speed v-belt drives for farm implements," in *SAE Transactions*, 1954.

[32] L. R. Oliver, "Torque sensing variable speed v-belt drive," in *PT-30 Continuously Variable Transmissions for Passenger Cars*, SAE Paper 720708, Warrendale, PA: SAE, 1972.

[33] L. R. Oliver, K. G. Hornung, J. E. Swenson, and H. N. Shapiro, "Design equations for a speed and torque controlled variable ratio v-belt transmission," in *SAE Paper 730003*, International Automotive Engineering Congress and Exposition, SAE, 1973.

[34] B. G. Gerbert, "Adjustable speed v-belt drives: Mechanical properties and design," in *SAE Paper 740747*, Off-Highway Vehicle Meeting and Exposition, (Milwaukee, Wisconsin), September 1974.

[35] B. G. Gerbert, "Some notes on v-belt drives," in *ASME 80-C2/DET-91*, Intl. Power Trans. Gearing Conf, ASME, August 1980.

[36] T. F. Chen and C. K. Sung, "Design considerations for improving transmission efficiency of the rubber v-belt cvt," *International Journal of Vehicle Design*, vol. 24, no. 1, pp. 320–333, 2000.

[37] D. O. Bents, "Axial force and efficiency tests of fixed center variable speed belt drive," in *SAE Paper 810103*, 1981.

[38] F. Ferrando, F. Martin, and C. Riba, "Axial force test and modelling of the v-belt continuously variable transmission for mopeds," *Journal of Mechanical Design*, vol. 118, pp. 266–273, June 1996.

[39] K. E. Bisshopp and D. C. Drucker, "Large deflection of cantilever beams," *Quarterly of Applied Mathmatics*, vol. 3, no. 3, pp. 272–275, 1945.

[40] R. Frisch-Fay, *Flexible Bars*. Washington, D.C.: Butterworth, 1962.

[41] W. Gorski, "A review of literature and a bibliography on finite elastic deflections of bars," *Transactions of the Institution of Engineers, Australia, Civil Engineering Transactions*, vol. 18, no. 2, pp. 74–85, 1976.

[42] P. F. Byrd and M. D. Friedman, *Handbook of Elliptic Integrals for Engineers and Physicists*. Berlin: Springer-Verlag, 1954.

[43] H. Nahvi, *Static and Dynamic Analysis of Compliant Mechanisms Containing Highly Flexible Members*. PhD thesis, Purdue university, West Lafayette, Indiana, 1991.

[44] G. E. Forsythe and W. R. Wasow, *Finite Difference Methods for Partial Differential Equations*. New York: Wiley, 1960.

[45] J. R. Wright and M. L. Baron, "A survey of finite-difference methods for partial differential equation," in *Numerical and Computer Methods in Structural Mechanics* (S. J. Fenve, N. Perrone, A. R. Robinson, and W. C. Schnobrich, eds.), pp. 265–289, San Diego, CA: Academic Press, 1973.

[46] P. K. Kythe, *An Introduction to Boundary Element Methods*. Boca Raton, FL.: CRC Press, 1995.

[47] H. B. Harrison, "Post-buckling analysis of non-uniform elastic columns," *International Journal for Numerical Methods in Engineering*, vol. 7, pp. 195–210, 1973.

[48] R. E. Miller, "Numerical analysis of a generalized plane elastica," *International Journal for Numerical Methods in Engineering*, vol. 15, pp. 325–332, 1980.

[49] B. A. Coulter and R. E. Miller, "Numerical analysis of a generalized plane elastica with non-linear material behavior," *International Journal for Numerical Methods in Engineering*, vol. 26, pp. 617–630, 1988.

[50] I. Her, *Methodology for Compliant Mechanism Design.* PhD thesis, Purdue University, West Lafayette, Indiana, 1986.

[51] T. C. Hill and A. Midha, "A graphical user-driven newton-raphson technique for use in the analysis and design of compliant mechanisms," *Journal of Mechanical Design*, vol. 112, no. 1, pp. 123–130, 1990.

[52] T. G. Boronkay and C. Mei, "Analysis and design of muliple input flexible link mechanisms," *Journal of Mechanisms*, vol. 5, pp. 29–40, 1970.

[53] M. V. Gandhi and B. S. Thompson, "The finite element analysis of flexible components of mechanical systems using a mixed variational principle," in *ASME Design Engineering Technical Conference*, pp. 1–9, 1981.

[54] E. P. Golebiewski and J. P. Sadler, "Analytical and experimental investigation of elastic slider-crank mechanisms," *ASME*, 1976. ASME Paper No. 76-DET-18.

[55] D. J. Peery and J. J. Azar, *Aircraft Structures.* College Custom, New York: McGraw-Hill, second ed., 1982.

[56] K. Tai, G. Y. Cui, and T. Ray, "Design synthesis of path generating compliant mechanisms by evolutionary optimization of topology and shape," *Journal of Mechanical Design*, vol. 124, pp. 492–500, September 2002.

[57] S. Kota, J. Joo, S. M. Rodgers, and J. Sniegowski, "Design of compliant mechanisms: Applications to mems," *Analog Integrated Circuits and Signal Processing-An International Journal*, vol. 29, pp. 7–15, 2001.

[58] G. K. Ananthasuresh and M. I. Frecker, *Optimal Synthesis with Continuum Models*, ch. 9, pp. 301–335. John Wiley & Sons, Inc., first ed., 2001.

[59] L. L. Howell and A. Midha, "The development of force-deflection relationships for compliant mechanisms," in *Machine Elements and Machine Dynamics*, vol. 71 of *23rd ASME Biennial Mechanisms Conference*, pp. 501–508, ASME, 1994.

[60] A. Saxena and S. N. Kramer, "A simple and accurate method for determining large deflections in compliant mechanisms subjected to end forces and moments," *Journal of Mechanical Design*, vol. 120, pp. 392–400, 1998.

[61] C. Kimbal and L.-W. Tsai, "Modeling of flexural beams subjected to arbitrary end loads," *Journal of Mechanical Design*, vol. 124, pp. 223–235, 2002.

[62] S. M. Lyon, *The Pseudo-Rigid-Body Model for Dynamic Predictions of Macro and Micro Compliant Mechanisms.* PhD thesis, Brigham Young University, Provo, Utah, 2003.

[63] M. H. Dado, "Variable parametric pseudo-rigid-body model for large-deflection beams with end loads," *International Journal of Non-Linear Mechanics*, vol. 36, pp. 1123–1133, 2000.

[64] J. Derderian, "The pseudo-rigid-body model concept and its application to micro compliant mechanisms," Master's thesis, Brigham Young University, Provo, Utah, 1996.

Appendix

Appendix A

Continuously Variable Transmissions (CVT)

A CVT has been shown to be more efficient than traditional transmissions. Stieg et. al. [28] showed that a rubber v-belt CVT for a front wheel drive car was 17.7% more efficient mechanically and 15.5% more efficient in fuel economy than a 3 speed automatic transmission in the same vehicle. Some of the other advantages of CVT's are a smooth speed change, lower cost, less maintenance, and in many cases they are a simpler mechanism.

A.1 Types

A CVT is a device that can take on any speed ratio that is found within its operational limits [29]. Beachley et. al. [30] stated that a CVT also implies that torque may be controlled independent of the speed ratio. The speed ratio is defined as the maximum to minimum output speeds possible for a given fixed input speed.

Beachley [30] discussed 5 principles upon which CVT's may operate: hydrostatic, friction, variable geometry, electric, and gearbox with slip clutch. All have their own mechanisms to transfer a variable amount of torque and speed. Any one of the five can be an infinitely variable transmission as well if it has the ability to produce zero output. Mortensen [29] created a sixth class by breaking the friction drives into two separate categories: friction drives and traction drives. Friction drives would include those whose relative motion between the transfer medium is static (i.e. a belt in contact with a sheave has no relative motion). A traction drive transmits power through hardened metallic rolling bodies and elastohydrodynamic fluid films.

A.2 V-Belt CVT's

The type of most interest to this work is a friction drive utilizing a composite v-belt and two pulleys. The pulleys consist of two sheaves each, one mobile and one stationary, which move together or apart according to a supplied axial force. These pulleys are also referred to as a driver or primary clutch and the driven or secondary clutch. The most common system consists of a velocity sensing driver and a torque sensing driven as shown in Figure A.1. This type of system is common in recreational vehicles, mopeds, agricultural equipment, machine tools, and some automobiles.

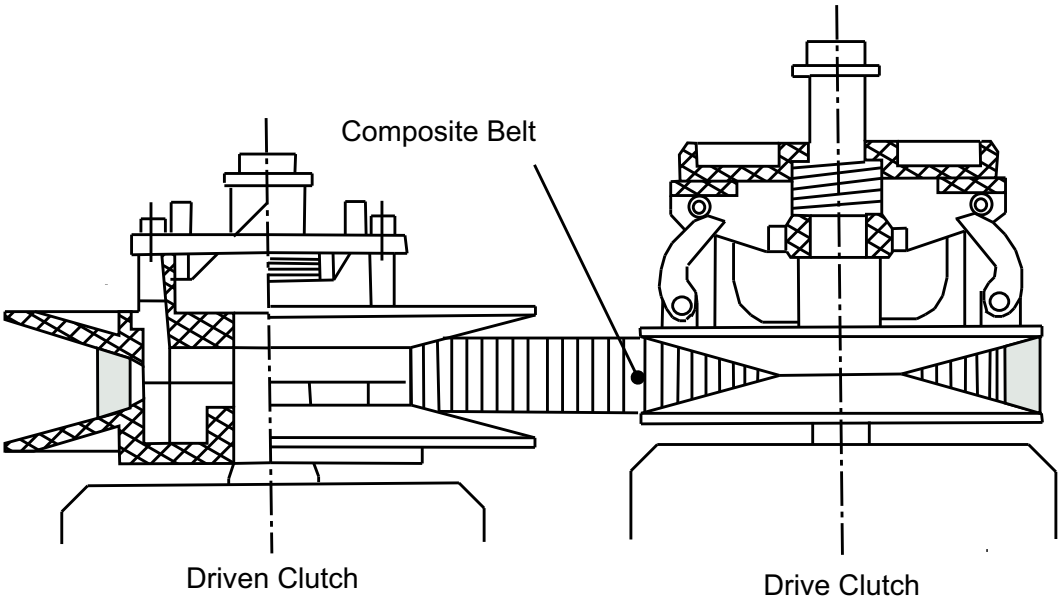

Figure A.1: Composite v-belt continuously variable transmission schematic.

Worley [31] was one of the first to publish literature on the design of adjustable-speed v-belt drives. Worley proposed belt standards along with information on how to design belts to those standards. He also stated that the sheave diameter is derived from the speed ratio.

Oliver [32] discussed the advantages of a torque sensing v-belt drive and made general recommendations for designing new ones. He also discussed the benefits

of torque actuated tensioning. Later Oliver [33] developed design equations which model the behavior of a speed and torque controlled variable ratio v-belt transmission. These fundamental equations allow a designer to analyze the axial forces present in a speed sensing driver and a torque sensing driven. The equations were based on the assumption of a constant friction angle between the sheaves and the belt. The effects of friction between the mobile sheave and shaft under belt tension were neglected.

Gerbert [34] investigated both manually and automatically regulated adjustable v-belt drives. Simple relationships were established and system drive characterizations were obtained for various combinations of axial loading equipment. Gerbert [35] later added to his original work.

Chen [36] described two types of losses in a rubber v-belt CVT: speed and torque. Three loss models were mentioned along with their characteristics. Chen proposed a method for modeling the belt system operating under four separate states. Power loss mechanisms were broken down and their relative significance to overall power loss quantified. The effects of belt parameters on efficiency were also studied.

Bents [37] stated that the most important part of designing a variable speed drive is the control system that actuates the mobile sheave. This system controls both the speed ratio and the belt tension. The key to a workable control system is the characterization of the drive parameters and their interactions. Bents also discussed the relationship between centerline and axial forces with the power transmitting efficiency. Stieg [28] discussed three criteria that must be met by the axial forces supplied by the control mechanism in a driver/driven system.

1. The belt should not slip under any load condition.

2. The axial forces should be as low as possible to maximize belt life.

3. The CVT speed ratio should be controlled to obtain the desired engine operating line.

A.3 Velocity Sensing Clutch

The velocity sensing clutch has evolved into a highly tunable part of a v-belt CVT system. The analysis of the axial forces generated in this clutch and how the main components interact with each other are critical to performance.

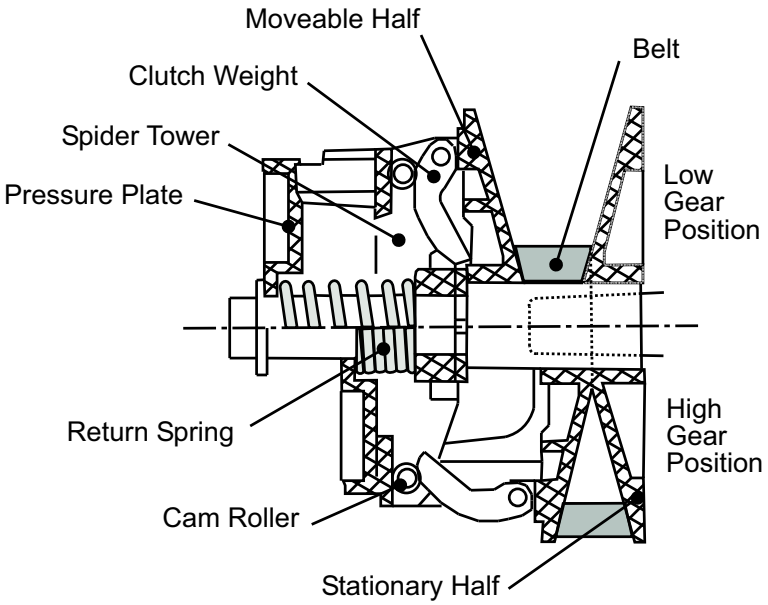

Figure A.2: A typical velocity sensing driver clutch at high and low gear ratios.

A basic driver clutch in a v-belt CVT utilizes a system of cams, weights, and springs to change its ratio. The weights pivot on the mobile sheave and have a cam profile which contacts cam rollers attached to the spider tower structure. The centrifugal forces cause the weights to extend which in turn push the mobile sheave toward the fixed sheave. This motion is resisted by the return spring pushing on the pressure plate. As the angular velocity in the engine increases the centrifugal forces on the weights overpower the return spring. As the velocity decreases the spring force becomes greater than the centrifugal forces and the sheaves are moved back apart.

There is a complex relationship between the angular velocity, weight, cam profile, and properties of the spring. Understanding the axial forces is critical to proper design.

There have been numerous models proposed for understanding the axial forces in a velocity sensing clutch. Ferrando [38] summarized and compared the various models used for predicting axial forces with a new empirical model developed therein. Ferrando showed that Gerbert's model [35] of the velocity-sensing driver was the most accurate for predicting axial forces when compared with experimental data.

A.4 CVT's & COPS's

Anderson et. al [4] articulated the possible benefits of applying COPS to a velocity sensing CVT. A CVT utilizing COPS would be more tunable to the novice recreational vehicle driver through adding or removing a COPS vs. purchasing a new coil spring for each desired setting. Additionally, the design would also provide benefits such as simplified part count, lower costs through manufacture and assembly, and decreased weight and space requirements. A prototype compliant ortho-planer spring was developed at Brigham Young University for use in a CVT with the objective of testing its feasibility under dynamic loads.

A number of configurations were designed to fit within the constraints of the existing P-90 Polaris driver clutch. Figure A.3 shows a CAD model of the P-90 and the modifications one might do to adapt a COPS to it. CAD models of COPS were developed and finite element analysis was used to confirm the calculated stresses. The N8S COPS design, shown in Figure 2.4, was selected as the prototype. Calculated stresses in the leg-platform, leg-base, and intermediary platform transition areas would lead to premature failure. Other problems were encountered in removing the pressure plate used by the pressure spring. One of its purposes is to provide a second bearing surface along the shaft for supporting the mobile sheave under the large moment created by belt tension.

Christiansen [5] experimentally determined the fatigue life of the N8S design subjected to simple quasi-static loads. At full deflection to one side it's fatigue life was found to be under 50,000 cycles. Adding centrifugal loads, vibrations, and

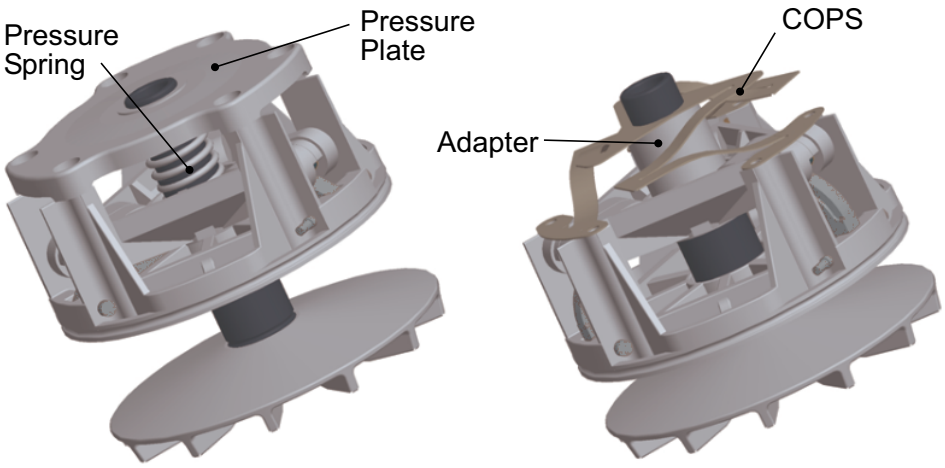

Figure A.3: A rendition of the P-90 Polaris Drive Clutch (a) and a COPS adapted to fit within the existing design.

other dynamic loads will decrease fatigue life further. A three factorial design using the spring constant, lubrication between layers, and hysteresis was performed under controlled conditions. Hysteresis and lubrication were insignificant while stacking was significant. Christiansen confirmed that COPS spring constants have a near linear relationship and can be added with a fair amount of accuracy to increase the total stiffness or K value of the COPS pack.

Appendix B

Compliant Mechanisms Analysis Methods Overview

B.1 Closed Form Methods

These methods employ the Bernoulli-Euler equation and elliptic integrals to derive closed form solutions which describe the beam path under certain loads. Howell [1] gives a brief history of key findings for closed form solutions of these types. Bisshopp & Drucker [39] were some of the first ones to employ the use of elliptic integrals of the first and second kind to this particular problem. Others contributed to the knowledge tables and summaries [40, 41].

Howell [10] reviewed the assumptions used for linearized beam equations and the reasons they are inadequate for large deflection analysis. When using the Bernoulli-Euler beam equation for small deflections the key assumption is that the slope of the transverse deflection is small which is not the case under large deflections.

The closed form solution for the deflection of a cantilever beam with combined end loads was derived by solving the Bernoulli-Euler equation for an initially curved beam for both follower and nonfollower loads [10]. The results were nondimensionalized and put in a form such that elliptic integrals of the first and second kind [42] could be used to solve them. The simple load case of a moment applied to the free end of a cantilever beam was presented.

Limitations of this type of derivation for both follower and nonfollower loads are due to the square roots and inverse trigonometric functions used in the elliptic integral solution. Nondimensionalized beam tip deflections were presented as functions of nondimensional parameters in graphical form [10]. They can be used to find

beam end coordinates for various loads, moments, modula, and beam dimensions for this particular load case given that the input stays within the specified limitations of the model. Although the resultant closed form solutions minimize the required computation time they are still by no means simple. Besides not having a physical representation of what is going on, this method can only be used on a limited number of geometries and load cases.

B.2 Numerical Methods

Numerical methods are good for determining both displacements and stresses in compliant mechanisms. There are a few instances when this type of method may have an advantage over others. First, when mechanism geometry already exists and the model needs either validation or further refinement. Second, these methods also become extremely valuable when the geometry of the mechanism does not lend itself well to other methods of analysis. In other words the geometry is too complex to be analyzed by simple models. This section will be limited to chain algorithms and finite element analysis. Nahvi [43] compared the behavior of finite element methods with the chain algorithm and found that the chain algorithm is more efficient in its computation. Finite element methods are powerful for complex geometry but inefficient for solving simpler models. They will briefly be discussed but there are other numerical methods which may be used such as the finite difference methods [44, 45] and boundary element methods [46].

Chain Algorithm The chain algorithm has been used by many to solve nonlinear problems [47, 48, 49]. Her [50] was the first to use the algorithm to analyze compliant mechanisms. It was subsequently improved upon by others [51, 43]. The chain algorithm has been verified against closed form solutions [50, 10].

The chain algorithm works by breaking the model up into a number of beam elements. Each element is analyzed in succession and then its results are used as inputs to the next element. Each element will have its own translations and rotations, which will be added to the deflections of the previous element. Thus each element is

analyzed as a deflected beam at the end of the previous one. See [10] for a detailed explanation on the chain algorithm.

The chain algorithm is a tool for solving nonlinear problems. Nonlinearities occur as the system changes, over the application of the load, and it becomes necessary to recalculate the moment arms and the matrices used for calculating displacements. Solution accuracy is proportional to both the number of load increments or steps used during the analysis and on the number of elements. Howell [10] has some useful graphs relating the absolute error associated with the number of load increments and the number of elements.

Finite Element Methods Boronkay & Mei [52] were the first to use this method for analyzing compliant mechanisms. They used finite element methods for analyzing a mechanical adder in which the pivot points were replaced with flexible members. A basic overview of how the method works was also presented.

Ghandi & Thompson [53] used FEA on a flexible connecting rod and found the results to be very similar to those obtained by others [54] applying a different method for the same geometry.

There are two types of finite element methods, the stiffness and flexibility methods. The stiffness method relates forces to corresponding displacements and the flexibility method is vice versa. Finite element methods are particularly useful when simple analytical models may no longer be applied with ease to a problem. It is the most widely used method of structural analysis for complex structures. A number of centuries ago the method was time consuming because of the lack of adequate computing power. Modern computers now have the capacity, in both time and memory, to evaluate extremely complicated problems [55].

Howell [1] gave some advice on using finite element methods for nonlinear analysis of compliant mechanisms.

- Ensure that the program you are using supports non-linear analysis and that this analysis capability is activated before solving. Also make sure that output graphics are shown to scale and not disproportioned.

- Simplify the model as much as possible. The nonlinearities associated with large displacements will add complexity to the computation as well as increase the required time. A simplified model will increase the possibility of converging to a solution.

- Use displacement loads for the inputs instead of force for large deflections in compliant mechanisms. This is emphasized for complex nonlinear analysis.

The details of this method can be found in a number of books and articles, so no further discussion is felt to be necessary for this thesis.

B.3 Structural Optimization & Homogenization Theory

Structural optimization and homogenization theory is a systematic design method which utilizes a series of tools and techniques to synthesize and analyze compliant mechanisms.

Sevak et. al. [9] used this method to successfully analyze a four bar linkage with compliant input and output linkages and a flexible coupler mechanism. Sevak's work validated the capability this design methodology has to successfully analyze and synthesize flexible link mechanisms.

Frecker et. al. [14] used this type of method for designing compliant stroke amplifiers. Tai et. al [56] used this method for synthesis of path generating compliant mechanisms. Others have used this methodology for creating compliant mechanisms on the micro level [57].

Unlike the PRBM, topology optimization uses continuum solid mechanics instead of rigid-body kinematics for mechanisms analysis and synthesis [58]. Tai et. al. [56] stated that there is also a ground structure approach which is used for designing frame or truss like structures. Both of these methods are aimed at creating distributed compliance in mechanisms as opposed to lumped compliance. Distributed compliance is the practice of having a large portion of the mechanism deform to get its motion.

The general inputs for structural optimization are an objective function, a design domain, prescribed force-deflection characteristics of the mechanism, and the

material properties. The design domain is the physical space that the resulting mechanism could occupy. Creating a mechanism from this empty space does not limit the possible configurations to known geometries that work. As mentioned before a series of design methodologies are used to process the inputs and obtain the results. Frecker & Ananthasuresh [58] list the methods and techniques they have identified as useful tools in optimal synthesis with continuum models.

Ananthasuresh et. al. [11] gives a simplified overview of structural optimization and suggests that future work should seek to create a hybrid method which incorporates kinematics with the continuum approach.

B.4 Pseudo-Rigid-Body Model

The purpose of the pseudo-rigid-body model (PRBM) is to provide a simplified method of analyzing systems that undergo large, nonlinear deflections. It is used to model compliant members using rigid-body components that have equivalent force-deflection characteristics. Its use allows rigid-body theory to be directly applied to compliant mechanisms. One advantage the PRBM has over other types of analysis is that it has a graphical model depicting its geometry.

This model was first researched and documented by Howell [10, 59]. Since that time there have been numerous models created for different types of compliant segments, deflection characteristics, and load cases. Howell [1] cites a number of PRBM's for many of these cases: small length flexural pivots [15], fixed-pinned or cantilever beams with an end force on the free end [16], fixed-guided segments [1], beams with end-moment loads [1], initially curved cantilever beams [17], pinned-pinned segments [18], and fixed-fixed segments [1]. There are also several papers on modeling combined end force and moment loads on fixed-pinned beams [60, 61, 62]

Dado [63] parameterized the load, P, and joint stiffness, K, with respect to the characteristic length factor, γ, and the pseudo-rigid-body angle, Θ, for a large deflection beam with end loads. His findings for the beam end path were comparable to those found in [59]. Dado's equations proved to be more accurate than using simple constant values for, γ, and k.

Derderian [64] explored the PRBM and its application to MEMS. In his work he studied parallel motion mechanisms in depth of which some use fixed-guided segments to achieve their motion. Fixed-guided segments are of particular interest to this study because a leg in a COPS design will be comprised of segments. The PRBM will be the first step in analyzing COPS designs and a basic overview of a cantilever beam and a fixed-guided beam will follow.

An important thing to note about the fixed-guided beam is that the inflection point somewhere along the beam has no curvature and therefore has no moment. If both beam ends are held at a 0 deg angle then the inflection point will occur in the middle of the beam. The segment can be split into two beams at the inflection point, and each can be modeled as a single cantilever beam with half the vertical displacement load as the fixed-guided segment. A diagram of such a cantilever beam, it's pseudo-rigid-body model, and key parameters can be seen in Figure B.1.

The only load situations in a COPS that can be analyzed using the PRBM are orthogonal loads. Even though a segment in a leg, like the one shown in Figure B.2, can be analyzed with the PRBM, there are still differences in beam end constraints which make it less useful in this situation.

PRBM for a Cantilever Beam The derivation of the PRBM for a cantilever beam with a load on the free end is discussed in detail in [10, 16]. Here is given a quick summary of the method used to derive it and the resulting equations pertinent to this thesis. Because there are few differences between the PRBM for a cantilever beam and a fixed-guided segment, only the differences will be pointed out.

The model assumptions included linearly elastic, inextensible, rigid in shear, and of constant cross section beams. Howell [10, 16] derives the equations describing the free-end coordinates (a, b) of the cantilever beam subject to a vertical force of P and a horizontal force of nP, where n is the axial load factor, as shown in Figure B.1.

The PRBM is a result of manipulating closed form solutions found using the Bernoulli-Euler equation and elliptic integrals. The data derived from these solutions was nondimensionalized by division of the beam length and plotted against each

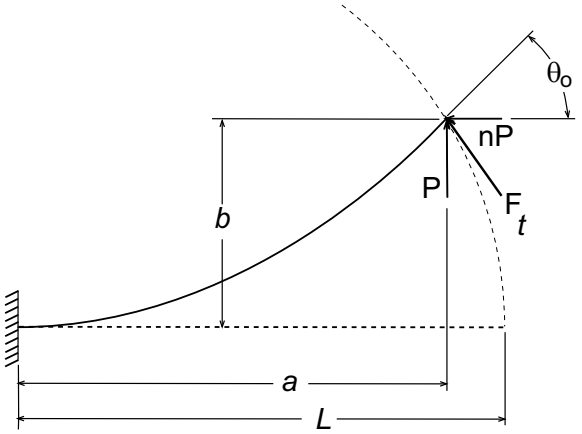

(a)

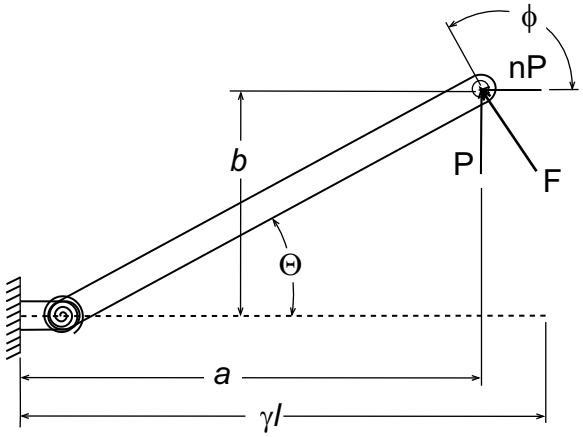

(b)

Figure B.1: (a) A cantilever beam with an end load (b) and it's pseudo-rigid-body model.

other. There were two significant results which form the basis of the parametric approximations for the PRBM. First, the deflection paths were similar over the load conditions $n = -5 \ldots 10$. Second, the paths were nearly circular in shape until the beam tip angle, θ_o, approached the equivalent applied load angle, ϕ, where $\phi = \tan^{-1}(\frac{1}{-n})$ and n is the axial load factor.

The center of the nearly circular path of the beam end lies at a point somewhere on the beam. At this point the model is divided into two rigid links connected by a pin joint. A torsional spring is also placed at the pivot to model the beams resistance

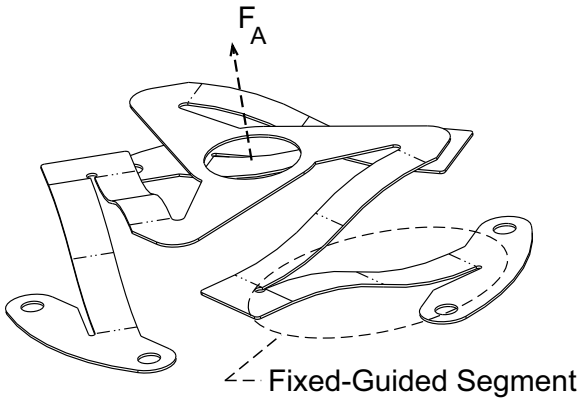

Figure B.2: COPS legs consist of segments which are easily analyzed under static load cases.

to deflection. The characteristic radius factor, γ, determines the length or radius, γl of the pseudo-rigid-body link and the location of the characteristic pivot on the cantilever beam.

The beam end point locations, beam end angle, and the load-deflection relationship were all parameterized with respect to the pseudo-rigid-body angle, Θ. The pseudo-rigid-body angle was maximized by solving for a γ which kept the error between the closed form solution and the PRBM prediction below 0.5%. The resulting piecewise functional relationship for γ as a function of the axial force coefficient, n, is

$$\gamma = \begin{cases} 0.841655 - 0.0067807 \cdot n + 0.000438 \cdot n^2 & (0.5 < n < 10.0) \\ 0.852144 - 0.0182867 \cdot n & (-1.8316 < n < 0.5) \\ 0.912364 + 0.0145928 \cdot n & (-5 < n < -1.8316) \end{cases} \tag{B.1}$$

Discrete values of γ can be found in Table B.1. The coordinates at the free end of the beam are described by

$$a = l(1 - \gamma(1 - \cos\Theta)) \tag{B.2}$$

$$b = \gamma l \sin \Theta \tag{B.3}$$

The beam end angle, θ_o, can be found using the parametric angle coefficient, c_θ and is described by

$$\theta_o = c_\theta \Theta \tag{B.4}$$

The torsional spring constant is

$$K = \gamma K_\Theta \frac{EI}{l} \tag{B.5}$$

where K_Θ is the stiffness coefficient. Values for K_Θ are also a function of the axial load coefficient and can be found using the following piecewise equation.

$$K_\Theta = \begin{cases} 3.024112 + 0.121290 \cdot n \\ \quad +0.003169 \cdot n^2 & (-5.0 < n < -2.5) \\ 1.967647 - 2.616021 \cdot n \\ \quad -3.738166 \cdot n^2 - 2.649437 \cdot n^3 \\ \quad -0.891906 \cdot n^4 - 0.113063 \cdot n^5 & (-2.5 < n < -1.0) \\ 2.654855 - 0.0509896 \cdot n \\ \quad -0.0126749 \cdot n^2 - 0.00142039 \cdot n^3 \\ \quad +0.584525 \cdot 10^{-4} \cdot n^4 & (-1.0 < n < 10) \end{cases} \tag{B.6}$$

Table B.1 shows specific values of γ, Θ, and K_Θ for calculating the beam end coordinates and the torsional spring constant for different values of the axial load coefficient, n. In order to get an accurate position prediction the pseudo-rigid-body angle must stay under $\Theta_{max}(\gamma)$ and for an accurate force prediction $\Theta_{max} < \Theta_{max}(K_\Theta)$.

The vertical force is a function of the load angle, ϕ, the stiffness coefficient, and other parameters.

Table B.1: Data for γ, c_θ, and K_Θ as a function of angles and force.

n	ϕ	γ	$\Theta_{max}(\gamma)$	c_θ	K_Θ	$\Theta_{max}(K_\Theta)$
0	90.0	0.8517	64.3	1.2385	2.67617	58.5
0.5	116.0	0.8430	81.8	1.2430	2.63744	64.1
1.0	135.0	0.8360	94.8	1.2467	2.61259	67.5
1.5	146.3	0.8311	103.8	1.2492	2.59289	65.8
2.0	153.4	0.8276	108.9	1.2511	2.59707	69.0
3.0	161.6	0.8232	115.4	1.2534	2.56737	64.6
4.0	166.0	0.8207	119.1	1.2548	2.56506	66.4
5.0	168.7	0.8192	121.4	1.2557	2.56251	67.5
7.5	172.4	0.8168	124.5	1.2570	2.55984	69.0
10	174.3	0.8156	126.1	1.2578	2.56597	69.7
-0.5	63.4	0.8612	47.7	1.2348	2.69320	44.4
-1.0	45.0	0.8707	36.3	1.2323	2.72816	31.5
-1.5	33.7	0.8796	28.7	1.2322	2.78081	23.6
-2.0	26.6	0.8813	23.2	1.2293	2.80162	18.6
-3.0	18.4	0.8669	16.0	1.2119	2.68893	12.9
-4.0	14.0	0.8522	11.9	1.1971	2.58991	9.8
-5.0	11.3	0.8391	9.7	1.1788	2.49874	7.9

$$P = \frac{K_\Theta \Theta}{\eta \gamma l_s \sin(\phi - \Theta)} \tag{B.7}$$

where

$$\eta = \sqrt{1 + n^2} \tag{B.8}$$

The static stress at the bottom and top of the beam can be found by

$$\sigma = \pm \frac{-(Pa + nPb)c}{I} - \frac{nP}{A} \tag{B.9}$$

where c is the distance from the neutral axis to the outer fibers.

PRBM for a Fixed-Guided Segment Figure B.3 depicts a fixed-guided segment with its PRBM model. There are several differences between the analysis of this type and that of the cantilever beam. First, the division of the beam occurs in two places now creating two characteristic pivots equally spaced from the ends. Equation B.5 for the torsional spring constant, K, changes to

$$K = 2K_\Theta \gamma \frac{EI}{l} \tag{B.10}$$

Note that there are now two characteristic pivots with torsional springs and the stiffness of a fixed-guided beam is four times greater than a cantilever beam of the same length.

Because there is no horizontal force component in a fixed-guided beam for a COPS under static loads, the fundamental equations become simple derivations of the

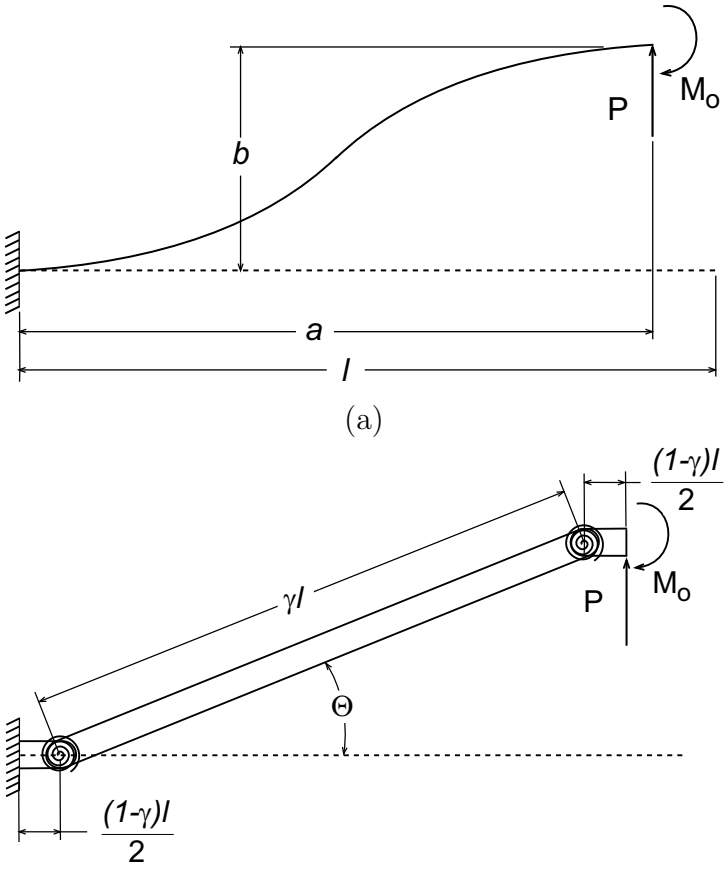

Figure B.3: (a) A fixed-guided segment with an end load (b) and it's pseudo-rigid-body model.

cantilever beam equations. Values of γ and K_θ become discrete at 0.8517 and 2.67617 respectively and the beam end has an applied moment now so that $\theta_o = 0$.

For a given vertical displacement, b, of a fixed-guided segment, the pseudo-rigid-body angle can be found by

$$\Theta = \arcsin\left(\frac{b}{\gamma l}\right) \tag{B.11}$$

This can then be used to find the horizontal displacement, a of the beam end with the following

$$a = l\,(1 - \gamma(1 - \cos\Theta) \tag{B.12}$$

The vertical force, P, for both springs is four times as stiff as that of the cantilever beam and is

$$P = \frac{4K_\Theta \Theta EI}{L^2 \cos\left(\Theta\right)} \tag{B.13}$$

An estimation of the total axial force a COPS can produce is found by multiplying P by the number of legs. With the vertical load force and the moment arm known the stress at both ends of the beam can be found with

$$\sigma_{max} = \frac{2K_\Theta Ec(1 - \gamma(1 - \cos\Theta))\Theta}{L\cos\Theta} \tag{B.14}$$

where c is the distance to the outer fibers. Check that $\Theta < \Theta_{max}(K_\Theta)$ to make sure the results are accurate.

Appendix C

ANSYS Batch Files

C.1 3D PRBM Beam Batch File

```
!=================================================================
!  Created by Nathan Rasmussen, 02/18/2004
!  This batch file uses 3D Elements to deflect a
!  beam in two dimensions.
!  RECTANGULAR CROSS-SECTION
!  /|
!  /|-------------------------
!  /|
!=================================================================
FINISH
/CLEAR
/TITLE,Analysis of a 3D-Cantilever Beam
/PREP7

!=================================================================
!               INPUT PARAMETERS
!=================================================================
!tz = 8             !*** Width of beam
!ty = 2             !*** Thickness of beam
!L = 130            !*** Length of beam
!
!Ey = 207000000
!Pr = 0.28
!
```

```
!rSteps=30          !*** Number of load steps
!nonlinear=1        !*** 1 = nonlinear, 0 = linear
!
!size=5             !*** 1 to 10 for fine to coarse meshing
!
!dz = .2            !*** Limit in z direction
!dy = .5            !*** Limit in y direction
!contours = 20
!contournumber = 11 !0 TO (CONTOURS) 0 IS ONLY Y AND 19 IS Z
!pi = 3.1415926
!theta = ((pi/2)/contours)*contournumber
!
!r = SQRT(((COS(theta)**2)/(dy**2)+(SIN(theta)**2)/(dz**2))**(-1))
!
!
!***  coordinates to end at
!dY = r*cos(theta)*L
!dZ = r*sin(theta)*L
!
! === Read from input file ===
/INPUT,ANSYS_3Dcant_inputs,txt

!=================================================================
!               MODEL SETUP
!=================================================================

!*** Base Face
K,1,0,0,0
K,2,0,-ty/2,0
K,3,0,ty/2,0

!*** Beam Tip
K,4,-L,ty/2,0
K,5,-L,-ty/2,0

!***  Beam Lines
```

```
L,1,2
L,1,3
L,3,4
L,2,5
L,4,5

!***   Beam Areas
AL,ALL

VEXT,1,1,1,0,0,tz/2,0,0
VEXT,1,1,1,0,0,-tz/2,0,0
VADD,1,2

!***Element Type: 3-D Structural Solid (20-Node)***
ET,1,SOLID186
MP,EX,1,Ey      !*** Youngs Modulus ***
MP,PRXY,1,Pr    !*** Poisson Ratio ***

VATT,1,,1,0
!SMRT,ON
SMRT,5      !*** Size, 1--fine, 10--course
MSHAPE,1,3D !*** Shape, 0--hexahedral, 1--tetrahedral
MSHKEY,0    !*** Key, 0--free, 1--mapped, 2--mapped if possible

!ESIZE,ty/3,0,
VMESH,ALL

!***Get Node Number at KeyPoint 1***
KSEL,s,kp,,1
NSLK,s
*GET,nkp1,node,0,num,max
NSEL,all
KSEL,all

FINISH
```

```
!=================================================================
!                        SOLUTION STEPS
!=================================================================
/SOLU

!**** Set to Nonlinear Deflection Analysis ****
*IF,nonlinear,EQ,1,THEN
  SOLCONTROL,ON     !*** Steps optimized for nonlin probs
  DELTIM            !*** Use default substeps
  NLGEOM,1          !*** For large deflection analysis
  CNVTOL,U,,0.0001,,0.01        !*** Convergence for Displacement
  CNVTOL,F,,0.0001,,0.01        !*** Convergence for Force
*ENDIF
ANTYPE,0            !*** Analysis Type is Static (0)

!*** Constraint Support
DA,5,ALL,0
DA,11,ALL,0

!---------------------- Apply a Displacement ------------------
*DO,mm,1,rSteps,1
  DK,1, ,mm*dY/rSteps, ,0,UY, , , , , , !*** take out first UY
  DK,1, ,mm*dZ/rSteps, ,0,UZ, , , , , , !*** take out first UZ
   lswrite,mm
*ENDDO

lssolve,1,rSteps

FINISH

!=================================================================
!                  OUTPUT for GUI MODE
!=================================================================

/POST1
```

```
*DIM,Xdis,TABLE,rSteps
*DIM,Ydis,TABLE,rSteps
*DIM,Zdis,TABLE,rSteps
*DIM,Yforce,TABLE,rSteps
*DIM,Zforce,TABLE,rSteps

mm = 0
*DO,mm,1,rSteps,1
  SET,mm
  *GET,disX,NODE,nkp1,U,X
  *SET,Xdis(mm),disX
  *GET,disY,NODE,nkp1,U,Y
  *SET,Ydis(mm),disY
  *GET,disZ,NODE,nkp1,U,Z
  *SET,Zdis(mm),disZ
  *GET,forceY,NODE,nkp1,RF,FY
  *SET,Yforce(mm),forceY
  *GET,forceZ,NODE,nkp1,RF,FZ
  *SET,Zforce(mm),forceZ
*ENDDO

! ************* The results file will be named
*VPLOT,Xdis(1,1),Ydis(1,1)
/output,ANSYS_3Dcant_results.txt
*VWRITE
                Xdis                 Ydis                 Zdis
               Yforce               Zforce
*VWRITE,Xdis(1),Ydis(1),Zdis(1),Yforce(1),Zforce(1)
%20e %20e %20e %20e %20e
/output

FINISH

/eof
```

C.2 COPS Leg Batch File

```
!=================================================================
!  ANSYS Batch File
!  Created by Nathan Rasmussen, 14 January 2005
!=================================================================
!
FINISH
/CLEAR
/TITLE, Angle Study on Ortho-Planar Spring Leg
/PREP7
!
!=================================================================
!                       INPUT PARAMETERS
!=================================================================
!pi=ACOS(-1)
!== Geometry ====================================================
!st = .000508           !thickness of spring
!lw = .01.7             !leg length
!ll = .07239            !leg width
!lrad = .003175         !gap width
!ip = .0127             !intermediate platform depth
!ipf = .5*ip            !intermediate platform fillet
!platrad = .00381       !platform radius
!legang = 135           !leg angle 0-135
!
!==-Material=============================================================
!Ey = 207000000000      !modulus of elasticity
!Pr = .30               !poissons ratio
!De = 7850              !density for inertial loads
!
!== Mesh Parameters=============================================
!gelsize =.00254        !global element size
!radsegs = 30           !# of divisions for meshing
!legsegs = 20           !# of divisions-lines close to ip rad
!legskew = .1           !skew of legseg lines
```

```
!
!== DOF Constraints=============================================
!zdisp = .0254          !othogonal displacement-m
!angvelz = 0            !angular velocity $(rad/s)$
!angaccz = 0            !angular acceleration-$(rad/s^2$
!
!== Number of Steps ============================================
!rSteps = 10
!nonlinear = 1 \        !1=true
!
!================================================================
!            Read from input file
!================================================================
/INPUT,ANSYS_anglestudy_inputs,txt

!== Set ElementType ============================================
ET,1,SHELL181
!== Set Options for Element ====================================
KEYOPT,1,1,0
KEYOPT,1,3,2
KEYOPT,1,8,2
KEYOPT,1,9,0
KEYOPT,1,10,0
ETCONTROL,SUGG,OFF

!== Set the Real Constants =====================================
R,1,st, , , , , ,

!== Set Material Properties=====================================
MP,EX,1,Ey
MP,PRXY,1,Pr
MP,DENS,1,De

!== Turn Degenerate Elements Off ===============================
ETCONTROL,SUGG,OFF
```

```
!================================================================
!                  Create Geometry
!================================================================
!== Keypoints ======================================================
K,1,lw/2,,,
K,2,-lw/2,,,
K,3,-(lw/2+2*lrad),,,
K,4,-(lw/2+2*lrad+lw),,,
K,5,-(lw/2+2*lrad+lw),ll,,
K,6,-(lw/2+2*lrad),ll,,
K,7,-lw/2,ll,,
K,8,lw/2,ll,,
K,9,lw/2,(ll+ip+lrad),,
K,10,-(lw/2+2*lrad+lw),(ll+ip+lrad),,
K,11,-(lw/2+lrad),(ll+lrad-.0001),,
K,12,-lw/2,(ll-lw),,
K,13,-(lw/2+2*lrad),(ll-lw),,
K,14,-(lw+2*lrad),,,        !*This will be the key point
!== Lines ======================================================
LSTR,1,2
LSTR,3,14
LSTR,14,4
LSTR,4,5
LSTR,5,6
LSTR,13,3
LSTR,12,2
LSTR,8,7
LSTR,8,1
LSTR,8,9
LSTR,9,10
LSTR,5,10
LSTR,12,7
LSTR,13,6

!== Create Arc ==================================================
LARC,7,6,11
```

```
!== Create Fillets ============================================
LFILLT,11,10,ipf, ,
LFILLT,12,11,ipf, ,

!== Create Areas ==============================================
AL,1,7,13,8,9
AL,2,3,4,5,6,14
AL,5,8,10,11,12,15,16,17

!== Move Geometry and change angle=============================
*AFUN,DEG            !sets angle types used in functions
AGEN, ,ALL, , ,platrad*sin(-legang),platrad*cos(legang), , , ,1

!== Global Element Mesh Size ==================================
ESIZE,gelsize,0,

!== Break up important lines for meshing ======================
!== Short Lines on Leg Segments ================================
LESIZE,13, , ,legsegs,legskew, , , ,1
LESIZE,14, , ,legsegs,legskew, , , ,1
'\
!== Intermediate Platform Radius ===============================
LESIZE,15, , ,radsegs,1, , , ,1

!== Lines across legs ==========================================
LESIZE,5, , ,legsegs,legskew, , , ,1
LESIZE,8, , ,legsegs,legskew, , , ,1

!== InterPlat Radii ============================================
LESIZE,16, , ,7,1, , , ,1
LESIZE,17, , ,7,1, , , ,1

!== IP Line ====================================================
LESIZE,11, , ,14,1, , , ,1
```

```
!== Sides of IP ================================================
LESIZE,10, , ,6,1, , , ,1
LESIZE,12, , ,6,1, , , ,1

!== Mesh Areas =================================================
MSHAPE,0,2D
MSHKEY,0
AMESH,ALL,,

!== Get Node Number at KeyPoint 14==============================
KSEL,s,kp,,14
NSLK,s
*GET,nkp1,node,0,num,max
NSEL,all
KSEL,all

FINISH
!================================================================
!                     Solution or Solver
!================================================================
/SOL

!== Set Analysis Type ==========================================
! Set to nonlinear Deflection Analysis
*IF,nonlinear,EQ,1,THEN
  SOLCONTROL,ON     !Steps optimal values for nonlinear problems
  PRED,0            !predictor off for 181SHELL elements
  DELTIM            !Use default substeps
  NLGEOM,1          !For large deflection analysis
  CNVTOL,U,,0.0001,,0.01    !Convergence for Displacement
  CNVTOL,F,,0.0001,,0.01    !Convergence for Force
*ENDIF
ANTYPE,0            !Analysis Type is Static (0)

!=== Apply DOF Constraints======================================
DL,1,,ALL,0,1
```

```
DL,3,,UX,0,1
DL,3,,UY,0,1
DL,3,,ROTX,0,1
DL,3,,ROTY,0,1
DL,2,,UX,0,1
DL,2,,UY,0,1
DL,2,,ROTX,0,1
DL,2,,ROTY,0,1

!== Apply Angular Loads ========================================
*DO,mm,1,rSteps,1
    OMEGA,0,0,angvelz,                    !*Angular Velocity
    !*DOMEGA,0,0,angaccz,                    !*Angular Acceleration
    DK,14, ,zdisp, ,0,UZ, , , , , ,
   lswrite,mm
*ENDDO

lssolve,1,rSteps

FINISH
!================================================================
!                          Post Processor
!================================================================
/POST1

*DIM,Smax,TABLE,rSteps
*DIM,Xdis,TABLE,rSteps
*DIM,Ydis,TABLE,rSteps
*DIM,Zdis,TABLE,rSteps
*DIM,Xforce,TABLE,rSteps
*DIM,Yforce,TABLE,rSteps
*DIM,Zforce,TABLE,rSteps
*DO,mm,1,rSteps,1
  SET,mm
  ETABLE,svonm,S,EQV
  ESORT,ETAB,svonm,0,1
```

```
  *GET,stress,SORT,0,MAX
  *SET,Smax(mm),stress
  *GET,disX,NODE,nkp1,U,X
  *SET,Xdis(mm),disX
 *GET,disY,NODE,nkp1,U,Y
  *SET,Ydis(mm),disY
  *GET,disZ,NODE,nkp1,U,Z
  *SET,Zdis(mm),disZ
  *GET,forceX,NODE,nkp1,RF,FX
  *SET,Xforce(mm),forceX
  *GET,forceY,NODE,nkp1,RF,FY
  *SET,Yforce(mm),forceY
  *GET,forceZ,NODE,nkp1,RF,FZ
  *SET,Zforce(mm),forceZ
*ENDDO

!== The results file will be named ============================
ANSYS_anglestudy_results.txt
*VPLOT,Xdis(1,1),Ydis(1,1)
/output,ANSYS_anglestudy_results.txt
*VWRITE
               Xdis                 Ydis                 Zdis
Xforce               Yforce               Zforce                Smax
*VWRITE,Xdis(1),Ydis(1),Zdis(1),Xforce(1),Yforce(1),Zforce(1),Smax(1)
\%20e \%20e \%20e \%20e \%20e \%20e \%20e
/output

FINISH
/eof
```

Appendix D

MatLab Files

D.1 MatLab Example EVAL File

```
function [disp,force,stress]=eval_anglestudy_lateral...
         (geom,mat,loads,ansys,params)
% ------------------------------------------------------------------------
% Study involving leg angles, angular velocity, and other geom parameters
% ------------------------------------------------------------------------
%
%   IMPORTANT: The names of the fields in the structure need to
%              match the variable names used in the ANSYS batch file.
%
%   geom.st = spring thickness
%   geom.lw = leg width
%   geom.ll = leg segment length
%   geom.lrad = leg radius
%   geom.ip = intermediate platform depth
%   geom.ipf = intermediate platform corner radii
%   geom.platrad = radius of the platform
%   geom.legang = leg angle in degrees
%
%   mat.Ey = Young's modulus
%   mat.Pr = Poisson's ratio
%   mat.De = Density
%
%   loads.zdisp = Maximum displacement in z-direction
%   loads.angvelz = Angular velocity about the z-axis
```

```
%   loads.angaccz = Angular acceleration about the z-axis
%
%   - ANSYS Parameters
%   ansys.rSteps = Number of load steps to displace to dZ
%   ansys.nonlinear = Logical (1=true) : Nonlinear deflection analysis
%   ansys.gelsize = global element size
%   ansys.radsegs = number of divisions for meshing radius
%   ansys.legsegs = number of segments on legs
%   ansys.legskew = skew for meshing legs
%   - MATLAB ANALYSIS Parameters (Not passed to ANSYS)
%   ** no params currently used (placeholder) **
%
% OUTPUTS:
%   disp - matrix of Xdis, Ydis, and Zdis
%   force - matrix of Yforce and Zforce for each displacement
%   stress - vector of maximum stress at each displacement
%
%  ANSYS setup:
%      ANSYS is run using the run_ANSYS.bat file, which contains the
%      full path to the ANSYS executable.  ANSYS creates files begin-
%      ning with the job name, or ANSYSJOB_*.* (these files may be
%      deleted). When changing computers or installing a new version
%      of ANSYS, you'll need to change the path in the batch file.
%
% ======================================================================
%                              Initialize
% ======================================================================
strWinBatchFile = 'run_ansys_anglestudy_lateral.bat';
strJobName = 'ANSYSJOB_anglestudy_lateral';   % Must match .bat batch file

% You can modify strWorkDir to use a temporary working directory
% where you can delete all the files later.
strAnsysDir = 'C:\ansystemp\';
strWorkDir = '.\';
inputFile = sprintf('%s%s',strAnsysDir,'ANSYS_anglestudy_inputs.txt');
batchFile = sprintf('%s%s',strWorkDir,'eval_ansys_anglestudy_lateral.inp');
```

```
outputFile = sprintf('%s%s',strAnsysDir,'ANSYS_anglestudy_results.txt');
errorFile = sprintf('%s%s%s',strAnsysDir,strJobName,'.err');

% Delete previous input/output/error files
fid = fopen(inputFile,'r');
if fid~=-1
    fclose(fid);
    syscommand = sprintf('del
    [eCode,retText]=system(syscommand);
end
%fid = fopen(outputFile,'r');
%if fid~=-1
%    fclose(fid);
%    syscommand = sprintf('del
%    [eCode,retText]=system(syscommand);
%end
fid = fopen(errorFile,'r');
if fid~=-1
    fclose(fid);
    syscommand = sprintf('del
    [eCode,retText]=system(syscommand);
end

% ========================================================================
%   Create the Input Parameter File
% ========================================================================
% When debugging, check to make sure input file is created correctly.

fid = fopen(inputFile,'w');
if fid==-1
   errordlg('ANSYS input parameter file open error','Error!','modal');
   error('ANSYS file open error.');
end

% Using the names within the structures
fprintf(fid,'\r\n');
```

```
paramNames = fieldnames(geom);
paramValues = struct2cell(geom);
for I = 1:length(paramNames)
    fprintf(fid,'%s = %f\r\n',paramNames{I},paramValues{I});
end

fprintf(fid,'\r\n');
paramNames = fieldnames(mat);
paramValues = struct2cell(mat);
for I = 1:length(paramNames)
    fprintf(fid,'%s = %f\r\n',paramNames{I},paramValues{I});
end

fprintf(fid,'\r\n');
paramNames = fieldnames(loads);
paramValues = struct2cell(loads);
for I = 1:length(paramNames)
    fprintf(fid,'%s = %f\r\n',paramNames{I},paramValues{I});
end

fprintf(fid,'\r\n');
paramNames = fieldnames(ansys);
paramValues = struct2cell(ansys);
for I = 1:length(paramNames)
    fprintf(fid,'%s = %f\r\n',paramNames{I},paramValues{I});
end

status=fclose(fid);
if status~=0
   errordlg('ANSYS input parameter file close error','Error!','modal');
   error('ANSYS file close error.');
end

% ======================================================================
%                                  RUN ANSYS
% ======================================================================
```

```
errCode=system(strWinBatchFile);
% errCodes: 8 - normal.  7 - no license file.  1 - no convergence
if errCode==1
   %errordlg('ANSYS failed to converge','Error!','modal');
   %error('ANSYS failed to converge.');
   disp=[];
   force=[];
   stress=[];
   return
end
if errCode==7
   %errordlg('ANSYS license unavailable','Error!','modal');
   %error('ANSYS license unavailable.');
   disp=[];
   force=[];
   stress=[];
   return
end

% ========================================================================
%                                READ the RESULTS
% ========================================================================
% Read results file.  Columns are displacement, force, stress
% rows are for each point in the force/displacement curve.

% Check if results file exists
fid=fopen(outputFile,'r');
if fid==-1
   %errordlg('Unable to open ANSYS results file.','Error!','modal');
   %error('Unable to open ANSYS results file. Check ANSYS .err file.');
   disp=[];
   force=[];
   stress=[];
   return
else
   fclose(fid);
```

```
end
% Read results
[Dmax Ydis Zdis Xforce Yforce Zforce Smax] = ...
    textread()outputFile,'%f %f %f %f %f %f %f','headerlines',1);

% ========================= Save/Return Results =========================
disp = [Dmax Ydis Zdis];
force = [Xforce Yforce Zforce];
stress = Smax;
```

D.2 MatLab 3D PRBM Script File

```
format short g
clear all
clc
% ============================================================================
%                           BEGINNING of INPUT Section
% ============================================================================
    geom.AR = 5;                    % geom.AR = tz/ty;
    geom.ty = 2;                    % beam thickness (mm)
    geom.tz = geom.ty*geom.AR;      % beam width (mm)
    geom.L = 100;                   % beam length (mm)
    geom.dy = .7;                   % nondimensional limit in y
    geom.dz = .2;                   % nondimensional limit in z

    mat.Ey = 207000000;             % modulus of elasticity (MPa) - mMKSV
    mat.Pr = 0.28;                  % poissons ratio

    loads.dY = geom.dy*geom.L;      % limit in y
    loads.dZ = geom.dz*geom.L;      % limit in z
    ansys.rSteps = 50;              % number of points on each contour
    ansys.nonlinear = 1;            % turns nonlinear solver on

% ------------------------- Used for analysis later ---------------------
    geom.Iy = (geom.ty*geom.tz^3)/12;   % moment of inertia about y axis
    geom.Iz = (geom.tz*geom.ty^3)/12;   % moment of inertia about z axis
```

```
% --- Define input displacements in polar coordinates using an ellipse ---
    cont = 20;                          % number of contours
    rZ = loads.dZ;                      % limit steps
    rY = loads.dY;                      % limit steps
    theta = linspace(0,pi/2,cont)';     % angles dividing quadrant
    dZmax = rZ*sin(theta);              % vector of z limits
    dYmax = rY*cos(theta);              % vector of y limits
% To verify ellipse:  plot(dZmax,dYmax); axis equal;

% ========================================================================
%                                 RUN the MODEL
% ========================================================================
dXdata = [];
dYdata = [];
dZdata = [];
FYdata = [];
FZdata = [];

for n = 1:cont
    loads.dZ = dZmax(n);
    loads.dY = dYmax(n);

    % ---------------------------- Run Ansys -----------------------------
    [disp,force,stress]=eval_3Dcant(geom,mat,loads,ansys,params);

    fprintf('Completed ANSYS run #%d of %d \n',n,cont);

    dXdata(:,n) = disp(:,1);
    dYdata(:,n) = disp(:,2);
    dZdata(:,n) = disp(:,3);
    Xdata = geom.L + dXdata;
    Ydata = dYdata;
    Zdata = dZdata;
    FYdata(:,n) = force(:,1);
    FZdata(:,n) = force(:,2);
```

```
    % --------------------- Real time update of plot ---------------------
    figure(1); clf;
    plot(Xdata,Ydata,'-x');
    axis equal;
    xlabel('X position');
    ylabel('Y position');

    % -------------------------- Update surface plot ---------------------
    if n > 1
        gscale = linspace(0.2,0.8,50)';
        gmap = [gscale, gscale, gscale];
        figure(2); clf;
        surface(Xdata,Ydata,Zdata);
        axis equal;
        view(30,20);
        grid;
        shading interp;
        colormap(gmap);
        alpha(0.6);
        hold on;
        line(Xdata,Ydata,Zdata,'LineStyle','-','Marker','o','MarkerSize',3);
        hold off;
        xlabel('X position');
        ylabel('Y position');
        zlabel('Z position');
    end

end

% ========================================================================
%                              SAVE RESULTS
% ========================================================================
save saved_3Dcant Xdata Ydata Zdata dXdata dYdata dZdata FYdata FZdata;
save saved_inputs geom mat loads ansys params cont theta dZmax dYmax;
```

D.3 MatLab COPS Leg Script File

```
format short g
clear all
clc

% ========================================================================
%                            Individual Runs
% ========================================================================

% ---------------------- BEGINNING of INPUT Section ----------------------
geom.st = .000508;          % units in m  ***spring thickness
geom.lw = .012700;          % units in m  ***leg width
geom.ll = .069850;          % units in m  ***leg length
geom.lrad = .002381;        % units in m  ****gap radius
geom.ip = geom.lw;          % units in m  ***intermediate platform width
geom.ipf = .5*geom.lw;      % units in m  ***radius on ip corners
geom.platrad = .050800;     % units in m  ***platform radius
geom.legang = 67.5;         % units in m  ***leg angle in degrees

mat.Ey = 207000000000;      % units in N/m^2
mat.Pr = 0.3;               % Poisson ratio
mat.De = 7850;              % units in kg/m^3

loads.zdisp = .0127;        % max displacement in the z direction
loads.angvelz = 325;        % angular velocity about the z axis rad/sec
loads.angaccz = 0;          % angular acceleration about the z axis

ansys.rSteps = 1;           % number of steps to move through z disp
ansys.nonlinear = 1;        % 1 = true
ansys.gelsize = geom.lw/.0127*.00254;    % global element size (m)
ansys.radsegs = 30;         % number of divisions for meshing radius
ansys.legsegs = 20;         % number of segments on legs
ansys.legskew = .1;         % skew for meshing legs

% ----------------------- END of INPUT Section --------------------------
```

```
% ========================================================================
%                              RUN the MODEL
% ========================================================================
Zmax = [];
Zdata = [];
FZdata = [];

for n = 1:ansys.rSteps

% ------------------------------ Run Ansys -----------------------------
    [disp,force,stress]=eval_anglestudy_lateral...
        (geom,mat,loads,ansys,params);

    fprintf'Completed ANSYS run #%d of %d \n',n,ansys.rSteps);

    Zmax = disp(:,1)
    Zdata = disp(:,3)
    FZdata(:,n) = force(:,3)

end

% ---------------------------- SAVE RESULTS ----------------------------
save saved_anglestudy Zmax Zdata FZdata;
save saved_inputs geom mat loads ansys params;
```